Order Number 9322693

Theory of optical nonlinearity in π-conjugated polymers and related materials

Guo, Dandan, Ph.D.

The University of Arizona, 1993

U·M·I
300 N. Zeeb Rd.
Ann Arbor, MI 48106

THEORY OF OPTICAL NONLINEARITY IN π-CONJUGATED POLYMERS AND RELATED MATERIALS

by

Dandan Guo

A Dissertation Submitted to the Faculty of the

DEPARTMENT OF PHYSICS

In Partial Fulfillment of the Requirements
For the Degree of

Doctor of Philosophy

In the Graduate College

THE UNIVERSITY OF ARIZONA

1 9 9 3

THE UNIVERSITY OF ARIZONA
GRADUATE COLLEGE

As members of the Final Examination Committee, we certify that we have read the dissertation prepared by Dandan Guo

entitled Theory of Optical Nonlinearity in pi-Conjugated Polymers and Related Materials

and recommend that it be accepted as fulfilling the dissertation requirement for the Degree of Doctor of Philosophy /Physics

Sumitendra Mazumdar	4/12/93 Date
J. D. Garcia	4/12/93 Date
Laurence McIntyre	4/12/93 Date
Robert Parmenter	4/12/93 Date
Nesser Peyghambrian	4/12/93 Date

Final approval and acceptance of this dissertation is contingent upon the candidate's submission of the final copy of the dissertation to the Graduate College.

I hereby certify that I have read this dissertation prepared under my direction and recommend that it be accepted as fulfilling the dissertation requirement.

Sumitendra Mazumdar — 4/12/93
Dissertation Director — Date
Sumitendra Mazumdar

STATEMENT BY AUTHOR

This dissertation has been submitted in partial fulfillment of requirements for an advanced degree at The University of Arizona and is deposited in the University Library to be made available to borrowers under rules of the library.

Brief quotations from this dissertation are allowable without special permission, provided that accurate acknowledgment of source is made. Requests for permission for extended quotation from or reproduction of this manuscript in whole or in part may be granted by the head of the major department or the Dean of the Graduate College when in his or her judgment the proposed use of the material is in the interests of scholarship. In all other instances, however, permission must be obtained from the author.

SIGNED: 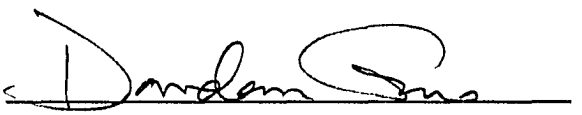

ACKNOWLEDGEMENTS

I would like to thank my advisor, Dr. Sumitendra Mazumdar, for his guidance during my thesis work. Without his help, encouragement, and criticism, my current achievements are impossible. What I have learned from him is invaluable.

I am very grateful to Dr. Chang-Yun Fan for helping me to come to the United States and for his supports and guidance during the ups and downs of my graduate student time.

I am greatly indebted to Dr. Markus Lindberg for his suggestion of working with Dr. Mazumdar, for his instructive scientific discussions with me, and for his many years friendship.

I would also like to thank Patrick McGuire who read my dissertation and gave many useful suggestions. Special thanks to Dr. Charles Nugent and his wife Peggy for their long time friendship since I came to Tucson.

My dissertation work has been supported by NSF under grant No. ECS-89-11960 and the Optical Circuitry Cooperative of the University of Arizona.

Last and most of all, my husband, Lifeng Li, and my mother, Liming Shen, have given me their unconditional love, support, and helps that are beyond measure.

To My Father

TABLE OF CONTENTS

LIST OF TABLES

LIST OF FIGURES

ABSTRACT

Within the framework of interacting-electron models, the optical nonlinearity in π-conjugated polymers is investigated theoretically. A complete microscopic many-body theory is developed for the mechanism of the third order nonlinearity in these materials. The universality and the predictability of the theory are well established.

It is found that the bulk of the optical nonlinearity in conjugated polymers is determined by four essential states although all the excited states are involved. It is also found that electron-electron Coulomb interactions in one-dimensional systems play key roles in the nonlinear optical processes and are responsible for the observed spectroscopic features.

The theoretical results are compared with experiments in wide variety of materials and excellent agreements between theory and experiments are obtained. With the essential-state theory, various experiments are explained within a single unified theory for the first time, and many controversies are resolved.

CHAPTER 1

INTRODUCTION

In recent years, scientists have shown enormous interests in one- and quasi-one-dimensional π-conjugated polymers and have conducted intense research on these materials. Due to their unique mechanical properties such as processibility and flexibility, their novel electronic conductivity, and their large optical nonlinearity[1], conjugated polymers have found new applications in electronics, optical communication, optical computing, and many other fields of technology. Furthermore, the development in molecular engineering has made it possible to tailor materials of desired properties and has made conjugated polymers more attractive than ever. As model quasi-one-dimensional electronic systems, π-conjugated polymers have been considered to be the prototypes for studying electron-electron correlations in reduced dimensions, the characteristics shared by many other novel electronic materials such as organic superconductors and high T_c superconductors. The research on conjugated polymers is providing valuable information for the research on more complicated materials.

As a new generation of nonlinear optical materials, π-conjugated polymers possess large nonresonant nonlinearities comparable to or larger than those of inorganic semiconductors[2], and with fast response in the order of pico- to femtoseconds[3]. However, due to the difficulties in numerical calculations and, hence,

[1]See, for example, "*Conjugated Conducting Polymers*", edited by Kiess, 1992.

[2]See, for example, Sauteret *et al.*, 1976.

[3]see, for example, Messier *et al.*, eds, 1989); Vadeny and Baker, eds, 1992; Chiang *et al.*, eds, 1991.

the lack of the complete knowledge of electron-electron interactions in these one-dimensional systems, there exist many controversies on and incorrect explanations for experimental results. In addition, in most available materials the figure of merit that measures the efficiency of a given nonlinear process is still below the ideal value for device applications. Therefore, there is a great need for a theory that captures the essential mechanism of the optical nonlinearity in π-conjugated polymers and provides guidance for searching and tailoring better materials.

The purpose of this research is to understand the underlying physics responsible for the optical nonlinearity in π-conjugated polymers and to find a theory that not only can explain the existing experiments but also can predict for future research.

1.1 Historical Review: Electronic structures

1.1.1 Modeling π-Conjugated Polymers

The lattice of a π-conjugated polymer consists of arrays of carbon atoms. In Fig. 1.1, the idealized structures of a few widely studied conjugated polymers are illustrated. Because a carbon atom has atomic configuration $1s^2 2s^2 2p^2$, four of the electrons are the valence electrons. Three of the valence electrons are in sp^2 hybridized orbitals; two of them are paired with their counterparts in the neighboring carbon atoms to form the so called σ bonds that construct the one-dimensional lattice, while the third forms a σ-bond with either an atomic or a molecular side group. The remaining valence electron, the π-electron, is in the $2p_z$ atomic orbital, with its charge density lobes perpendicular to the molecular plane defined by the other three (see Fig. 1.2). The overlap between two adjacent π-electron orbitals forms a π bond. Since each π-orbital overlaps with a similar orbital at both left- and right-hand side (see Fig. 1.2), the π-electrons are delocalized over the whole lattice,

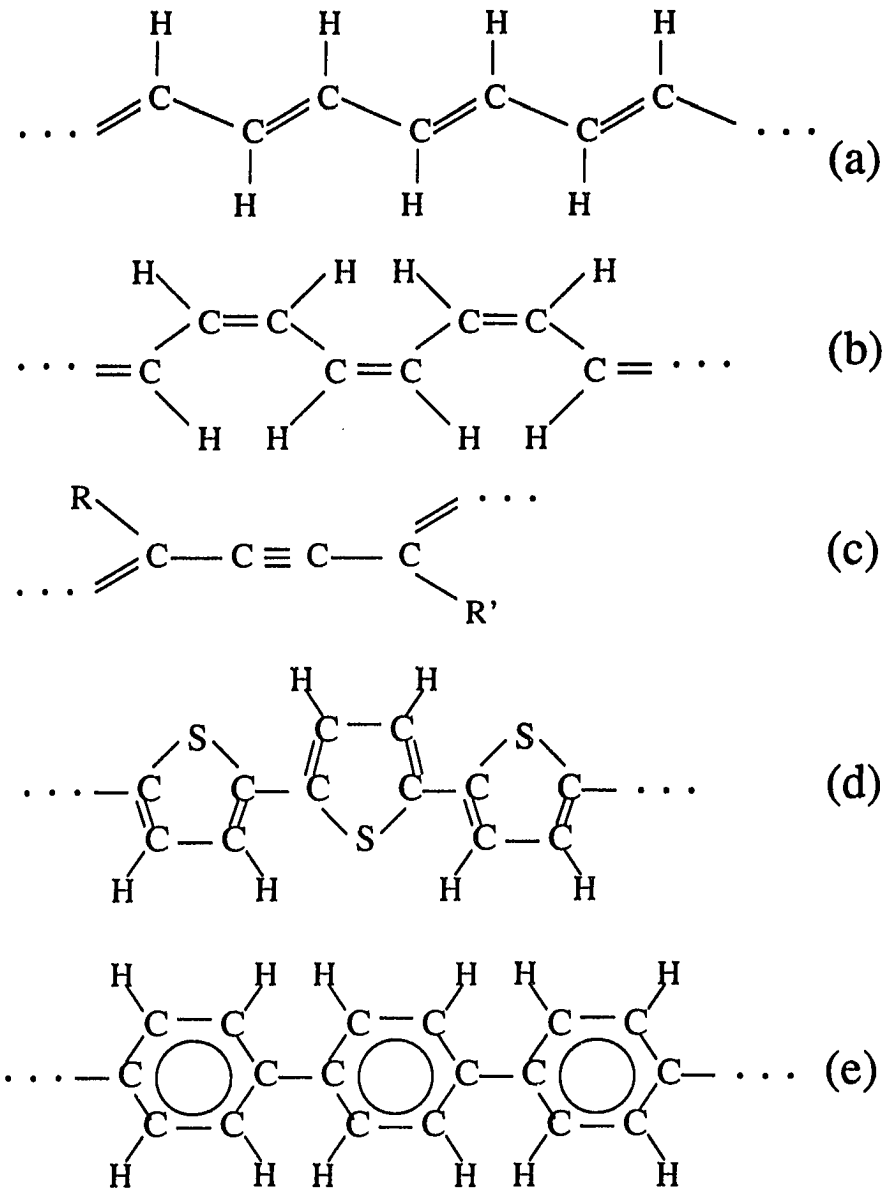

Figure 1.1: The idealized chemical structure of several π-conjugated polymers. (a) *trans*-$(CH)_x$ polymer chain. (b) *cis*-$(CH)_x$ polymer chain. (c) Polydiacetylene. (d) Polythiophene. (e) Polyaraphenylene.

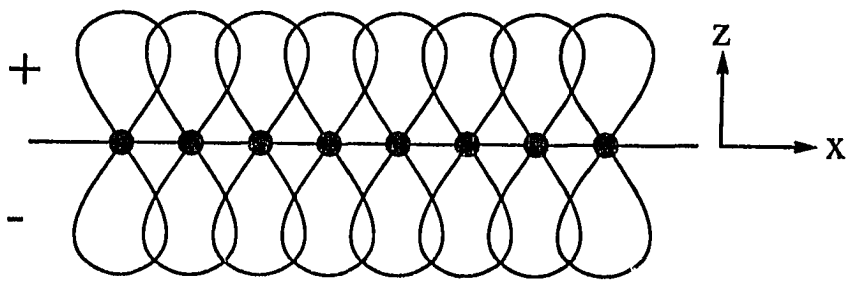

Figure 1.2: Schematic presentation of π-electron $2p_z$ orbitals and the overlaps between the orbitals. The molecular plane is in the x-y plane.

which characterizes the conjugated molecules. To a first approximation, no conjugation between the main chain and the side groups is assumed. Because of the large inter-chain spacings, particularly in polydiacetylenes with large molecules as side groups, and the observed highly anisotropic electric and optical properties, the conjugated polymers with delocalized π-electrons are considered as one-dimensional π-electron networks. Furthermore, the tight-binding approximation that neglects the overlaps between non-nearest neighbor π-electron orbitals has been widely accepted in all the theoretical models for π-conjugated polymers because of the good agreement between the prediction of the one-dimensional tight-binding models and experiments[4].

For the purpose of gaining insight into the general properties of π - conjugated polymers, one often uses the simplified structure shown in Fig. 1.3 in theoretical modeling. In the figure, each site represents a (CH) unit. With such

[4]See, for example, Heeger *et al.*, 1988.

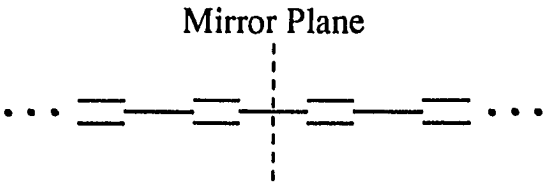

Figure 1.3: Simplified molecular structure in the theoretical modelings.

simplification, the wave functions possess mirror plane and centro-inversion symmetries. The group notations for the mirror plane symmetries are A (symmetric) and B (antisymmetric), and those for the inversion symmetries are g (symmetric) and u (antisymmetric). The ground state is the $1A_g$ and the first optical state dipole coupled to the ground state is necessarily the $1B_u$. Hereafter, A_gs and B_us are used for describing the total energy states of the one-dimensional molecular chains.

1.1.2 Many-Body Problems

Contrary to the prediction of conventional band theory, π-conjugated polymers with half-filled bands (i.e. number of electrons = number of carbon sites N) are semiconductors with alternating bond lengths[5] rather than conductors with equal bond length. The origin of the semiconducting gap (or optical gap) has been debated for a long time, and the prediction of a gap and bond alternation has been considered as a must for an appropriate theoretical model to these one-dimensional systems.

The independent-electron theory for polyenes was developed by Hückel (Hückel, 1931) and was reformulated in the model of Su, Schrieffer, and Heeger

[5]See, for example, Fincher *et al.*, 1982; Yannoni *et al.*, 1983.

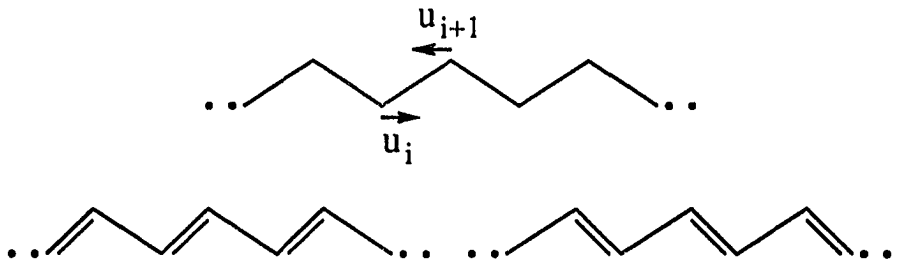

Figure 1.4: The $2k_F$ lattice distortion and the two dimerized phases of *trans*-$(CH)_x$.

(SSH) (Su, Shrieffer, and Heeger, 1979) to include the electron-lattice vibration (phonon) couplings explicitly. Within the tight-binding and the Born-Oppenheimer approximations, the SSH Hamiltonian is written as

$$H_{SSH} = -\sum_{i,\sigma}[t + \alpha(u_i - u_{i+1})][c^+_{i,\sigma}c_{i+1,\sigma} + c^+_{i+1,\sigma}c_{i,\sigma}] + \frac{\kappa}{2}\sum_i (u_i - u_{i+1})^2 \ , \quad (1.1)$$

where the operator $c^+_{i,\sigma}(c_{i,\sigma})$ creates (annihilates) a π-electron of spin σ at site i (the ith carbon atom), $t(> 0)$ is the overlap integral that measures the overlap between the nearest neighbor atomic orbitals $(2p_z)$ of the π-electrons, u_i is the displacement of the ith carbon atom in the one-dimensional lattice, α is the coupling constant of electron-phonon interactions, and κ is the spring constant for the lattice energy when expanded to second order about the equilibrium in dimerized systems. Within such a model, the lattice is unstable with respect to a periodic distortion with a wave vector being equal to $\pm 2k_F$ (see Fig. 1.4), which leads to dimerization (or bond alternation) for a half-filled band, and a gap is resulted in for arbitrarily weak electron-photon couplings. From Peierls theorem (Peierls, 1955), such instability is known to be the consequence of the one-dimensionality within mean-field approximation. The two dimerized phases of *trans*-$(CH)_x$ are shown in Fig. 1.4.

Besides giving physical interpretations to the semiconductor gap and dimerizations, the SSH model predicts the presence of topological defects in infinite

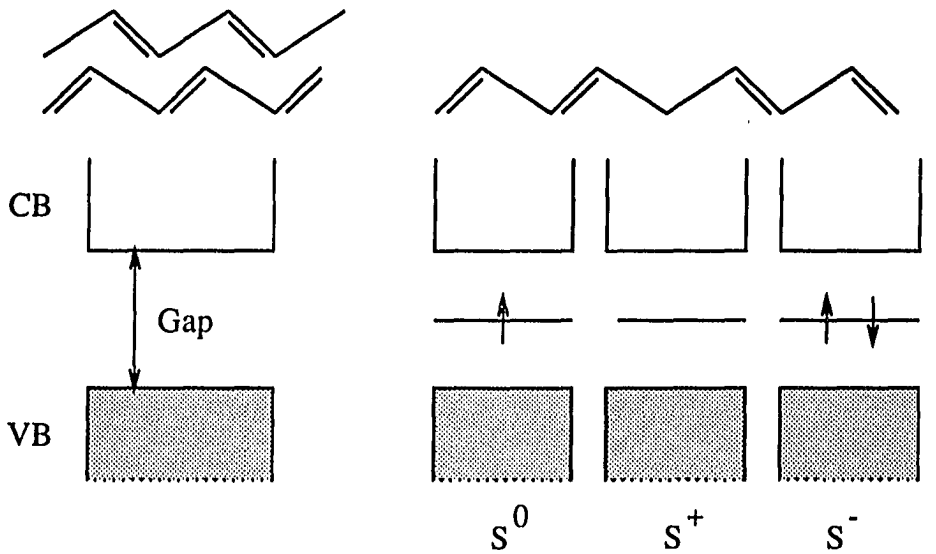

Figure 1.5: Soliton configurations and the corresponding single-particle energy spectra. S^0, S^+, and S^- represent, respectively, the neutral, positively charged, and negatively charged solitons.

chains whose boundaries have different asymptotic limits at $x \to \pm\infty$ and in odd-membered rings. This defect corresponds to a phonon field configuration that approaches one dimerized phase for $N \to -\infty$ and another phase for $N \to \infty$, and is called a neutral soliton since the system is neutral and the shape of the defect is preserved while it moves along the chain. Charged solitons are resulted by doping a hole or an electron. which is attached to the neutral defect. The occurrence of a soliton leads to a localized eigenstate around the defect, which gives rise to a nonbonding orbital at the middle of the energy gap. The middle gap orbital is half-occupied in the case of neutral soliton and empty (doubly occupied) in the case of a positively (negatively) charged soliton. The geometric structures and the energy spectra of neutral and charged solitons are illustrated in Fig. 1.5. The presence of solitons in conjugated polymers explains the observed electric conductivity in

doped polyacetylene (Chiang *et al.*, 1977).

Although the independent-electron theory and the SSH model lead to qualitatively good understanding of some of the properties of conjugated polymers, there are, however, many experimental facts that cannot be explained within the simple single particle picture. One of the examples is about the optical absorption of solitons. According to the SSH model, neutral and charged solitons absorb at the same energy, which is half of the optical gap (see Fig. 1.5). However, experimental results show that the neutral soliton absorption is at an energy near the gap while the charged solitons at an energy below the half-gap (Weinberger *et al.*, 1984). Another important result that renders the one-electron theory suspect is the occurrence of negative spin densities (Hanna *et al.*, 1962) at the carbon sites, which are expected to have zero spin densities within the framework of independent-electron models.

The discrepancies between experiments and the one-electron theory initiated the efforts to incorporate electron-electron Coulomb interactions in theoretical models. A simplified interacting-electron model that has been popularly applied to the studies of conjugated polymers and other low-dimensional systems is the Hubbard model, which was originally suggested by Hubbard (Hubbard, 1963) to describe the Coulomb correlations among the electrons in the d-bands of transition metals that exhibit behavior characteristic of both band model and atomic model. The Hubbard Hamiltonian is written as

$$H_{Hubbard} = -t \sum_{i,\sigma} (c^{+}_{i,\sigma} c_{i+1,\sigma} + c^{+}_{i+1,\sigma} c_{i,\sigma}) + U \sum_{i} n_{i,\uparrow} n_{i,\downarrow} \qquad (1.2)$$

where U is the on-site Coulomb repulsion and $n_i = \sum_\sigma c^{+}_{i,\sigma} c_{i,\sigma}$ is the density operator at site i.

The Hubbard model has been widely accepted because of the following reasons. First, as a consequence of electron-electron Coulomb interaction, a gap is retained even in the case of equal bond lengths. Second, the research in the

Peierls-Hubbard model that includes both electron-electron and electron-phonon interactions indicates that the bond alternation in one-dimensional chains not only persist for arbitrary values of U but also can be enhanced by U (Mazumdar and Dixit, 1983). Third, within the Hubbard model, the problems such as soliton absorptions (Campbell *et al.*, 1984; Mazumdar and Dixit, 1989) and negative spin densities (McConnell and Chesnut, 1957; Hirsh, 1983) are naturally solved. For example, in the limit $U >> t$, the optical absorption of a neutral soliton corresponds to creating a double occupancy, which costs an energy $\sim U$, while a charged soliton absorption corresponds to an electron hopping with numbers of double occupancy conserved (see Fig. 1.5) and, hence, costs much less energy. This explains qualitatively the neutral and charged soliton absorption spectra.

For optical properties, the most relevant issue to many-body effects is about the nature of the lowest excited state. From the definition of the wavefunction symmetries, the ground state is the $1A_g$ and the first optical state that is dipole coupled to the ground state is necessarily the $1B_u$.

In the one-electron Hückel or SSH model, a single particle state corresponds to a molecular orbital (MO) with energy

$$E_k = \pm 2t\sqrt{cos^2 k + \delta^2 sin^2 k} \tag{1.3}$$

where k is the wave vector and, for open linear chains[6], $k = m\frac{\pi}{N+1}$, m = 1, 2, ... The "+" sign in Eq. 1.3 is for the MOs in the conduction band, while the "-" sign is for the orbitals in the valence band. The ground state corresponds to a fully filled valence band and an unoccupied conduction band. The $1B_u$ is reached from the ground state by exciting one electron from the highest occupied molecular orbital to the lowest empty molecular orbital. The MO occupations of the $1A_g$, the $1B_u$, the $2A_g$ and the $2B_u$ states are given in Fig. 1.6. From Fig. 1.6, it is apparent that the lowest excited state is the $1B_u$, whose symmetry is different from that of the ground state, and the $2A_g$ must have a higher energy than that of the $1B_u$.

[6]see Salem, 1964.

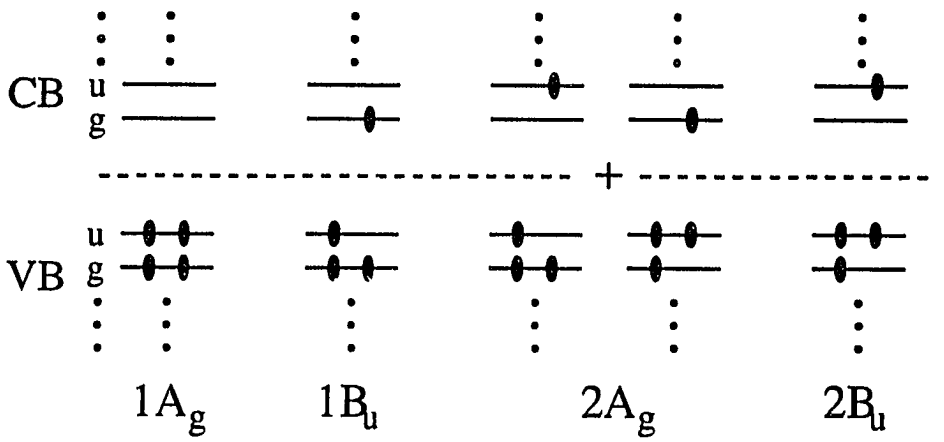

Figure 1.6: Molecular orbitals and electron occupancies of the $1A_g$, $1B_u$, $2A_g$, and $2B_u$ states. The symmetry of MO alternates (g or u) in a given state.

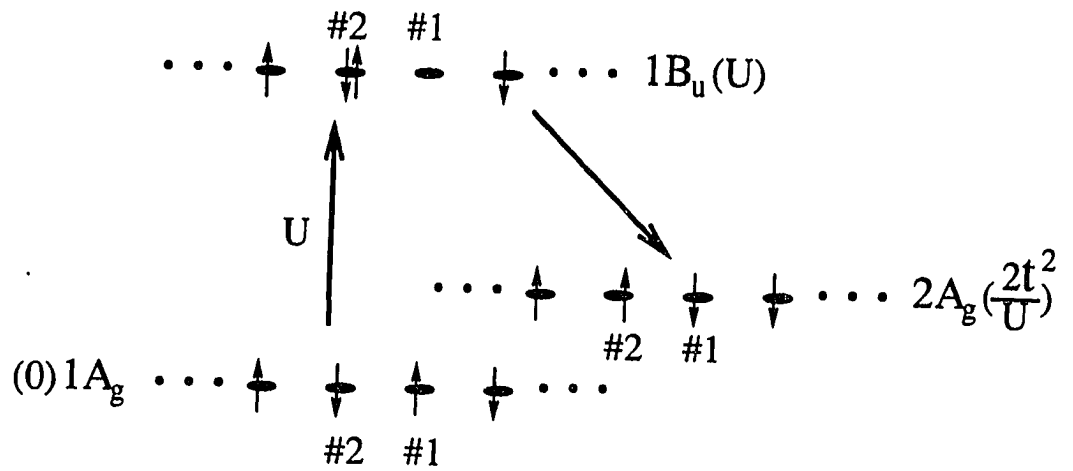

Figure 1.7: Dominant spin configurations for the $1A_g$, the $1B_u$, and the $2A_g$ states in strong Coulomb interaction limit. In this case, the $1B_u$ is at an energy $\sim U$ with respect to that of the ground state while the $2A_g$ is $\sim t^2/U$ above the $1A_g$.

However, it is experimentally observed that the first singlet excited state in finite polyenes is an A_g state located below the $1B_u$ (Hudson and Kohler, 1974; Kohler *et al.*, 1988), which has been attributed to the $2A_g$. Although the occurrence of subgap states is impossible in the one-electron theory, it is well understood within interacting-electron models (Schulten *et al.*, 1976; Ramasesha and Soos, 1984). A qualitative illustration of the subgap $2A_g$ is shown in Fig. 1.7 for the strong coupling limit of the Hubbard model. In the limit of large U, the ground state $1A_g$ is dominantly covalent with each site occupied by an electron. The optical transition to the $1B_u$ corresponds to a charge transfer from one site (denoted by 1) to a neighboring site (denoted by 2) and necessarily leads to a double occupancy, which raises the energy by $\sim U$. Further charge transfer of the electron that is originally at site #2 to site #1 results in a lower energy state, which is covalent and has a different spin configuration from that of the ground state. This state is the $2A_g$ and has an energy $\sim t^2/U$ in the perturbative limit. In fact, there is a band of covalent states below the $1B_u$ in long polyenes within the Hubbard model. These states become degenerate with the ground state and correspond to gapless spin excitations for $U \rightarrow \infty$ in undimerized chains. In general, the number of subgap states is a function of U and the dimerization parameter.

1.2 Nonlinear Optical Properties

Unlike other properties mentioned in the last section, nonlinear optical properties involve, in principle, *all* the excited states and the study of the optical nonlinearity can provide complete information on the electronic structure. Therefore, by comparing with experiments, it is possible to test the appropriateness of a theoretical model in describing real materials.

1.2.1 Third Order Optical Nonlinearity

Nonlinear optics deals with nonlinear interactions of light and matter. In general, the response of a medium to an input light (or electromagnetic field) is always nonlinear. However, nonlinear effects were not observable until the advent of lasers that produce intense and coherent light.

A nonlinear optical process is composed of (a) the nonlinear response of a medium to the input light, and (b) the nonlinear modification of the field by the reacting medium. For a non-magnetic medium, the nonlinear response to an input field $\mathbf{E}$ is described by the equation[7]

$$\mathbf{D} = \epsilon^{(1)} \cdot \mathbf{E} + \epsilon^{(2)} : \mathbf{EE} + \epsilon^{(3)} : \mathbf{EEE} + \cdots, \tag{1.4}$$

where $\mathbf{D}$ is the electric displacement resulted from the medium-field interaction and $\epsilon^{(n)}$ is the $(n+1)$th-rank electric permittivity tensor.

Since in most materials the electric quadruple and higher order multipoles are completely negligible, we are only interested in the electric dipole polarization $\mathbf{P}$. Corresponding to the nonlinear relation in Eq. 1.4, the nonlinear polarization vector $\mathbf{P}$ has the form

$$\mathbf{P} = \chi^{(1)} \cdot \mathbf{E} + \chi^{(2)} : \mathbf{EE} + \chi^{(3)} : \mathbf{EEE} + \cdots, \tag{1.5}$$

where $\chi^{(n)}$ is the nth-order nonlinear susceptibility.

The nonlinear susceptibility $\chi^{(n)}$ characterizes the optical properties of a medium. Because $\chi^{(n)}$ is related to the microscopic structure of the medium, full quantum-mechanical calculations are required for its proper evaluations. Once the optical susceptibilities are known, the optical problems in a medium become, in principle, solvable via Eq. 1.5 and the Maxwell equations.

Since polyacetylene and polydiacetylenes, which are the most widely studied polymers, have centro-inversion symmetry, the second order susceptibility $\chi^{(2)}$

[7]See, for example, Jackson, 1975.

vanishes and the lowest order nonlinear susceptibility is the $\chi^{(3)}$ in these materials. Therefore, only $\chi^{(3)}$ is discussed in this dissertation. The general expression of the third order optical nonlinear susceptibility is written as[8]

$$\chi^{(3)}(-\omega_\sigma;\omega_1,\omega_2,\omega_3) = K\hat{P}\sum_{glmn}\rho(g)[\frac{\mathbf{e}^*_\sigma\cdot\mu_{gl}\mathbf{e}_1\cdot\mu_{lm}\mathbf{e}_2\cdot\mu_{mn}\mathbf{e}_3\cdot\mu_{ng}}{(\omega_{lg}-\omega_\sigma)(\omega_{mg}-\omega_2-\omega_3)(\omega_{ng}-\omega_3)}$$
$$+\frac{\mathbf{e}_1\cdot\mu_{gl}\mathbf{e}^*_\sigma\cdot\mu_{lm}\mathbf{e}_2\cdot\mu_{mn}\mathbf{e}_3\cdot\mu_{ng}}{(\omega_{lg}+\omega_\sigma-\omega_2-\omega_3)(\omega_{mg}-\omega_2-\omega_3)(\omega_{ng}-\omega_3)}$$
$$+\frac{\mathbf{e}_1\cdot\mu_{gl}\mathbf{e}_2\cdot\mu_{lm}\mathbf{e}^*_\sigma\cdot\mu_{mn}\mathbf{e}_3\cdot\mu_{ng}}{(\omega_{lg}+\omega_\sigma-\omega_2-\omega_3)(\omega_{mg}+\omega_\sigma-\omega_3)(\omega_{ng}-\omega_3)}$$
$$\frac{\mathbf{e}_1\cdot\mu_{gl}\mathbf{e}_2\cdot\mu_{lm}\mathbf{e}_3\cdot\mu_{mn}\mathbf{e}^*_\sigma\cdot\mu_{ng}}{(\omega_{lg}+\omega_\sigma-\omega_2-\omega_3)(\omega_{mg}+\omega_\sigma-\omega_3)(\omega_{ng}+\omega_\sigma)}] \quad (1.6)$$

where K is a constant, $\hat{P}$ is the permutation operator that permutes the indexes 1, 2, and 3, and, hence, there are totally 24 terms in the sum, $\omega_\sigma = \omega_1+\omega_2+\omega_3$, $\mathbf{e}_k$ is the unit vector of the field $\mathbf{E}_k = \mathbf{e}_k\mathcal{E}(\mathbf{r})e^{-i\omega_k t}$ with an amplitude $\mathcal{E}(\mathbf{r})$, $\hbar\omega_{ij} = [E(i)-E(j)]$ is the energy difference between the state i and j, μ is the dipole operator and $\mu_{ij} \equiv \langle i|\mu|j\rangle$. In general, there are 16 components[9] for a fourth-rank tensor $\chi^{(3)}_{\alpha\beta\lambda\eta}$, where α, β, λ, $\eta = x$, y, z, and x is along the direction of the molecular chain. For *trans*-polyenes, the five non-zero coefficients are for the components $xxxx$, $yxxx$, $yyxx$, $xxxy$, $yyyy$[10]. The largest coefficient is $\chi^{(3)}_{xxxx}$. Hereafter, I denote $\chi^{(3)}_{xxxx}$ with $\chi^{(3)}$.

The measurement of the $\chi^{(3)}(-\omega_\sigma;\omega_1,\omega_2,\omega_3)$ can be achieved via various experimental methods. For example, degenerate four wave mixing or two-photon absorption (TPA) with $\omega_1 = \omega_2 = -\omega_3 = \omega$ measures $\chi^{(3)}_{TPA} \equiv \chi^{(3)}(-\omega;\omega,\omega,-\omega)$, third harmonic generation (THG) with $\omega_1 = \omega_2 = \omega_3 = \omega$ measures $\chi^{(3)}_{THG} \equiv \chi^{(3)}(-3\omega;\omega,\omega,\omega)$, and coherent-anti-Stokes-Raman-spectroscopy with $\omega_1 = \omega_2 = \omega$, $\omega_3 = -\omega'$ measures $\chi^{(3)}_{CARS} \equiv \chi^{(3)}(-2\omega+\omega';\omega,\omega,-\omega')$[11]. Here, I discuss $\chi^{(3)}_{THG}$ and $\chi^{(3)}_{TPA}$. The schematic descriptions of third harmonic generation and two-photon absorption are given in Fig. 1.8.

[8]See, Orr and Ward, 1971.
[9]See, for example, Shen, 1984.
[10]see, for example, Shen, 1984, or Hann, Yuratich and Cotter, 1979.
[11]See, for example, Shen, 1984).

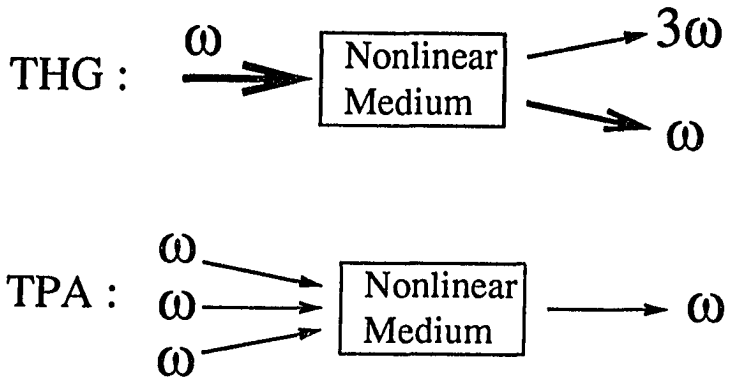

Figure 1.8: The schematic descriptions of third harmonic generation and two-photon absorption.

The expression of $\chi^{(3)}_{THG}$ is written as

$$\chi^{(3)}_{THG} = \sum_{jkl} \langle 1A_g|\mu|jB_u\rangle\langle jB_u|\mu|kA_g\rangle\langle kA_g|\mu|lB_u\rangle\langle lB_u|\mu|1A_g\rangle \times [D_1(\omega) + D_1(-\omega) + D_2(\omega) + D_2(-\omega)]. \quad (1.7)$$

where K has been taken to be 1, and the denominators are

$$D_1^{-1}(\omega) = (\omega_{jB_u} - 3\omega + i\Gamma)(\omega_{kA_g} - 2\omega + i\Gamma)(\omega_{lB_u} - \omega + i\Gamma),$$
$$D_2^{-1}(\omega) = (\omega_{jB_u} - \omega + i\Gamma)(\omega_{kA_g} - 2\omega + i\Gamma)(\omega_{lB_u} + \omega + i\Gamma), \quad (1.8)$$

with $\hbar\omega_{jB_u} = E(jB_u) - E(1A_g)$ etc. being the energies with respect to the ground state, Γ^{-1} is a characteristic relaxation time between an excited state and the ground state, which is assumed to be equal for all the states, and the triple sum is over all the excited states.

The $\chi^{(3)}_{TPA}$ is written as

$$\chi^{(3)}_{TPA} = \sum_{j,k,l} \langle 1A_g|\mu|jB_u\rangle\langle jB_u|\mu|kA_g\rangle\langle kA_g|\mu|lB_u\rangle\langle lB_u|\mu|1A_g\rangle$$

$$\times [d_1(\omega) + d_1(-\omega) + d_2(\omega) + d_2(-\omega) + d_3(\omega) + d_3(-\omega)], \quad (1.9)$$

where

$$\begin{aligned} d_1(\omega)^{-1} &= (\omega_{jB_u} - \omega + i\Gamma)(\omega_{kA_g} + i\Gamma)(\omega_{lB_u} - \omega + i\Gamma), \\ d_2(\omega)^{-1} &= (\omega_{jB_u} - \omega + i\Gamma)(\omega_{kA_g} + i\Gamma)(\omega_{lB_u} + \omega + i\Gamma), \\ d_3(\omega)^{-1} &= (\omega_{jB_u} - \omega + i\Gamma)(\omega_{kA_g} - 2\omega + i\Gamma)(\omega_{lB_u} - \omega + i\Gamma). \end{aligned} \quad (1.10)$$

Note that states jB_u, kA_g, and lB_u are the virtual states and their real contributions to the nonlinearity are via the dipole moments. There are no real transitions to these states since the frequency of the input field is limited to be less than the energy of the gap ($1B_u$) in nonlinear optical experiments. The issue of virtual states is important to understanding the origin of optical nonlinearity in materials such as polyacetylene in which solitons can be photo-generated when real transitions to B_u states occur. This will be discussed in Chapter 4.

According to the expression of $\chi^{(3)}_{THG}$ and $\chi^{(3)}_{TPA}$ a third order nonlinear process corresponds to a dipole coupling pathway

$$1A_g \rightarrow jB_u \rightarrow kA_g \rightarrow lB_u \rightarrow 1A_g, \quad (1.11)$$

(see the numerators in Eq. 1.7 and 1.9) and resonances are expected whenever a denominator becomes zero. The resonance at $\hbar\omega = \frac{1}{3}E(jB_u)$ is called a three-photon resonance, and that at $\hbar\omega = \frac{1}{2}E(kA_g)$ a two-photon resonance, and that at $\hbar\omega = E(lB_u)$ a one-photon resonance. Since the interesting frequency range for nonlinear optical experiments is below the $1B_u$, there is no one-photon resonance in the $\chi^{(3)}$ spectra within that region.

Because of the triple sum in the $\chi^{(3)}$ expression, the number of the terms (pathways) increases rapidly as the chain length N increases, and there is a great difficulty in the numerical computations of the third order susceptibilities. For N = 6, 8, and 10, the possible numbers of pathways to be calculated are of the orders 10^5, 10^8, and 10^{11} respectively. Therefore, it is impossible to perform

computations in long chains, and searching for the infinite chain behavior and the mechanism of optical nonlinearity is a formidable task.

1.2.2 Experimental $\chi^{(3)}_{THG}$ Spectrum and Its Implications

Instead of great complexity as revealed in the theoretical formula, the experimental $\chi^{(3)}$ spectra have surprisingly simple structures. Such a simplicity casts a new light on the underlying physics of the optical nonlinearity in conjugated polymers.

After the first reported large optical nonlinearities in conjugated systems—a long polyene (Hermann *et al.*, 1973) and in a single-crystalline polydiacetylene (Sauteret *et al.*, 1976), the research on the third order nonlinearity in conjugated polymers was initially focused on the absolute magnitude of the $\chi^{(3)}$. Wide varieties of polymeric materials have been investigated and sizable $\chi^{(3)}$ has been reported not only in many π-conjugated polymers but also in some of the σ-conjugated polymers (Hesagawa *et al.*, 1992; Kepler and Soos, 1991). The frequency spectra of $\chi^{(3)}$ were measured in polyacetylene via third-harmonic-generation experiments (Kajzar *et al.*, 1987; Fann *et al.*, 1989). The experimental $\chi^{(3)}_{THG}$ spectrum by Fann *et al.* is given in Fig. 1.9. Two distinct features have been recognized from the spectrum. Considering that the optical gap of polyacetylene is 1.8 eV, the peak at 0.6 eV is apparently a three-photon resonance to the $1B_u$. The peak at about 0.9 eV, which is half of the gap energy, has been attributed to a two-photon resonance due to an A_g state since there is no observable feature at either 0.9 eV or 3×0.9 eV in the linear absorption spectrum (Suzuki *et al.*, 1980; Weinberger *et al.*, 1984).

In spite of origins of the resonances, the strikingly simple $\chi^{(3)}_{THG}$ spectrum of polyacetylene raises the questions about the possible relation between complicated electronic structure and simple mechanism for the nonlinearity. The questions to be answered are the following. If the two-photon resonance in the experimental spectrum is due to a single two-photon A_g state, what are the roles played by the

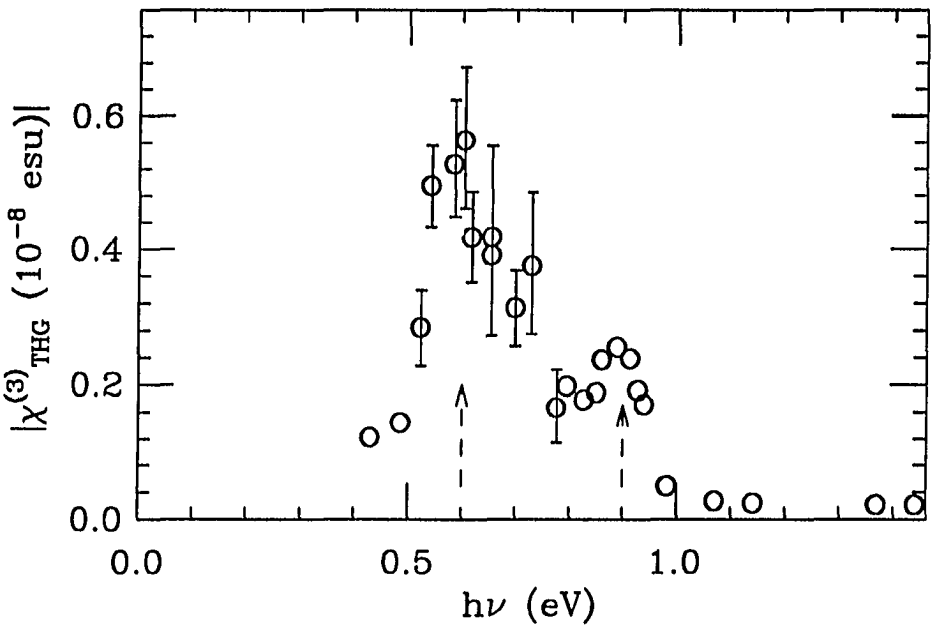

Figure 1.9: Experimental $\chi^{(3)}_{THG}$ spectrum in polyacetylene (Fann *et al.*, 1989).

rest of the two-photon states? Is the bulk of $\chi^{(3)}$ determined by *a few* states that are most relevant to the third order optical nonlinearity? What are the natures of these most important states if they do exist and why are they special? These questions will be answered in the following chapters.

1.2.3 Existing Theoretical Interpretations of the $\chi^{(3)}_{THG}$ Spectrum

Since the measurement of $\chi^{(3)}_{THG}$ frequency spectrum in polyacetylene, theoretical attention has been focused on the origin of the two-photon resonance in the spectrum, and controversies have been generated on the strength of electron-electron Coulomb interactions in polyenes and on what an appropriate theoretical model should be for conjugated polymers.

In the earlier works on electron-electron correlation in finite polyenes, it is found that the energy of the $2A_g$ is strongly affected and is lowered below that of

the $1B_u$. Due to this result, the $2A_g$ has been considered as responsible for the two-photon resonance in the $\chi^{(3)}_{THG}$ spectrum of polyacetylene (Kajzar *et al.*, 1987; Wu, 1988; Fann *et al.*, 1989; Soos and Ramasesha, 1989). However, such assignment has to place the $2A_g$ at the level of the $1B_u$ in order to explain the observed two-photon resonance at half of the gap, which is contrary to the earlier results from other experiments that predict much lower energy for the $2A_g$ in long polyenes (Hudson *et al.*, 1982; Soos and Ramasesha, 1984). Therefore, it is suggested that the the effective Coulomb interaction is weak due to inter-chain screening and one-electron theory is able to describe the nonlinear optical properties of polyenes (Kajzar *et al.*, 1987 Fann *al.*, 1989). However, numerical results within the one-electron SSH model predicts that the intensities of all the two-photon resonances vanish in the $\chi^{(3)}_{THG}$ spectrum for long chains (Yu *et al.*, 1989), implying that the one-electron theory is inappropriate.

The theoretical works within interacting-electron models found a two-photon state above and strongly coupled to the $1B_u$ (Heflin *et al.*, 1988; McWilliams *et al.*, 1991). This two-photon state is considered as the one that causes the resonance peak in the $\chi^{(3)}_{THG}$ spectrum. The numerical results within a long range interacting-electron Pariser-Parr-Pople (PPP) model[12], however, show that the energy of this two-photon state is well above the gap, which would lead to a two-photon resonance at an energy much higher than that in the experimental spectrum (McWilliams *et al.*, 1991). The explanation for the difference between the PPP and the experimental results has been that the inter-chain interactions lower the energies of two-photon states and this particular two-photon state is shifted to the level of the $1B_u$. Again, the interchain effects have to be invoked except that, in this case, the purpose is to lower the energies of the two-photon states as opposed to raising them (Kajzar *et al.*, 1987). Contrary to the results of McWilliams *et al.*, a recent study finds that the inter-chain Coulomb interactions have little effects on the energy of the high energy two-photon state and cannot lead to such a big

[12]See, for example, Pariser, 1956; Ohno, 1964.

shift (Mazumdar and F. Guo, 1992).

Based on the observation that there are only two peaks in the $\chi^{(3)}_{THG}$ spectrum of polyacetylene, a phenomenological model that includes three states — the ground state $1A_g$, the first one-photon state $1B_u$, and the first excited A_g state, the $2A_g$ that is below the $1B_u$ — has been suggested for describing nonlinear optical properties of π-conjugated polymers (Chollet *et al.*, 1989). Later works by Dixit, Guo, and Mazumdar (Dixit *et al.*, 1991) and by Hasegawa *et al.* (Hasegawa *et al.*, 1991) propose a three-level model with the two-photon state being just above the $1B_u$, which finds a two-photon resonance at about half of the optical gap. However, the three-level model predicts a rapid increase in the magnitude of $\chi^{(3)}$ as a function of chain length. Because such an increase of the nonlinearity in the three-level models is even faster than those with power law dependence in exact calculations for short chains (Heflin *et al.*, 1988; Herman and Ducuing, 1974), the calculated $\chi^{(3)}$ would exceed the observed values well before reaching the long chain limit. The saturation in the third order nonlinearity renders the three-level models at least incomplete for an accurate description of the nonlinear optical processes in π-conjugated polymers.

1.3 Addressed Issues and Organization of the Dissertation

Based on the analysis of the previous works, two issues are addressed in this dissertation. The first is about the effects of electron-electron Coulomb interactions on the electronic structures, which is directly related to the second issue on the mechanism of the nonlinearity in conjugated polymers.

Chapter 2 investigates the nonlinear optical properties within one-electron model. From investigating the nonlinear pathways leading to the $2A_g$ two-photon resonance, two-photon processes in the third order nonlinearity are understood. The conclusion on the appropriateness of one-electron models is obtained.

Chapter 3 presents a many-body theory for the optical nonlinearity in π-conjugated polymers. After the summary of a phenomenological essential states model, the rest of the chapter discusses how this model is developed. The physical meanings of the essential states and the universality of the theory are revealed via both numerical results and intuitive physical pictures. A method that combines physical considerations and numerical computations is applied to the analysis of the nonlinear optical processes for the purpose of understand infinite chain behavior from small cluster results. Based on the theory developed in this chapter, predictions are made for experimentally observable properties.

Chapter 5 compares the theoretical predictions with different experimental results in a variety of materials. Chapter 6 summarizes the dissertation and concludes according to the findings of this research.

CHAPTER 2

OPTICAL NONLINEARITY IN INDEPENDENT-ELECTRON MODELS

According to Eq. 1.7 and 1.9, the $\chi^{(3)}_{THG}$ and $\chi^{(3)}_{TPA}$ are determined by the energy structure and the dipole coupling behavior of the system under consideration. These two factors are therefore the focus of the study on the optical nonlinearities.

The energy spectrum of an infinitely long chain in a one-electron model is known to consist of a valence band and a conduction band when represented in the momentum space (see Fig. 2.10(a)), and a ground state and a continuum of states while represented in the total energy space (see Fig. 2.10(b)). The electron-hole symmetry ensures that each MO at energy $-\epsilon$ in the valence band corresponds to a MO at $+\epsilon$ in the conduction band (see Eq. 1.3), and that the dipole moment between two MOs in the valence band is equal to that between their counterparts in the conduction band. Namely, $|m_{\frac{N}{2}+i,\frac{N}{2}+j}| = |m_{\frac{N}{2}-i+1,\frac{N}{2}-j+1}|$, where $j > i$, $m_{s,t}$ is the dipole moment between the sth and the tth MOs, $E(\frac{N}{2}+i) = -E(\frac{N}{2}-i+1)$, and $E(\frac{N}{2}+j) = -E(\frac{N}{2}-j+1)$.

In linear chains, the dominant inter-band dipole couplings are between the MOs that are symmetrically placed at the two sides of the Fermi-surface, i.e. between the $(\frac{N}{2}-i+1)$th and the $(\frac{N}{2}+i)$th MOs. All the "asymmetric couplings" vanish in infinite chain limit. This can be understood by comparing with the case of ring, in which no asymmetric couplings are allowed and considering that an infinite chain is equivalent to an infinite ring. The dipole moments between

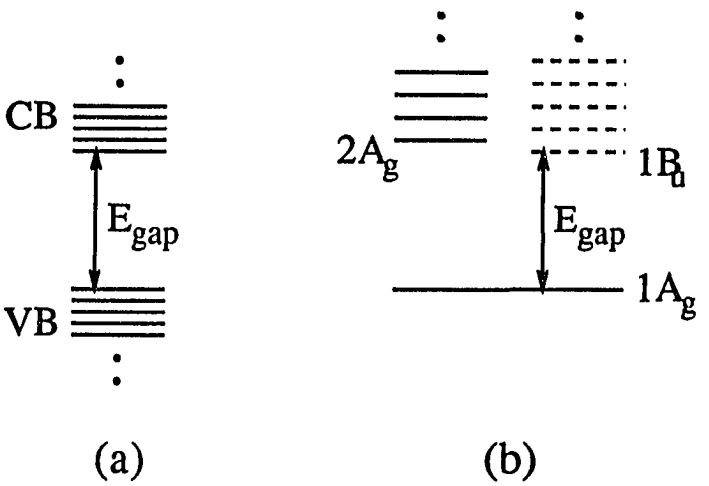

Figure 2.10: Energy spectra of one-electron models. (a) Single particle energy levels. (b) Total energy states.

symmetrically placed levels and between asymmetrically placed levels as functions of chain length are shown in Fig. 2.11. It is clearly seen that the asymmetric couplings vanish while the symmetric couplings saturate in long chain limit.

The dominant intra-band dipole couplings are between nearest neighbor MOs because the coupling strengths between nearest neighbor MOs increase much faster than those between non-nearest neighbor MOs. The numerical results of the two kinds of intra-band dipole coupling moments are depicted in Fig. 2.12. The presence of dominant dipole couplings, the symmetric inter-band and the nearest neighbor intra-band couplings, simplifies the analysis of nonlinear optical processes in linear chains and lays foundation for an essential-states description of the optical nonlinearity.

The dipole moments among the ground state $1A_g$, the B_u states that are reached from the the ground state via symmetric inter-band electron transfers (for

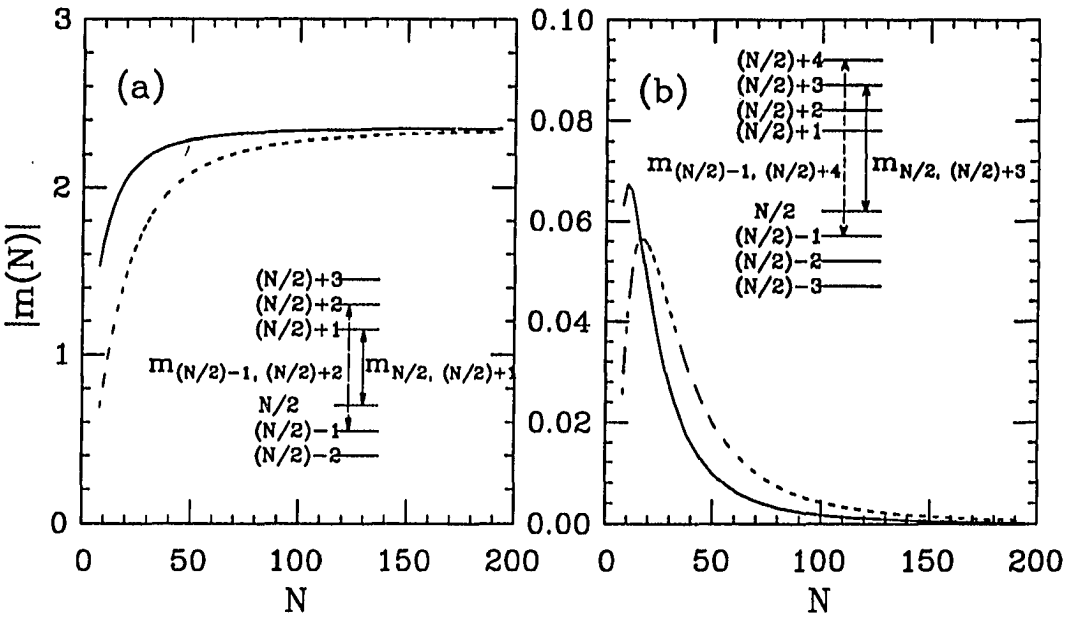

Figure 2.11: Dipole moments of symmetric and asymmetric couplings as functions of chain length N for $\delta = 0.2$. (a). Dipole moments between molecular orbitals that are symmetrically placed at the two sides of the Fermi-surface. (b) Dipole moments between molecular orbitals that are asymmetrically placed at the two sides of the Fermi-surface.

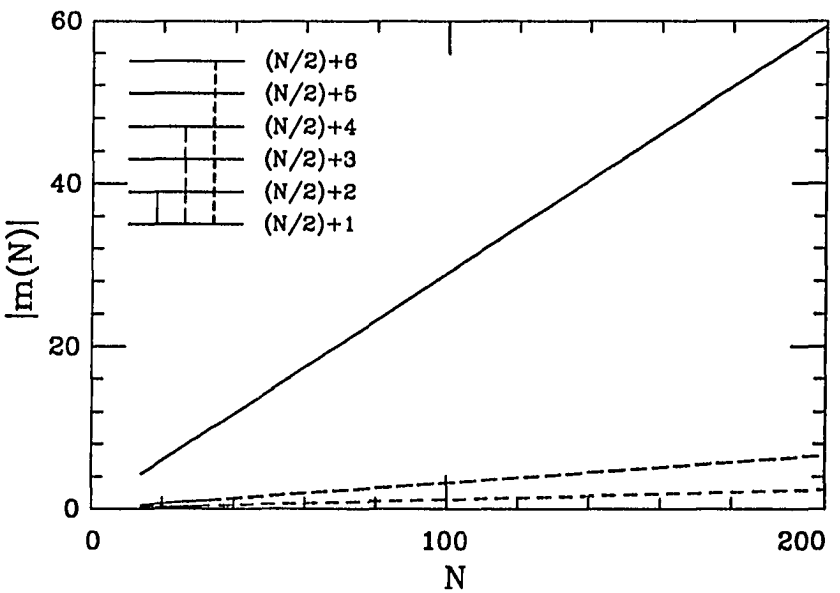

Figure 2.12: Intra-band dipole moments as functions of chain length N.

example, the $1B_u$ and the $2B_u$ in Fig. 1.6), and the A_g states that are coupled to these B_u states via nearest neighbor intra-band electron transfer (for example, the $2A_g$ in Fig. 1.6) have unique and significant properties, which leads to the absence of two-photon resonances in the $\chi^{(3)}_{THG}$ and $\chi^{(3)}_{TPA}$ spectra.

In order to demonstrate the special behavior of the dipole couplings, the following notations are used to representing these states.

Since the ground state corresponds to the MOs in the valence band being doubly occupied and those in the conduction band being empty, it can be written as

$$|1A_g\rangle = \frac{1}{\sqrt{N!}}\hat{P}\Pi_{k<k_F} a^+_{k,\uparrow} a^+_{k,\downarrow}|0\rangle \ , \tag{2.12}$$

where the operator $a^+_{k,\sigma} = \frac{1}{\sqrt{N}}\sum_n c^+_{n,\sigma} e^{ikn}$ creates an electron at the MO with momentum k and spin σ, $|0\rangle$ is the vacuum state, and the permutation operator $\hat{P}$ gives rise to $N!$ terms of the operator products and insures the exchange symmetry of the wave function.

The B_u state, denoted as l_1B_u, that is coupled to the ground state via a symmetric inter-band electron transfer can be expressed as

$$|l_1B_u\rangle = \frac{1}{\sqrt{2}}\sum_\sigma a^+_{u,\sigma} a_{v,\sigma}|1A_g\rangle \ , \tag{2.13}$$

where the vth MO is in the valence band with an energy E_v and the uth MO is in the conduction band with an energy E_u, and $0 < E_u = -E_v$.

The A_g state, denoted as kA_g, that is coupled to the l_1B_u via an nearest neighbor intra-band electron transfer and is above the l_1B_u is written as

$$|kA_g\rangle = \frac{1}{2}[\sum_\sigma a^+_{u+1,\sigma} a_{v,\sigma} - \sum_\sigma a^+_{u,\sigma} a_{v-1,\sigma}]|1A_g\rangle \ . \tag{2.14}$$

The B_u state, denoted as l_2B_u, that is coupled to the kA_g via a nearest neighbor intra-band electron transfer and is above the kA_g is written as

$$|l_2B_u\rangle = \frac{1}{\sqrt{2}}\sum_\sigma a^+_{u+1,\sigma} a_{v-1,\sigma}|1A_g\rangle \tag{2.15}$$

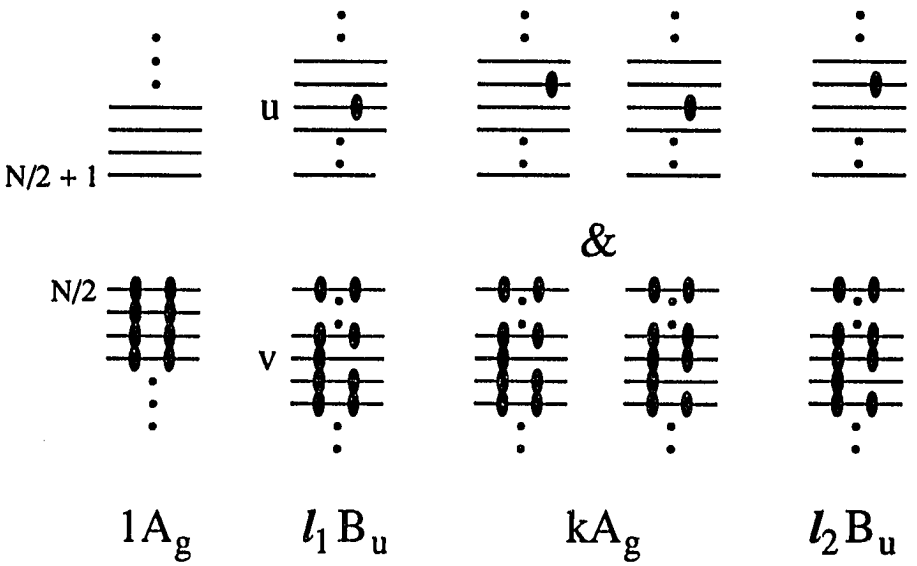

Figure 2.13: The states $1A_g$, l_1B_u, kA_g, and l_2B_u and the corresponding MO occupancies.

The MO occupancies of the state l_1B_u, kA_g, and l_2B_u are schematically shown in Fig. 2.13 and their special cases with $v = N/2$, $u = \frac{N}{2} + 1$ have been given in Fig. 1.6, in which they correspond to the $1B_u$, the $2A_g$, and the $2B_u$.

From the above, it is shown that only the two-photon processes that involve the $1A_g$, the l_1B_u, the kA_g, and the l_2B_u are important because of the dominant dipole couplings among them. The intensity of the two-photon resonance due to a kA_g vanishes in long chain as a result of cancellation among nonlinear pathways, which is discusses in the next section. In the following, I discuss the origin of the cancellation in the kA_g two-photon resonance, the signs of the dipole products involving the l_1B_u and the l_2B_u states.

The dipole operator, when represented in the molecular orbital representation, is written as

$$\mu = \frac{1}{\sqrt{2}} \sum_{\sigma} \sum_{i<j} m_{i,j} (a^{+}_{i,\sigma} a_{j,\sigma} + a^{+}_{j,\sigma} a_{i,\sigma}) \ . \tag{2.16}$$

where m_{ij} is chosen to be positive without lossing generality. For the nearest neighbor intra-band dipole couplings, one can write the dipole operator as

$$\mu_{intra} = \frac{1}{\sqrt{2}} \sum_{\sigma} \sum_{i \neq \frac{N}{2}} m_{i,i+1} (a^{+}_{i,\sigma} a_{i+1,\sigma} + a^{+}_{i+1,\sigma} a_{i,\sigma}) \ , \tag{2.17}$$

and for the inter-band couplings, one has

$$\mu_{inter} = \frac{1}{\sqrt{2}} \sum_{\sigma} \sum_{v',u'} m_{v',u'} (a^{+}_{v',\sigma} a_{u',\sigma} + a^{+}_{u',\sigma} a_{v',\sigma}) \ , \tag{2.18}$$

where $v'(\leq N/2)$ and $u'(\geq \frac{N}{2}+1)$ are the quantum numbers of the MOs in the valence and the conduction bands respectively.

The dipole moments among the $1A_g$, l_1B_u, kA_g and l_2B_u can be found by operating the dipole operator on these states. For the inter-band dipole coupling moments, $\langle 1A_g|\mu|l_1B_u\rangle$ and $\langle 1A_g|\mu|l_2B_u\rangle$ are found from

$$\begin{aligned} \mu_{inter}|l_1B_u\rangle &= \frac{1}{\sqrt{2}} \sum_{\sigma} \sum_{v',u'} m_{v',u'} (a^{+}_{v',\sigma} a_{u',\sigma} + a^{+}_{u',\sigma} a_{v',\sigma}) \frac{1}{\sqrt{2}} \sum_{\sigma} a^{+}_{u,\sigma} a_{v,\sigma} |1A_g\rangle \\ &= \frac{1}{2} m_{v,u} \sum_{\sigma} a^{+}_{v,\sigma} a_{v,\sigma} |1A_g\rangle + \ldots \\ &= m_{v,u} |1A_g\rangle + \ldots \quad , \end{aligned} \tag{2.19}$$

and,

$$\mu_{inter}|l_2B_u\rangle = m_{v-1,u+1}|1A_g\rangle + \ldots \ , \tag{2.20}$$

where, as mentioned above, the vth and the uth MOs are, respectively, in the valence and the conduction bands, and $E_v = -E_u$. In the infinite chain limit, the gaps between the nearest neighbor MOs vanish and $m_{v,u} = m_{v-1,u+1}$, and, therefore, $\langle 1A_g|\mu|l_1B_u\rangle = \langle 1A_g|\mu|l_2B_u\rangle$ (see, for example, Fig. 2.11(a)).

For intra-band dipole coupling moments, $\langle kA_g|\mu|l_1B_u\rangle$ and $\langle kA_g|\mu|l_2B_u\rangle$ are found from

$$\mu_{intra}|l_1B_u\rangle = \frac{1}{\sqrt{2}}\sum_{\sigma}\sum_{i\neq\frac{N}{2}} m_{i,i+1}(a^{+}_{i,\sigma}a_{i+1,\sigma} + a^{+}_{i+1,\sigma}a_{i,\sigma})\ \frac{1}{\sqrt{2}}\sum_{\sigma} a^{+}_{u,\sigma}a_{v,\sigma}|1A_g\rangle$$

$$= \frac{1}{2}(m_{u,u+1}\sum_{\sigma} a^{+}_{u+1,\sigma}a_{v,\sigma} - m_{v-1,v}\sum_{\sigma} a^{+}_{u,\sigma}a_{v-1,\sigma})|1A_g\rangle$$

$$+ \frac{1}{2}m_{u-1,u}\sum_{\sigma} a^{+}_{u-1,\sigma}a_{v,\sigma}|1A_g\rangle - \frac{1}{2}m_{v,v+1}\sum_{\sigma} a^{+}_{u,\sigma}a_{v+1,\sigma}|1A_g\rangle\ , \qquad (2.21)$$

and

$$\mu_{intra}|l_2B_u\rangle = \frac{1}{\sqrt{2}}\sum_{\sigma}\sum_{i\neq\frac{N}{2}} m_{i,i+1}(a^{+}_{i,\sigma}a_{i+1,\sigma} + a^{+}_{i+1,\sigma}a_{i,\sigma})\ \frac{1}{\sqrt{2}}\sum_{\sigma} a^{+}_{u+1,\sigma}a_{v-1,\sigma}|1A_g\rangle$$

$$= -\frac{1}{2}(m_{v-1,v}\sum_{\sigma} a^{+}_{u+1,\sigma}a_{v,\sigma} - m_{u,u+1}\sum_{\sigma} a^{+}_{u,\sigma}a_{v-1,\sigma})|1A_g\rangle$$

$$+ \frac{1}{2}m_{u+1,u+2}\sum_{\sigma} a^{+}_{u+2,\sigma}a_{v-1,\sigma}|1A_g\rangle - \frac{1}{2}m_{v-2,v-1}\sum_{\sigma} a^{+}_{u+1,\sigma}a_{v-2,\sigma}|1A_g\rangle\ . \qquad (2.22)$$

As a result of the electron-hole symmetry, $m_{v-1,v} = m_{u,u+1}$, Eq. 2.21 and 2.22 become

$$\mu_{intra}|l_1B_u\rangle = m_{v-1,v}\frac{1}{2}\sum_{\sigma}(a^{+}_{u+1,\sigma}a_{v,\sigma} - a^{+}_{u,\sigma}a_{v-1,\sigma})|1A_g\rangle + ...$$

$$= m_{v-1,v}|kA_g\rangle\ +\ ...\ , \qquad (2.23)$$

and

$$\mu_{intra}|l_2B_u\rangle = -m_{v-1,v}\frac{1}{2}\sum_{\sigma}(a^{+}_{u+1,\sigma}a_{v,\sigma} - a^{+}_{u,\sigma}a_{v-1,\sigma})|1A_g\rangle + ...$$

$$= -m_{v-1,v}|kA_g\rangle\ +\ ...\ . \qquad (2.24)$$

Therefore,

$$\langle kA_g|\mu|l_1B_u\rangle = -\langle kA_g|\mu|l_2B_u\rangle\ = m_{v-1,v}. \qquad (2.25)$$

and, as $N \rightarrow \infty$,

$$\langle 1A_g|\mu|l_1B_u\rangle\langle kA_g|\mu|l_1B_u\rangle = -\langle 1A_g|\mu|l_2B_u\rangle\langle kA_g|\mu|l_2B_u\rangle\ . \qquad (2.26)$$

Note that although Eq. 2.25 is obtained by chosing the phases of the wave functions such that $m_{ij} > 0$ and hence $\langle 1A_g|\mu|l_1B_u\rangle$ and $\langle 1A_g|\mu|l_2B_u\rangle$ have the same sign, Eq. 2.26 is valid in general. The use of proper phases is to simplify the demonstration of the general property of Eq. 2.26.

An example of Eq. 2.26 is for $v = N/2$, $u = \frac{N}{2} + 1$. In this case, the l_1B_u is the $1B_u$, the kA_g is the $2A_g$, and the l_2B_u is the $2B_u$, and

$$\langle 1A_g|\mu|1B_u\rangle\langle 1B_u|\mu|2A_g\rangle = -\langle 1A_g|\mu|2B_u\rangle\langle 2B_u|\mu|2A_g\rangle \qquad (2.27)$$

Eq. 2.26 has significant effect on the two-photon process involving a kA_g and on the optical nonlinearities of non-interacting one-dimensional chains. This is discussed next.

2.1 Nonlinear Pathways and Intensities of Two-Photon Resonances

Although the $2A_g$ is expected to become degenerate with the $1B_u$ in an infinitely long chain, which leads to a two-photon resonance at half of the gap energy, the intensity of the $2A_g$ two-photon resonance may not be strong enough to be observable in the $\chi^{(3)}$ spectra. According to the discussion in the last section, for the two-photon states that involve only one-electron excitations the corresponding intensities of two-photon resonances in the $\chi^{(3)}$ spectrum can be figured out from the analysis of the nonlinear pathways without actually calculating the $\chi^{(3)}$ itself. Here the $2A_g$ is used as an example.

From the expression of $\chi^{(3)}$, the nonlinear pathways that lead to the $2A_g$ two-photon resonance are the following two kinds.

I. The "direct" paths:

$$1A_g \rightarrow jB_u \rightarrow 2A_g \rightarrow jB_u \rightarrow 1A_g \quad j = 1,\ 2\ . \qquad (2.28)$$

Their resonant contributions to $\chi^{(3)}_{THG}$ and $\chi^{(3)}_{TPA}$ are, respectively,

$$T^{THG}_{jj} = \frac{\langle 1A_g|\mu|jB_u\rangle^2\langle 2A_g|\mu|jB_u\rangle^2}{(\omega_{jB_u} - 3\omega)(\omega_{2A_g} - 2\omega)(\omega_{jB_u} - \omega)} , \tag{2.29}$$

and

$$T^{TPA}_{jj} = \frac{\langle 1A_g|\mu|jB_u\rangle^2\langle 2A_g|\mu|jB_u\rangle^2}{(\omega_{jB_u} - \omega)(\omega_{2A_g} - 2\omega)(\omega_{jB_u} - \omega)} . \tag{2.30}$$

II. The "cross" paths:

$$1A_g \rightarrow iB_u \rightarrow 2A_g \rightarrow jB_u \rightarrow 1A_g \quad i,\ j = 1,\ 2;\ i \neq j , \tag{2.31}$$

and their resonant contributions to the $\chi^{(3)}_{THG}$ and $\chi^{(3)}_{TPA}$ are, respectively,

$$T^{THG}_{ij} = \frac{\langle 1A_g|\mu|iB_u\rangle\langle iB_u|\mu|2A_g\rangle\langle 2A_g|\mu|jB_u\rangle\langle jB_u|\mu|1A_g\rangle}{(\omega_{iB_u} - 3\omega)(\omega_{2A_g} - 2\omega)(\omega_{jB_u} - \omega)} , \tag{2.32}$$

and

$$T^{TPA}_{ij} = \frac{\langle 1A_g|\mu|iB_u\rangle\langle iB_u|\mu|2A_g\rangle\langle 2A_g|\mu|jB_u\rangle\langle jB_u|\mu|1A_g\rangle}{(\omega_{iB_u} - \omega)(\omega_{2A_g} - 2\omega)(\omega_{jB_u} - \omega)} . \tag{2.33}$$

For nonresonant contributions, there exist the same two kinds of paths.

In the limit $N \rightarrow \infty$, a consequence of $\langle 1A_g|\mu|1B_u\rangle\langle 1B_u|\mu|2A_g\rangle =$ $-\langle 1A_g|\mu|2B_u\rangle\langle 2B_u|\mu|2A_g\rangle$ (Eq. 2.27) and $E(1B_u) = E(2B_u)$ is that the two kinds of $\chi^{(3)}$ contributions cancel exactly at all the frequencies since $T_{jj} = -T_{ij}$ ($i,\ j = 1,\ 2$). Therefore, the intensity of the $2A_g$ two-photon resonance is expected to vanish in long chains. Similarly, the intensities of the two-photon resonances due to other kA_g states also vanish for $N \rightarrow \infty$, and, therefore, there is not a single observable two-photon resonance in the $\chi^{(3)}$ spectra within one-electron models.

The calculated $\chi^{(3)}_{THG}$ spectra for $N = 20,\ 60,\ 80,\ 120$ are plotted in Fig. 2.14. As the chain length increases, the intensities of the two-photon resonances (for example, the $2A_g$, whose location is marked by "V" in the figure) decrease. For $N = 120$, there is no two-photon resonance peak in the spectrum, which is expected from the above argument.

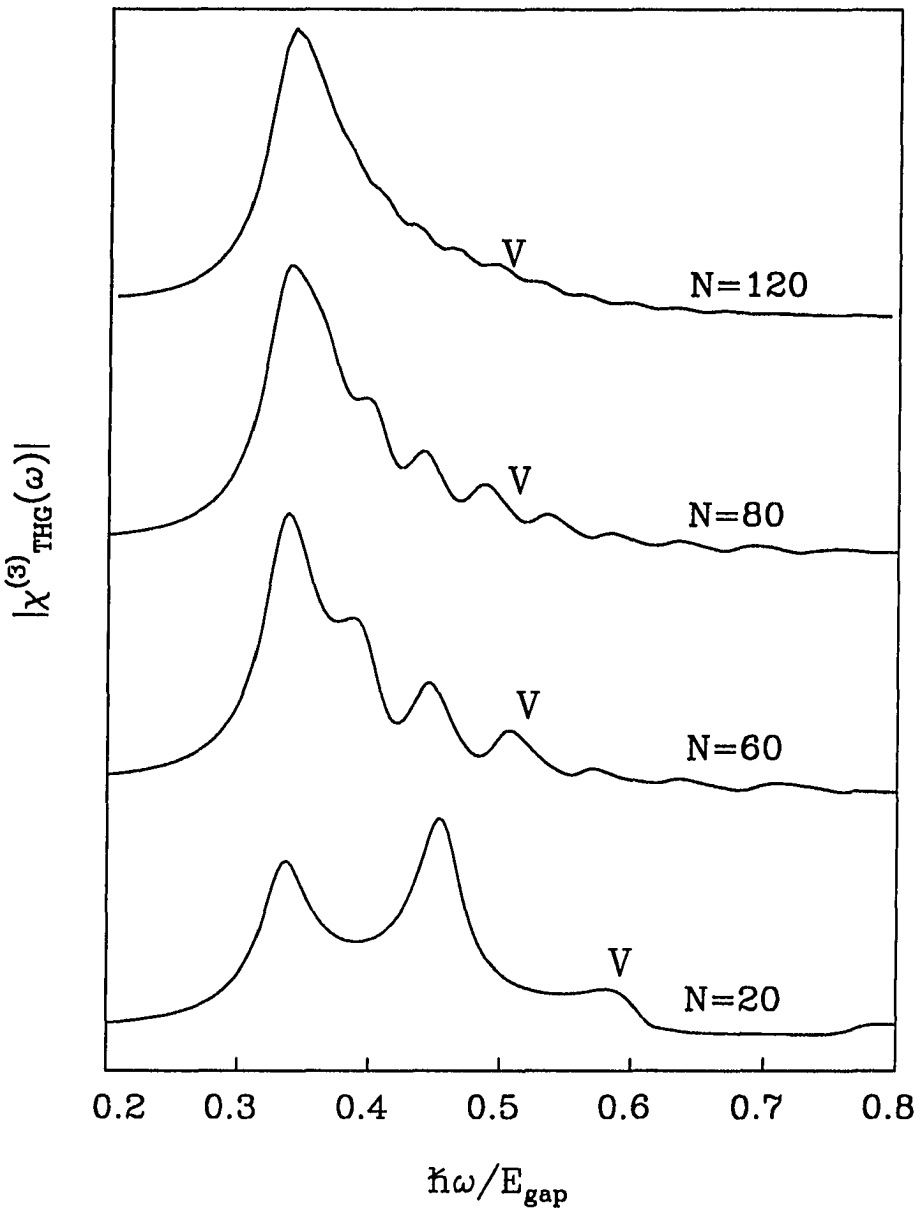

Figure 2.14: The calculated $\chi^{(3)}_{THG}$ spectrum in a one-electron model (Hückel model) for $N = 120$, $\delta = 0.2$, $\Gamma = 0.05E(1B_u)$. The location of the $2A_g$ is marked with V.

2.2 Conclusions on One-Electron Models

In this chapter, it is found that within one-electron theory, the intensities of two-photon resonances in the $\chi^{(3)}$ spectra are diminished due to the cancellation between two kinds of nonlinear pathways. In the long chain limit the cancellations are exact as a result of degeneracy between the two B_u states that are strongly intra-band coupled to the two-photon states, and the intensities vanish completely. It is shown that understanding the intensity of the two-photon resonance is important to understanding the mechanism of nonlinearity.

The prediction from independent-electron models does not agree with what has been observed experimentally, indicating that the single particle picture is not appropriate to describing nonlinear optical properties of conjugated polymers. The presence of a two-photon resonance in experimental $\chi^{(3)}$ spectra is a signature of pronounced electron-electron Coulomb interactions in real materials.

CHAPTER 3

OPTICAL NONLINEARITY IN INTERACTING-ELECTRON MODELS

As shown in Chapter 1, one-electron theory is not appropriate for studying many of the properties of conjugated polymers, and the Hubbard model has been successfully applied to study many-body effects on these properties. Therefore Hubbard-type models capture the essence of electron Coulomb correlations in these low-dimensional systems. This research on the optical nonlinearity of π-conjugated polymers is carried out within the extended Hubbard model.

The Hamiltonian of the extended Hubbard model for a dimerized rigid lattice is written as

$$H_{ext.-Hubbard} = -t\sum_{i,\sigma}[1-(-1)^i\delta](c^+_{i,\sigma}c_{i+1,\sigma} + c^+_{i+1,\sigma}c_{i,\sigma}) + U\sum_i n_{i,\uparrow}n_{i,\downarrow}$$
$$+ V\sum_i (n_i - 1)(n_{i+1} - 1) \qquad (3.34)$$

where $n_i = \sum_\sigma n_{i,\sigma}$, V is the nearest neighbor Coulomb repulsion parameter, and $\delta \equiv \alpha/t$ is the bond alternation parameter.

In the extended Hubbard model the nearest neighbor electron-electron Coulomb interactions is added to the simple Hubbard Hamiltonian. The introduction of nonzero V leads to only quantitative differences in the properties involving low energy states from those of simple Hubbard model[1], while it can cause qualitative changes in the nonlinear optical properties involving higher energy states, which will be shown in the rest of the chapter.

[1]See, for example, Mazumdar and Dixit, 1984.

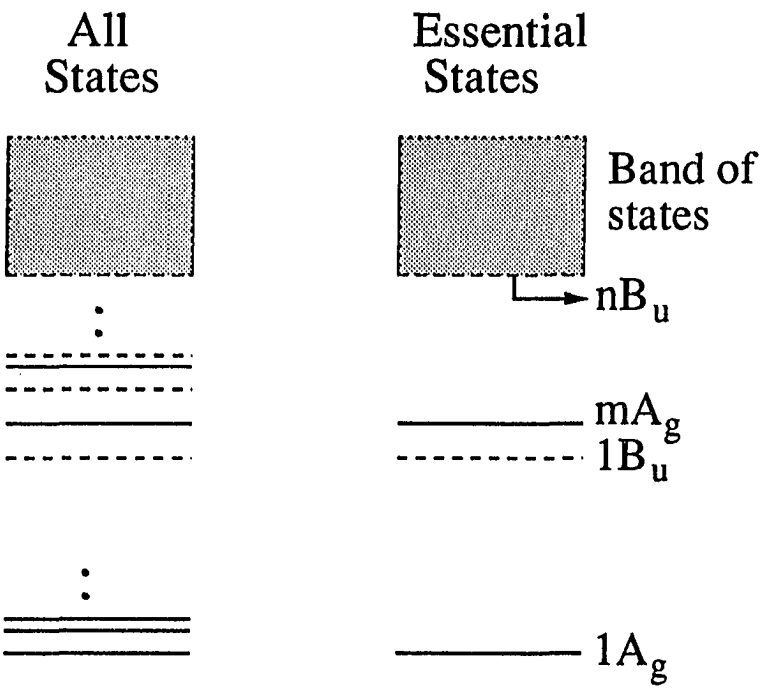

Figure 3.15: The four essential states versus all the states.

3.1 A Summary on Essential States Mechanism

The essential states mechanism for the third order optical nonlinearity of π-conjugated polymers (Guo *et al.*, 1992b, 1992c, 1992d, 1992e) is summarized as follows. In spite of great numbers of states involved, the bulk of the third order nonlinearity $\chi^{(3)}$ is determined by four essential states. The four essential states are the ground state, the first odd-parity exciton state ($1B_u$), the first even-parity exciton state (denoted as mA_g), and the conduction band threshold (denoted as nB_u). The quantum numbers m and n are parameter dependent, but the characteristics of the mA_g and the nB_u are parameter independent. The four essential states are shown schematically in Fig. 3.15. The essential two-photon

state mA_g is located above and nearly degenerate with the $1B_u$ in the long chain limit. The subgap $2A_g$ and other subgap A_g states are irrelevant to the nonlinearity.

The essentiality of the states in the phenomenological four-level model stems from the strong and dominant dipole couplings among them. Such couplings are unique to the essential states since the couplings among the rest of states are much weaker. A physical picture for qualitatively describing the coupling behavior, the natures of the four essential states, and the charge transfer processes in the transitions from one essential state to another is shown in Fig. 3.16 for strong Coulomb interaction limit. The quantitative numerical results are given in the next section.

Fig. 3.16 can be understood along the line drawn as follows.

(1) For each state shown in the figure only two or three dominant configuration diagrams are given, and for each diagram only six sites are plotted. The weights of the diagrams in a state are not the same and are not given in the figure.

(2) Each diagram in a state represents the whole class of diagrams that can be obtained from the symmetry operations on it. The linear combination of the same class of diagrams is symmetric for an A_g state while antisymmetric for a B_u state with respect to the mirror plane passing through the center of the chain. For example, the $1B_u$ and the mA_g have the same but the different combinations of dominant diagrams.

(3) The dipole moment between two states is proportional to the overlaps between diagrams in the states. An overlap is maximized if the two diagrams are the same. From the figure, it is apparent that the largest dipole moment is between the $1B_u$ and the mA_g since the two states have the same dominant diagrams, while the dipole moment between the $1B_u$ and the $2A_g$ or between the $1B_u$ and a bi-exciton A_g state is much smaller due to much less overlaps.

(4) The natures of the essential excited states are determined by the nature of

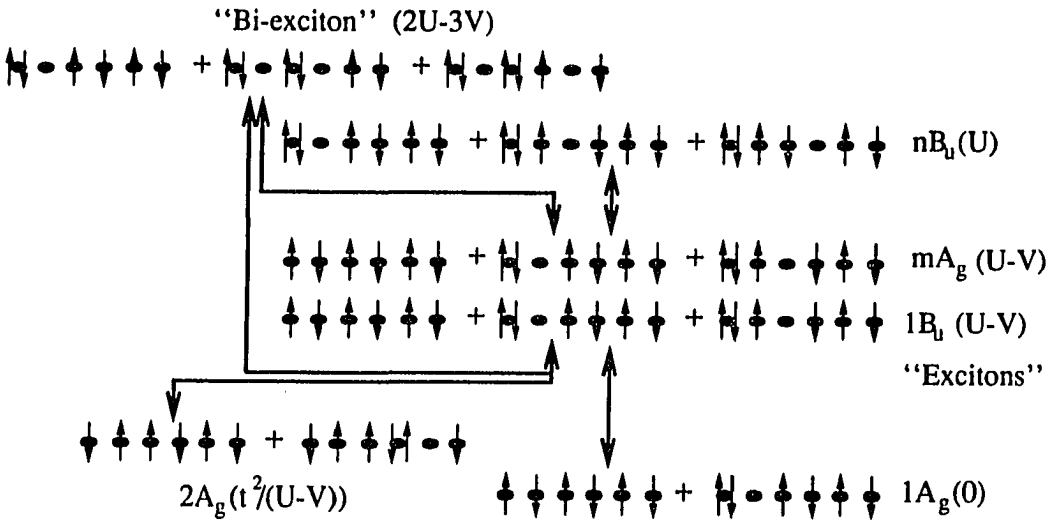

Figure 3.16: The dominant real-space-configuration diagrams of the essential states, the $2A_g$, and the bi-exciton state. A charge transfer from one diagram to another, which corresponds to an inter-band transition, is pointed out by a pair of arrows that connect the two diagrams. The quantities in the parentheses are the energies (in the units of t) of the corresponding states in the strong correlation limit with $U >> V >> t$. See text for detailed explanations.

the ground state. In the strong correlation limit, the ground state is dominantly covalent. The lowest energy optical transition or a charge transfer from the mostly covalent ground state leads to the mostly excitonic (one double occupancy) $1B_u$ state at an energy $U - V$ with respect to the ground state. Besides going back to the ground state, the further charge transfer from the $1B_u$ can end up at either the covalent $2A_g$ at $\sim t^2/(U - V)$ or the bi-exciton state at $\sim 2U - 3V$. However, the dipole coupling between the $1B_u$ and the $2A_g$ or the bi-exciton A_g state is very weak and these two states are, therefore, not important to nonlinear optical properties. The intra-band transition from the $1B_u$ to the excitonic mA_g state costs little energy, and the $1B_u$ and the mA_g are strongly coupled. From the mA_g, a charge transfer leads either to the conduction band threshold nB_u with the doubly occupied and the empty sites being separated or to a bi-exciton (coupled two excitons) B_u state. The dipole moment between the mA_g and the nB_u is larger than that between the mA_g and the bi-exciton B_u state, which can be seen from the number of same dominant diagrams in these states.

From the above, it is evident that for a system with covalent ground state and $V \neq 0$, the essential excited states have to be the first excitonic B_u state, the first excitonic A_g state, and the conduction band threshold. Other states are not as important as the essential states because of either their weak dipole couplings with the essential states or the cancellation in their $\chi^{(3)}$ contributions, which is quantitatively discussed next.

3.1.1 Numerical Results about the Essential States

The numerical results that show the uniqueness and the characteristics of the essential states are demonstrated in this section. The computations have been done for hundreds of parameter sets that cover wide range of parameter space. The data given here are the representatives of the numerical results.

The mA_g and the nB_u are Unique

For any nonlinear optical process in which the initial state is the ground state, the most important states are the $1A_g$ and the $1B_u$ since the dipole moment $|\langle 1A_g|\mu|1B_u\rangle|$ is the largest inter-band coupling moment. The essential two-photon A_g state, therefore, is necessarily the one that has the largest dipole monent with the $1B_u$.

It has been mentioned above that the mA_g is the unique two-photon state that most strongly coupled to the $1B_u$. In Fig. 3.17 the dipole moments between the $1B_u$ and A_g states are given for $N = 8$ chains. For all the parameters, there is only *one* excited A_g state that has large dipole moment with the $1B_u$. This A_g state — the mA_g — is always above the $1B_u$ and is expected to become nearly degenerate with the $1B_u$ in long chain limit for weak bond alternation, which leads to a two-photon resonance at about half of the gap energy ($E(1B_u)/2$).

Having found the essential two-photon state, the mA_g, the criterion for an essential B_u state besides the $1B_u$ is a large dipole moment with the mA_g. The dipole moments between the mA_g and several B_u states are shown in Fig. 3.18 for $N = 8$. From the data it is clear that, besides the $1B_u$, there is only one B_u state — the nB_u — that is strongly coupled to the mA_g. The larger the Coulomb parameters, the more unique the nB_u is.

The Natures of the Essential States

From examining dipole moments, the four essential states can be recognized. However, the physical characteristics of these states in infinitely long chains are far more difficult to determine from numerical results of small clusters. The major problems in short chain calculations originate from the discreteness of the energy spectrum and hence the overlaps between energy bands (here "band" implies collection of states of similar properties), which results in character mixing of states and creates great obstacles for distinguishing one state from another.

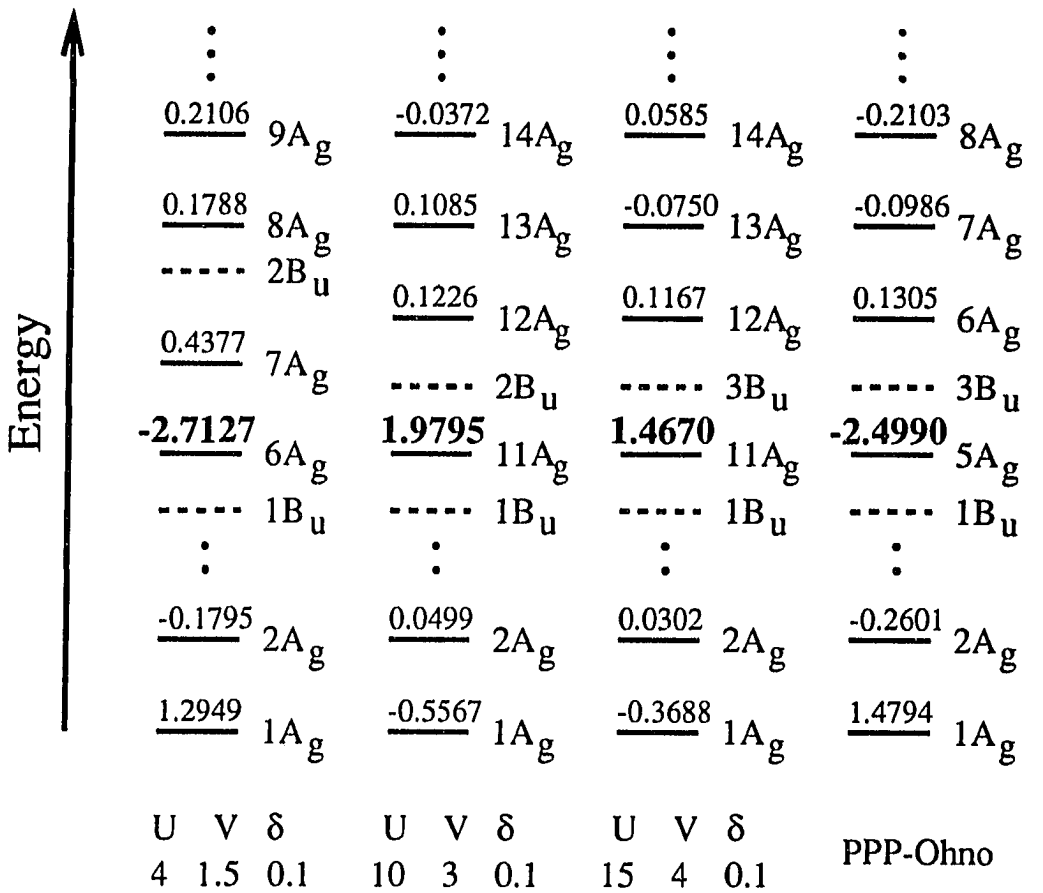

Figure 3.17: Dipole moments between the $1B_u$ and A_g states for various of parameters. Here U and V are in the units of t and t is set to be 1. The solid lines represent the A_g states and the dashed lines represent the B_u states. The numbers against the solid lines are the dipole moments between the corresponding A_g state and the $1B_u$. The A_g states not shown have very small dipole moments with the $1B_u$. The levels are plotted not in the real scale of energy The last set of results is obtained from the PPP model whose Hamiltonian is that of the simple Hubbard model plus a long range Coulomb potential term $\sum_{i<j} V_{ij}(n_i - 1)(n_j - 1)$, and $V_{ij} = \frac{U}{[1+0.6117|i-j|^2]^{1/2}}$ for the Ohno variant (Ohno, 1964).

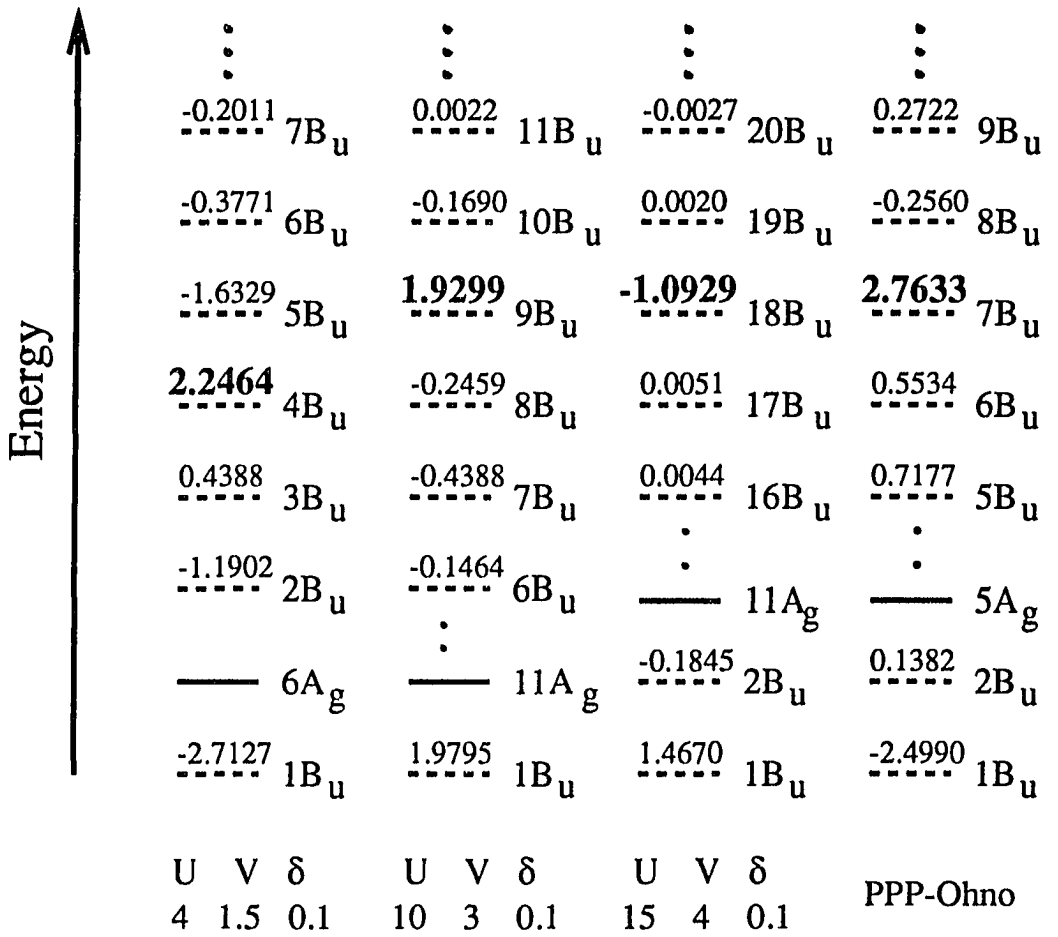

Figure 3.18: Dipole moments between the mA_g and the B_g states for various of parameters ($t = 1$). The solid lines represent the A_g states and the dashed lines represent the B_u states. The numbers against the dashed lines are the dipole moments between the corresponding B_u state and the mA_g. The B_u states not shown have very small dipole moments with the mA_g. The levels are plotted not in the real scale of energy.

The technique used to overcome the finite size effects in short chain calculations (Guo*et al.*, 1992e) is the following. First, the computations are carried out in the strong correlation limit, in which the energy bands are well separated and the natures of states are recognizable. The properties such as intra-band couplings and the density-density correlations are understood for the essential states in this limit. Second, the computations are extended to moderate Coulomb parameter regime, in which partial overlaps occur. The intra-band couplings and correlation functions are examined and the behavior of essential states that are recognized from the dipole moments between them are compared with those in the large parameter limit. If the same behavior is found for the two kinds of parameter choices, the natures of the essential states determined in strong correlation limit are proved to be valid in a moderate parameter region, and a universality is shown to exist.

Strong Correlation Limit

The energy spectrum for $N = 8$, $U = 50$, $V = 15$, $\delta = 0.1$ is depicted in Fig. 3.19. The energy bands are centered at about 0, $U - V$, U, etc.. The four essential states in this case are the $1A_g$, the $1B_u$, the $11A_g$, and the $20B_u$. From the spectrum, the four states are recognized as the covalent ground state, the first exciton B_u state at an energy $\sim U - V$ above the ground state, the first exciton A_g state also at $\sim U - V$, and the conduction band threshold at $\sim U$.

The dipole moments between A_g and B_u states for the same set of parameters are plotted in Fig. 3.20. The onset of strong intra-band couplings, characteristic of a band with closely spaced states, is at the $20B_u$, indicating that the $20B_u$ is the conduction band threshold.

A more quantitative way to determine the characteristics of states is to study the density-density correlations, which are defined as the expectation values

$$g_0 \equiv \frac{1}{N}\langle | \sum_{i=1}^{N-1} n_{i,\uparrow} n_{i,\downarrow} | \rangle \tag{3.35}$$

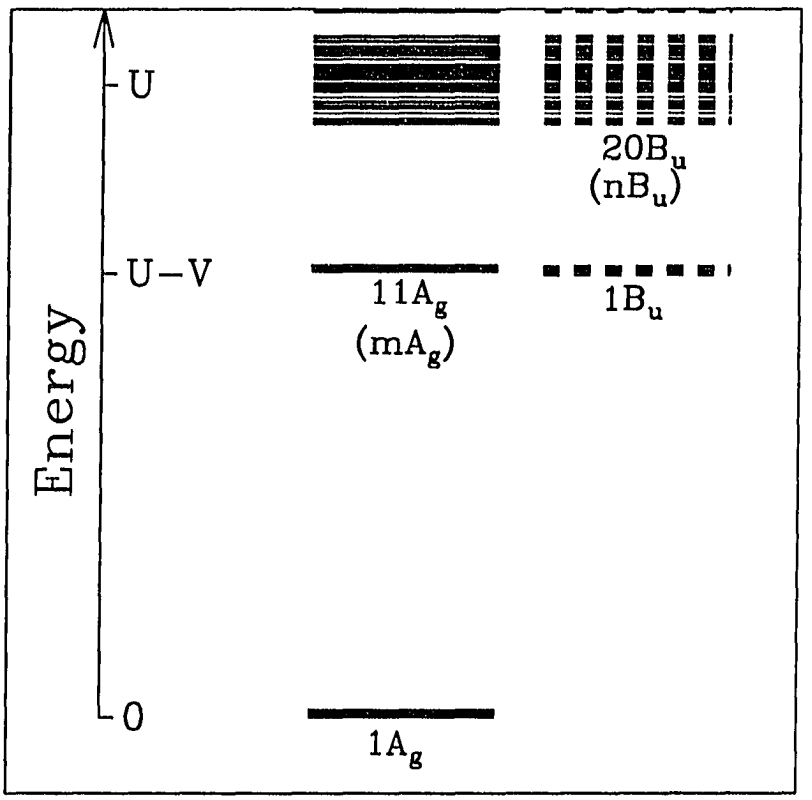

Figure 3.19: The energy spectrum for $N = 8$, $U = 50$, $V = 15$, $\delta = 0.1$.

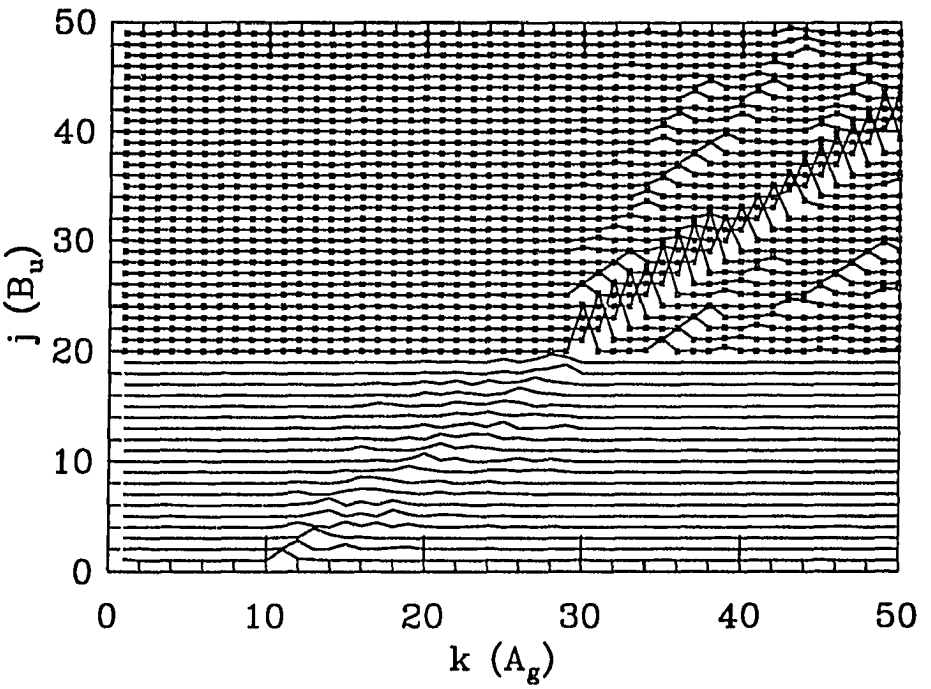

Figure 3.20: The dipole moments between the first 50 A_g and first 50 B_u states for $N = 8$, $U = 50$, $V = 15$, $\delta = 0.1$. Each curve $d_j(k) \equiv |\langle jB_u|\mu|kA_g\rangle|$ in the figure is a function of k. The dotted curves are for the conduction band B_u states.

and

$$g_l \equiv \frac{1}{N}\langle|\sum_{i=1}^{N-l}(n_i-1)(n_{i+l}-1)|\rangle, \quad l=1,2,...,N-1\ , \tag{3.36}$$

where l is the distance between two sites.

For the purpose of understanding the relation between the values of correlation functions and the property of a state, valence bond (VB) diagrams are used to describe the real space configurations of states. A more detailed description of the VB theory is given in Appendix A. The construction of the VB diagrams is summarized as follows. If one denotes the up-spin and down-spin by α and β respectively, a site doubly occupied with two electrons of opposite spins by a cross ($\times$), an empty site by a dot ($\cdot$), and a pair of singlet-coupled singly occupied sites by a line or "bond" joining them, then, using the creation operators c^+s, one has

$$\underset{site\ \ i\ \ j}{|\text{—}\rangle} \equiv \tfrac{1}{\sqrt{2}}(c^+_{i,\alpha}c^+_{j,\beta}-c^+_{i,\beta}c^+_{j,\alpha})|0\rangle\ , \tag{3.37}$$

$$\underset{site\ \ i\ \ j}{|\times\ \cdot\rangle} \equiv c^+_{i,\alpha}c^+_{i,\beta}|0\rangle\ , \tag{3.38}$$

where only two sites (i, j) are shown. All the other VB diagrams can be generated from these. For example, for a chain of 4 sites,

$$\underset{site\ \ 1\ 2\ 3\ 4}{|\ \overset{\frown}{\times\ \cdot}\ \rangle} \equiv \tfrac{1}{\sqrt{2}}c^+_{2,\alpha}c^+_{2,\beta}(c^+_{1,\alpha}c^+_{4,\beta}-c^+_{1,\beta}c^+_{4,\alpha})|0\rangle\ . \tag{3.39}$$

The VB representations of the A_g and the B_u states for an $N=4$ chain are illustrated in Fig. 3.21.

The criteria for a state to be covalent, excitonic, conducting, and biexcitonic are as follows.

(1) Covalent states :

$$g_0 \sim 0, \quad g_l \sim 0\ for\ l>0, \tag{3.40}$$

since there is no double occupancies in a covalent configuration diagram (see $|1+\rangle$ and $|2+\rangle$ in Fig. 3.21).

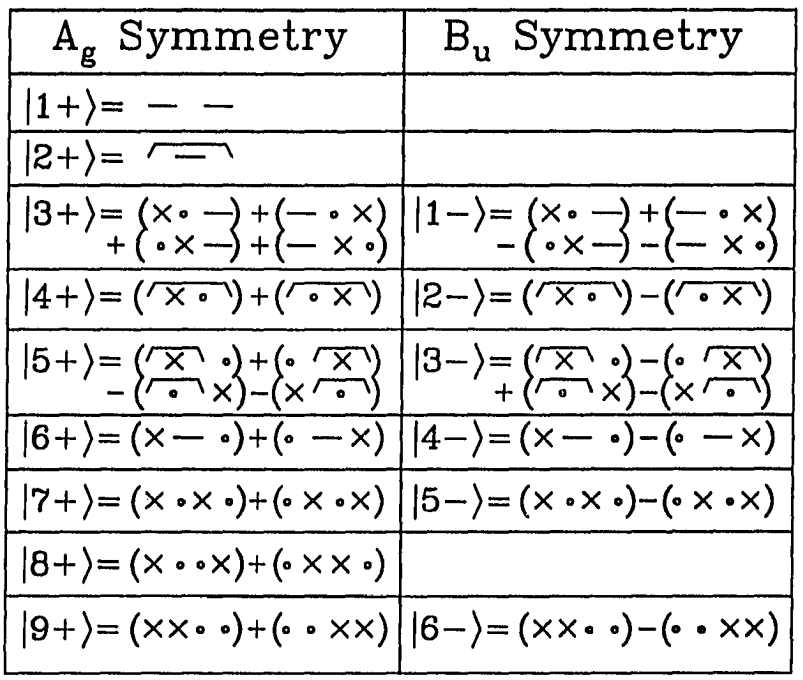

Figure 3.21: The VB basis functions for the A_g and the B_u states in an $N = 4$ chain.

(2) Exciton states :

$$g_0 \sim \frac{1}{N}, \quad g_1 \sim -\frac{1}{N}, \quad g_l \sim 0 \; for \; l > 1, \tag{3.41}$$

because an exciton state contains a nearest neighbor particle(×)-hole(·) pair (see $|3+\rangle$ and the $|4+\rangle$ in Fig. 3.21).

(3) Conduction band states :

$$g_0 \sim \frac{1}{N}, \quad g_l \sim 0 \; for \; l > 0, \tag{3.42}$$

since particles and holes are separated and uncorrelated in the conduction band (see $|5+\rangle$ and $|6+\rangle$ in Fig. 3.21).

(4) Bi-exciton states :

$$g_0 \sim \frac{2}{N}, \quad g_1 \sim -\frac{3}{N}, \quad g_2 \sim \frac{2}{N}, \quad g_3 \sim -\frac{1}{N}, \quad g_l \sim 0 \; for \; l > 3. \tag{3.43}$$

where a biexciton state contains a pair of neighboring particle-hole pairs (excitons) (see $|7+\rangle$ in Fig. 3.21).

The values of the correlation functions for $N = 8$, $U = 50$, $V = 15$, $\delta = 0.1$ are listed in Table 3.1. From the table, it is again confirmed that the ground state is a covalent state due to vanishingly small value of g_0, the $1B_u$ is the first B_u exciton with $g_0 \sim \frac{1}{N}$, $g_1 \sim -\frac{1}{N}$, and g_l for $l > 1$, the mA_g $(11A_g)$ is the first A_g exciton, and the nB_u $(20B_u)$ is the conduction band threshold with small $g_l \sim 0$ for $l \neq 0$.

Moderate Coulomb Parameter Regime

In this parameter region, there are overlaps between energy bands and it is impossible to recognize all the edges of the bands from the energy spectrum. The energy spectrum for $N = 8$, $U = 10$, $V = 3$, $\delta = 0.1$ is plotted in Fig. 3.22. From examining the dipole moments, the excited essential states are recognized as the $1B_u$, the $11A_g$, and the $9B_u$. However, the excitonic characters of the $1B_u$ and

	STATES	l							
		0	1	2	3	4	5	6	7
Covalent	$1A_g$	0.002	-.002	0	0	0	0	0	0
	.	.	.	.	.	.	.	.	.
	.	.	.	.	.	.	.	.	.
	$10A_g$	0	0	0	0	0	0	0	0
Exciton	$1B_u$	0.128	-.128	.002	-.002	0	0	0	0
	.	.	.	.	.	.	.	.	.
	$19B_u$	0.125	-.125	0	-.002	0	0	0	0
	$11A_g$	0.127	-.128	.003	-.002	0	0	0	0
	.	.	.	.	.	.	.	.	.
	$29A_g$	0.125	-.124	0	0	0	0	0	0
Conduction Band	$20B_u$	0.128	-.006	-.006	-.029	-.038	-.030	-.015	.004
	.	.	.	.	.	.	.	.	.
	$76B_u$	0.126	-.004	-.009	-.030	-.038	-.029	-.013	.003
	$30A_g$	0.128	-.006	-.006	-.029	-.038	-.030	-.015	.004
	.	.	.	.	.	.	.	.	.
	$86A_g$	0.126	-.004	-.009	-.030	-.038	-.029	-.013	.004
Bi-exciton	$77B_u$	0.241	-.345	.227	-.123	.001	-.001	0	0
	.	.	.	.	.	.	.	.	.
	$82B_u$	0.238	-.338	.221	-.120	-.001	0	0	0
	.	.	.	.	.	.	.	.	.
	$87A_g$	0.241	-.345	.227	-.123	.001	-.001	0	0
	.	.	.	.	.	.	.	.	.
	$92A_g$	0.238	-.338	.221	-.120	-.001	0	0	0

Table 3.1: Correlation functions $g_l = \frac{1}{N}\langle\sum_{i=1}^{N-l}(n_i - 1)(n_{i+l} - 1)\rangle$ as a function of l for $N = 8$, $U = 50$, $V = 15$, $\delta = 0.1$. Large negative value implies strong particle-hole correlation. The states at the lower part of the table are in higher energies. The numbers with magnitudes smaller than 0.001 are listed as 0. For $N = 8$, $1/N = 0.125$, $2/N = 0.250$, $3/N = 0.375$.

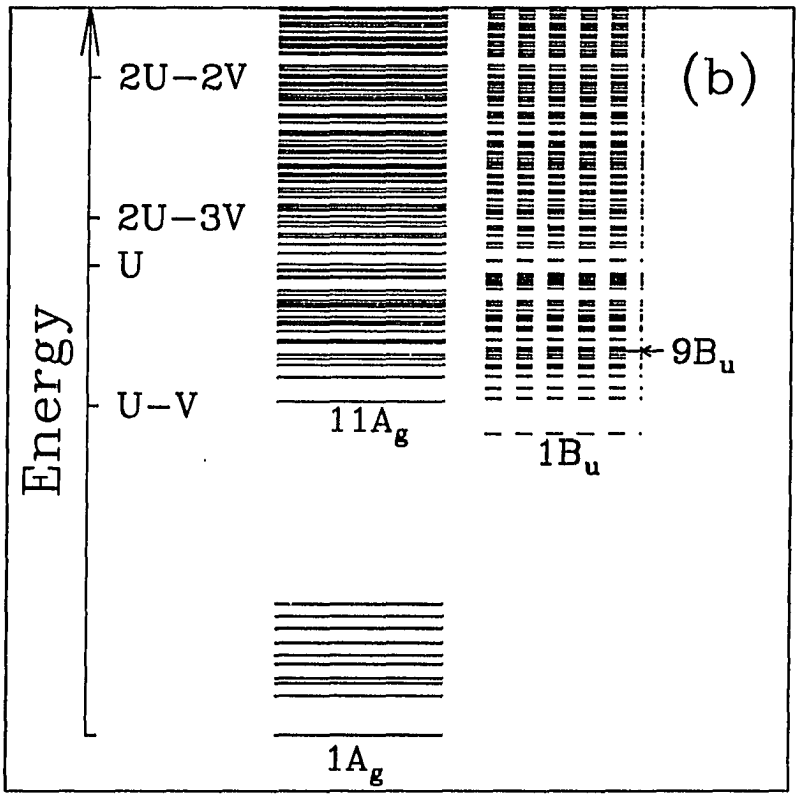

Figure 3.22: The energy spectrum for $N = 8$, $U = 10$, $V = 3$, $\delta = 0.1$.

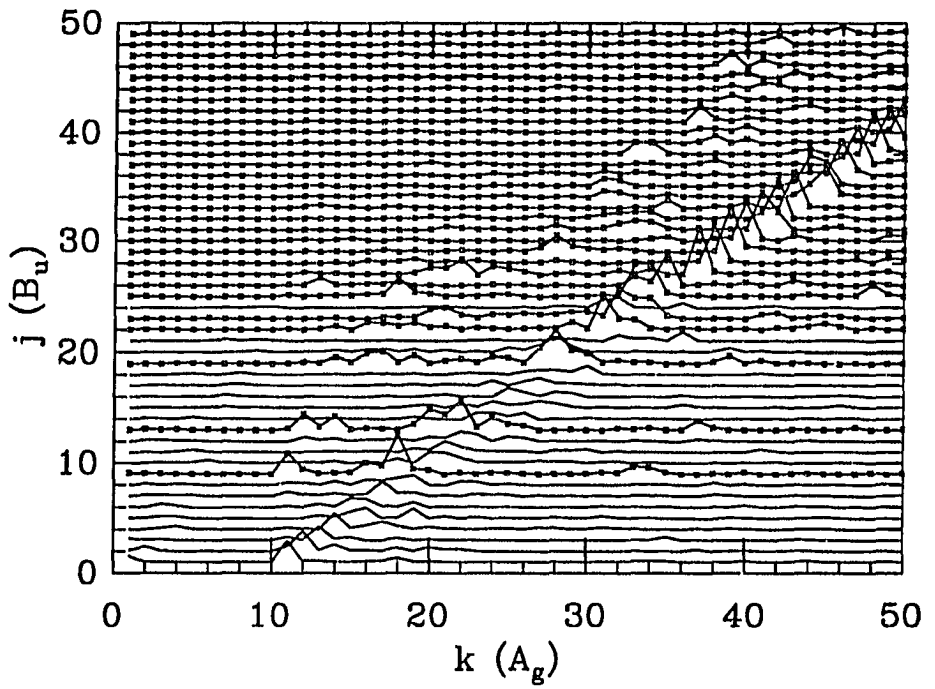

Figure 3.23: The dipole moments between the first 50 A_g and first 50 B_u states for $N = 8$, $U = 10$, $V = 3$, $\delta = 0.1$. Each curve $d_j(k) \equiv |\langle jB_u|\mu|kA_g\rangle|$ in the figure is a function of k. The dotted curves are for the conduction band B_u states.

the mA_g, and the band character of the $9B_u$ cannot be unambiguously identified from the spectrum. It is shown next that these characteristics can be identified from studying the wave-function properties, namely, the dipole moments and the correlation functions.

The dipole moments between A_g and B_u states for the same set of parameter are given in Fig. 3.23, in which the overlap between the exciton states and the conduction band states is clearly seen. In spite of the presence of the overlap, the onset of large intra-band couplings at $9B_u$ is recognizable and the $9B_u$ is evidently the conduction band threshold.

The calculated density-density correlations for the same set of parameters are listed in Table 3.2. The overlaps leads to less sharp edges of the energy bands,

	STATES		l							
			0	1	2	3	4	5	6	7
Covalent	$1A_g$		0.044	-.044	.001	-.001	0	0	0	0
	.		.	.	.	.	.	.	.	.
	$10A_g$		0.003	-.003	0	0	0	0	0	0
Conduction Band		$1B_u$	0.169	-.115	.027	-.032	.001	-.008	0	-.002
	.		.	.	.	.	.	.	.	.
		$11A_g$	0.158	-.112	.017	-.035	-.011	-.013	-0.003	-.002
	.		.	.	.	.	.	.	.	.
		$8B_u$	0.143	-.117	-.011	-.014	0	0	0	0
	$9B_u$		0.152	-.068	.011	-.010	.020	-.030	-.022	-.013
		$10B_u$	0.142	-.121	.008	-.023	-.004	-.002	0	0
		.	.	.	.	.	.	.	.	.
		$12B_u$	0.142	-.127	-.008	0	-.002	-.009	.009	-.005
	$13B_u$		0.145	-.057	.007	-.008	-.019	-.031	-.027	-.010
		$14B_u$	0.139	-.126	-.012	-.005	.007	-.004	0	0
		.	.	.	.	.	.	.	.	.
		$18B_u$	0.136	-.126	-.005	-.005	.002	.001	0	-.001
	$19B_u$		0.138	-.049	.005	-.010	-.026	-.030	-.020	-.070
		$20B_u$	0.135	-.119	.002	-.006	-.005	-.003	-.003	-.001
		$21B_u$	0.129	-.120	-.007	-.001	-.001	0	0	0
	$22B_u$		0.140	-.038	.002	-.022	-.042	-.026	-.011	-.003
	$23B_u$		0.131	-.027	.002	-.012	-.030	-.036	-.022	-.006
		$24B_u$	0.129	-.125	.001	0	-.001	-.002	-.001	0
	$25B_u$		0.142	-.035	-.002	-.026	-.022	-.011	-.021	-.025
	.		.	.	.	.	.	.	.	.
	$54B_u$		0.150	-.056	-.020	-.018	-.036	-.004	-.010	-.005
		$55B_u$	0.181	-.141	.054	-.043	-.032	-.013	-.002	-.002
	$56B_u$		0.147	-.057	-.032	-.017	-.021	-.014	-.006	-.011
	.		.	.	.	.	.	.	.	.
	$63B_u$		0.157	-.081	.009	-.026	-.023	-.017	-.009	-.010
		$64B_u$	0.188	-.140	.047	-.067	.017	-.031	-.005	-.009
	.		.	.	.	.	.	.	.	.
	$84B_u$	.	0.148	-.081	.009	-.026	-.023	-.017	-.009	-.010
		$85B_u$	0.219	-.188	.034	-.031	-.022	.008	-.013	-.007
		.	.	.	.	.	.	.	.	.

Exciton

Bi-exciton

Table 3.2: Expectation values $\frac{1}{N}\langle\sum_{i=1}^{N-l}(n_i-1)(n_{i+l}-1)\rangle$ as a function of l for $N=8$, $U=10$, $V=3$, $\delta=0.1$. Large negative value implies strong particle-hole correlation. The numbers with magnitudes smaller than 0.001 are listed as 0. For $N=8$, $1/N=0.125$, $2/N=0.250$, $3/N=0.375$.

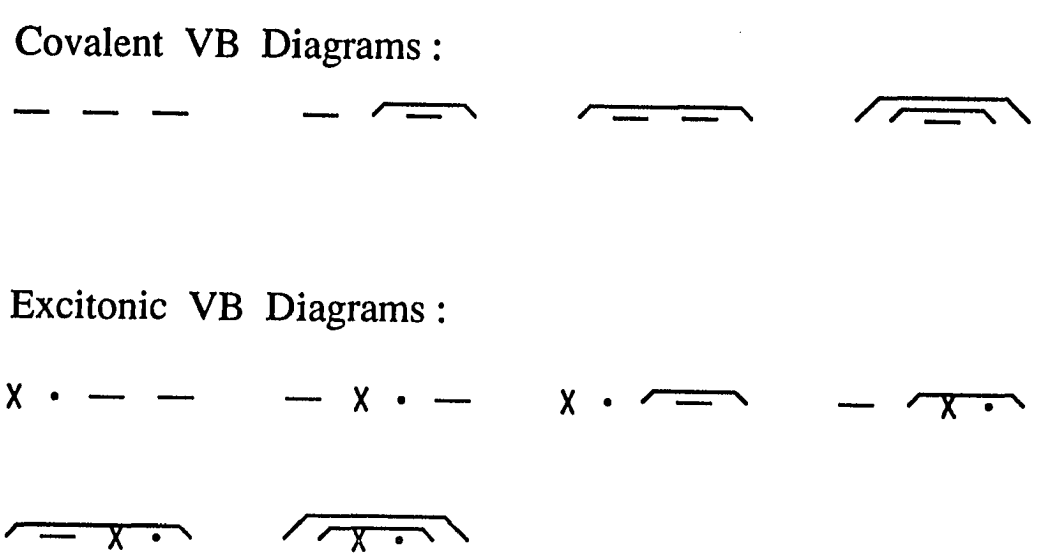

Figure 3.24: The four covalent and six excitonic VB diagrams for an $N = 6$ chain.

while the covalent character of the $1A_g$, the exciton characters of the $1B_u$ and the mA_g ($11A_g$), and the conduction band character of the nB_u ($9B_u$) are retained.

Another method that can also provide explanations for the natures of the mA_g and the nB_u is to study the quantum numbers m and n. For a given chain length N, the values of m and n increase as the Coulomb parameters increase and saturate at certain values m_s and n_s. The values of m_s and n_s are equal to the number of covalent VB diagrams (N_{cov}) +1 and the number of the excitonic diagrams (N_{exc}) +1, respectively. For $N = 6$, $N_{cov} = 4$, $N_{exc} = 6$, and for $N = 8$, $N_{cov} = 10$, $N_{exc} = 19$, which explains why the mA_g and the nB_u are, respectively, the $5A_g$ and the $7B_u$ for $N = 6$, and the $11A_g$ and the $20B_u$ for $N = 8$, in large parameter limit. The four covalent diagrams and six excitonic diagrams for $N = 6$ are depicted in Fig. 3.24. Furthermore, the saturation values of m and n tell that the mA_g is the first A_g exciton state and the nB_u is the conduction band threshold.

For smaller parameters, the values of m and n are less than the saturation values as a result of band overlaps. The natures of the mA_g and the nB_u, however, are preserved as shown in the above numerical results.

3.2 Nonlinear Pathways and Intensities of Two-Photon Resonances

From the four essential states, two kinds of nonlinear pathways can be constructed. The first includes the paths that give rise to three-photon resonances at $\frac{1}{3}E(1B_u)$ and $\frac{1}{3}E(nB_u)$, which are

$$1A_g \rightarrow jB_u \rightarrow 1A_g \rightarrow jB_u \rightarrow 1A_g \quad j = 1,\ n\ . \tag{3.44}$$

The second includes the paths that lead to mA_g two-photon resonance at $\frac{1}{2}E(mA_g)$, which are

$$1A_g \rightarrow iB_u \rightarrow mA_g \rightarrow jB_u \rightarrow 1A_g \quad i,\ j = 1,\ n\ . \tag{3.45}$$

where the $\chi^{(3)}$ contributions from the paths in Eq. 3.45 can be eighter positive and negative depending on the values of i and j. The effect of this is discussed next. In order to compare with the one-electron theory, the intensity of the $2A_g$ two-photon resonance within the extended Hubbard model is also discussed in this section.

Intensity of the mA_g Two-Photon Resonance

Similar to the $2A_g$ in the one-electron models, the mA_g two-photon resonance has contributions from two kinds of paths, the "direct" paths that involve only one B_u state in each path,

$$1A_g \rightarrow jB_u \rightarrow mA_g \rightarrow jB_u \rightarrow 1A_g \quad j = 1,\ n\ , \tag{3.46}$$

and the "cross" paths that involve both essential B_u states in each path,

$$1A_g \rightarrow iB_u \rightarrow mA_g \rightarrow jB_u \rightarrow 1A_g \quad i,\ j = 1,\ n;\ i \neq j\ . \tag{3.47}$$

The resonant $\chi^{(3)}_{THG}$ and $\chi^{(3)}_{TPA}$ contributions from the two kinds of pathways are, respectively,

$$T^{THG}_{jj} = \frac{\langle 1A_g|\mu|jB_u\rangle^2\langle mA_g|\mu|jB_u\rangle^2}{(\omega_{jB_u}-3\omega)(\omega_{mA_g}-2\omega)(\omega_{jB_u}-\omega)}\ , \tag{3.48}$$

$$T^{TPA}_{jj} = \frac{\langle 1A_g|\mu|jB_u\rangle^2\langle mA_g|\mu|jB_u\rangle^2}{(\omega_{jB_u}-\omega)(\omega_{mA_g}-2\omega)(\omega_{jB_u}-\omega)}\ , \tag{3.49}$$

and

$$T^{THG}_{ij} = \frac{\langle 1A_g|\mu|iB_u\rangle\langle iB_u|\mu|mA_g\rangle\langle mA_g|\mu|jB_u\rangle\langle jB_u|\mu|1A_g\rangle}{(\omega_{iB_u}-3\omega)(\omega_{mA_g}-2\omega)(\omega_{jB_u}-\omega)}\ , \tag{3.50}$$

$$T^{TPA}_{ij} = \frac{\langle 1A_g|\mu|iB_u\rangle\langle iB_u|\mu|mA_g\rangle\langle mA_g|\mu|jB_u\rangle\langle jB_u|\mu|1A_g\rangle}{(\omega_{iB_u}-\omega)(\omega_{mA_g}-2\omega)(\omega_{jB_u}-\omega)}\ . \tag{3.51}$$

Again, as in the case of $2A_g$ in the one-electron models, the dipole-moment products $\langle 1A_g|\mu|1B_u\rangle\langle 1B_u|\mu|mA_g\rangle$ and $\langle 1A_g|\mu|nB_u\rangle\langle nB_u|\mu|mA_g\rangle$ have opposite signs and the $\chi^{(3)}$ contributions T_{jj} and T_{ij} from different kinds of paths cancel since the denominators of the two terms have the same signs for $\omega \sim \omega_{mA_g}/2$. However, for $V \neq 0$, there is a gap between the exciton $1B_u$ and the conduction band threshold nB_u and, hence, $E(nB_u) \neq E(1B_u)$, $|\langle 1A_g|\mu|1B_u\rangle| \neq |\langle 1A_g|\mu|nB_u\rangle|$, and $|\langle mA_g|\mu|1B_u\rangle| \neq |\langle mA_g|\mu|nB_u\rangle|$ even for $N \rightarrow \infty$. As a result, the cancellation is only partial and the intensity of the mA_g two-photon resonance does not vanish in either the $\chi^{(3)}_{THG}$ or the $\chi^{(3)}_{TPA}$ spectrum.

Intensity of the $2A_g$ Two-Photon Resonance

In the previous works, the two-photon resonance in the experimental $\chi^{(3)}_{THG}$ spectrum has been attributed to the sub-gap state $2A_g$, while the essential-state theory shows that the $2A_g$ and other sub-gap states are not important to the third

N	U	V	δ	$P^-/P+$
4	3	1	0.1	0.4952
6	3	1	0.1	0.5988
8	3	1	0.1	0.5136
6	PPP			0.5141
8	PPP			0.5319
4	4	0	0.1	0.6585
6	4	0	0.1	0.7060
8	4	0	0.1	0.7938
4	6	2	0.1	0.9377
6	6	2	0.1	0.9642
8	6	2	0.1	0.9779
4	10	3	0.1	0.9902
6	10	3	0.1	0.9849
8	10	3	0.1	0.9991

Table 3.3: The ratio P^-/P^+ that measures the degree of cancellation in the $\chi^{(3)}_{TPA}$ contributions. See text for the definitions of P^+ and P^-.

order nonlinearity. In this section, the irrelevancy of the $2A_g$ and other sub-gap A_g states is further proved by investigating cancellation effect in the nonlinear pathways leading to the two-photon resonances within the interacting-electron models.

The two kinds of pathways for the subgap $2A_g$ state are the same as those in the independent-electron models (see Eq. 3.46 and 3.47), i.e. the $2A_g$ is coupled to the $1B_u$ and the $2B_u$. The cancellations between the "direct" and the "cross" paths remain strong due to the near degeneracy between the $1B_u$ and the $2B_u$ in the long chain limit. The calculated ratios of the resonance $\chi^{(3)}_{TPA}$ contributions $P^+ \equiv \sum_{j=1}^{2} T_{jj}(2A_g)$ and $P^- \equiv \sum_{i \neq j} T_{ij}(2A_g)$, P^-/P^+ are given in Table 3.3 for various of parameters. An exact cancellation corresponds to $P^-/P^+ = 1$. Despite their deviation from unity due to the finite size effects, the results in Table 3.3 for these short chain lengths ($N \leq 8$) have already shown strong cancellation between the two terms. Therefore, the intensity of the $2A_g$ two-photon resonance in a long chain is also expected to vanish within the interacting-electron models. The same kind cancellation is also expected for all the sub-gap A_g states (F. Guo, D. Guo,

and S. Mazumdar, 1993).

3.3 Theoretical Predictions

Based on the essential states study in this chapter, three predictions are made for the optical properties of π-conjugated polymers.

(1) Because of the presence of two essential B_u states, there should be *three* resonance peaks in the $\chi^{(3)}_{THG}$ spectrum. They are the three-photon resonance due to the $1B_u$ at $\frac{1}{3}E(1B_u)$, the three-photon resonance due to the band threshold nB_u at $\frac{1}{3}E(nB_u)$, and the two-photon resonance due to the mA_g at $\frac{1}{2}E(mA_g)$. The three peak $\chi^{(3)}_{THG}$ spectrum is expected for any excitonic ($V \neq 0$) system.

(2) Since the mA_g is the only important two-photon state, there should be only *one* two-photon resonance peak in the $\chi^{(3)}_{TPA}$ spectrum of a material containing long molecular chains. From its excitonic nature, the mA_g is expected to be very close to the $1B_u$ in energy.

(3) As a conduction band state, the nB_u is strongly intra-band coupled to the band A_g states, which leads to a strong state-mixing in the presence of an applied electric field and hence a large energy shift — the Stark shift — and a reduced absorption strength due to the weakened dipole coupling with the ground state. The field induced changes in the nB_u are, therefore, observable in the electroabsorption spectrum, which measures the difference between the zero field and nonzero field absorptions, although the nB_u may not be seen in the zero-field absorption spectrum due to the relatively weaker $1A_g$-nB_u coupling compared to the $1A_g$-$1B_u$ coupling.

CHAPTER 4

COMPARISON WITH EXPERIMENTS

Although the first $\chi^{(3)}_{THG}$ frequency spectrum in polyacetylene has been considered to be a two-peak spectrum (Kajzar *et al.*, 1987), the essential states mechanism of optical nonlinearity predicts the observable resonance feature from the conduction band threshold and, consequently, a three-peak $\chi^{(3)}_{THG}$ spectrum and reveals the universality that exists in many of the one-dimensional π-conjugated polymers. It is found that the complete information on the nonlinearity has to be extracted from various experiments rather than a single $\chi^{(3)}_{THG}$ measurement. In this chapter, the theoretical conclusions obtained from the essential-state model are compared with the experimental results obtained from the measurements such as third harmonic generation, two-photon absorption, and electro-absorption.

4.1 Third Harmonic Generations

The theoretical $\chi^{(3)}_{THG}$ spectrum for $N = 8$, $U = 10$, $V = 3.5$, $\delta = 0.1$ is given in Fig. 4.25, where three resonance peaks due to the $1B_u$, the nB_u and the mA_g are present. The solid curve in the figure is obtained from the four-state calculation while the dashed curve is obtained from the exact calculation that includes all the states. The quantitatively good agreement between the four-level and the exact results indicates that the four states discovered in this work are the essential states. In order to show the role played by the band threshold nB_u, a three-level spectrum (without the nB_u) is also given in Fig. 4.25(b). Without the nB_u, the intensity of the mA_g two-photon resonance is much larger. In addition,

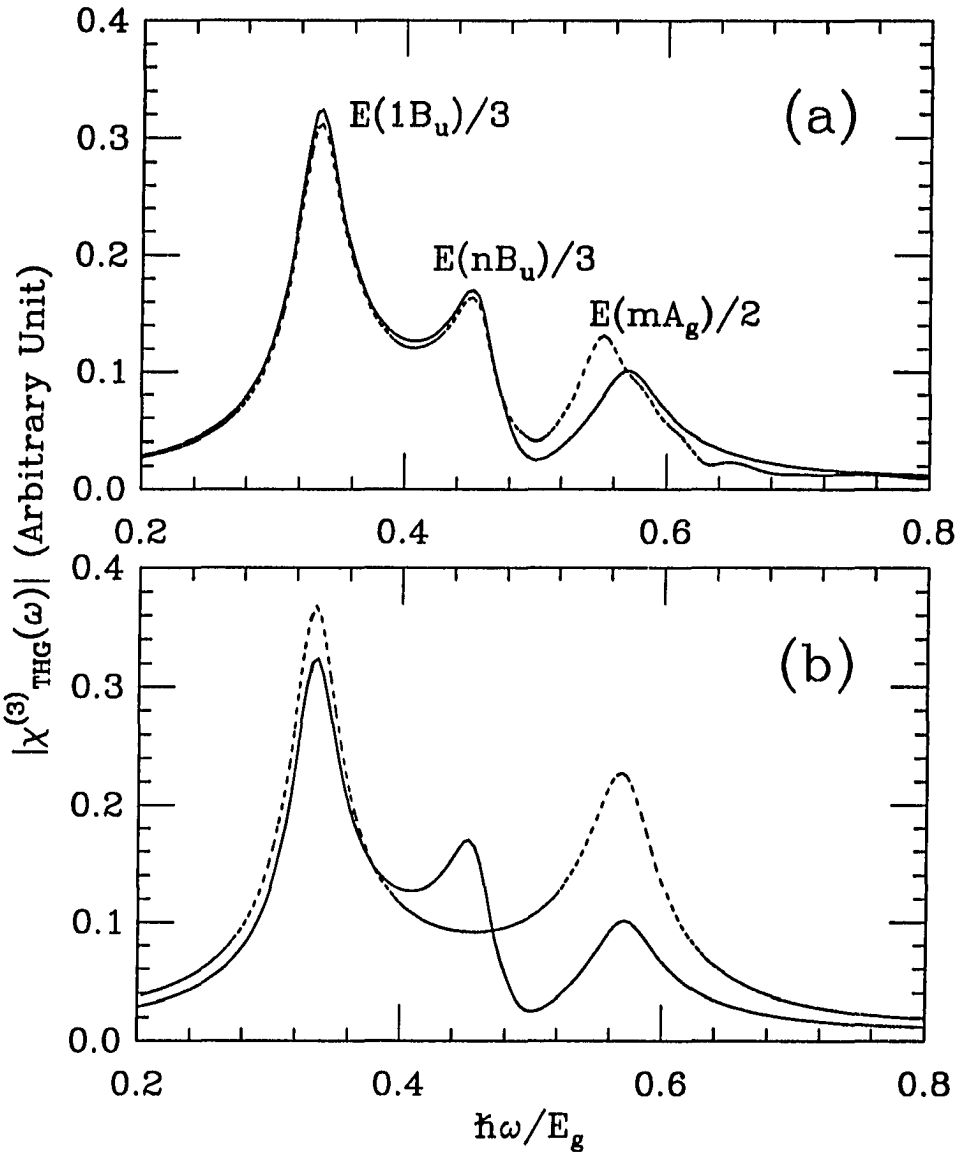

Figure 4.25: Theoretical $\chi^{(3)}_{THG}$ spectra for $N = 8$, $U = 10$, $V = 3.5$, $\delta = 0.1$, $\Gamma = 0.05E(1B_u)$. (a) The solid curve is obtained from the four-state calculation and the dashed curve is from the exact calculation that includes all the states. (b) Solid curve is the four-level spectrum and the dashed curve is the three-level (without the nB_u) spectrum.

in the absence of the nB_u the overall magnitude of $\chi^{(3)}$ would increase rapidly to an unrealistically large value as the chain length increases.

The experimental $\chi^{(3)}_{THG}$ spectrum by Hasegawa *et al.* (Hasegawa *et al.*, 1992) is shown in Fig. 4.26. The measurement is conducted in a polydiacetylene, PDA-C_4UC_4, which is polymerized from a diacetylene monomer RC≡C-C≡R powder, with R being the substitutional urethane side group R = $(CH_2)_4$-OCONH-C_4H_9, that is considered as being most suitable for the preparation of highly oriented films (Kanetake *et al.*, 1989). From electro-absorption experiment the energies of the $1B_u$ and the mA_g are found to be about 1.95 eV and 2.5 eV respectively (Hasegawa *et al.*, 1990). Therefore, in the $\chi^{(3)}$ spectrum, the resonances at 0.65 eV and 1.25 eV are the three-photon resonances due to the $1B_u$ and the two-photon resonance due to the mA_g. Photo-conduction experiment shows that the conduction threshold is at 2.8 eV[1], which leads to a three-photon resonance at about 0.93 eV in the $\chi^{(3)}_{THG}$ spectrum. The theoretical results (solid curves in Fig. 4.26) are obtained from the four-level calculation that uses the experimental values for the energies of the $1B_u$, mA_g, and nB_u and adjusts the dipole moments to get the best fits to the the experimental data. The fitting parameters are listed in Table 4.4 together with the parameters for other fittings.

Three-peak $\chi^{(3)}$ spectrum has also been found in many other materials such as polythiophenes[2] and polysilanes (Hasegawa *et al.*, 1992), which demonstrates explicitly the importance of the conduction band threshold in the third order optical nonlinearity.

4.2 Two-Photon Absorption

One of the theoretical predictions from the last chapter is that the intensities of the two-photon resonances due to all the A_g states are vanishingly small

[1]See Hasegawa *et al.*, 1992.

[2]See, Guo, Mazumdar, and Stegeman *et al.*, 1992).

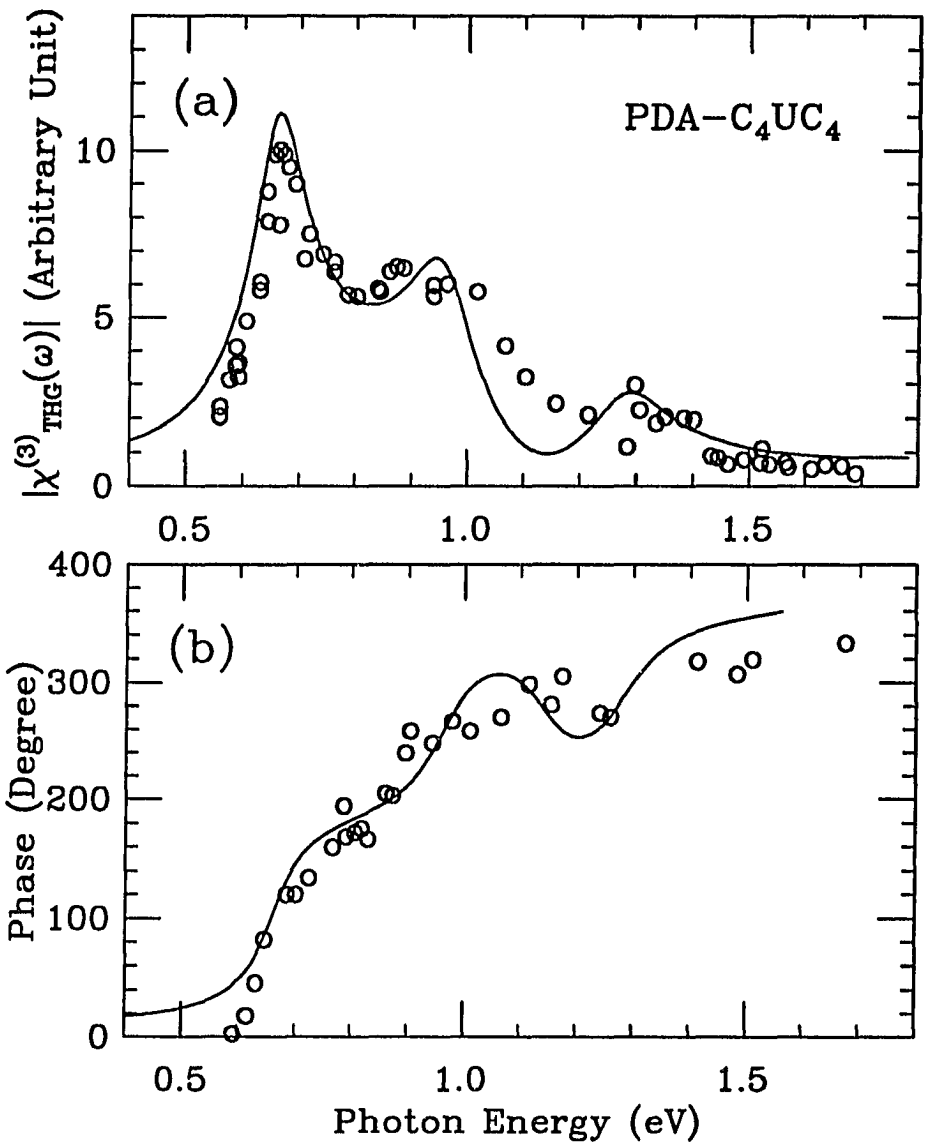

Figure 4.26: Experimental $\chi^{(3)}_{THG}$ spectra in PDA-C_4UC_4 film. The solid curves are the theoretical results from the four essential-state model. The theoretical calculations use the experimental values for the energies of the $1B_u$, mA_g and the nB_u and adjust the relative values of the dipole moments to get the best fits. The parameters are listed in Table 4.4

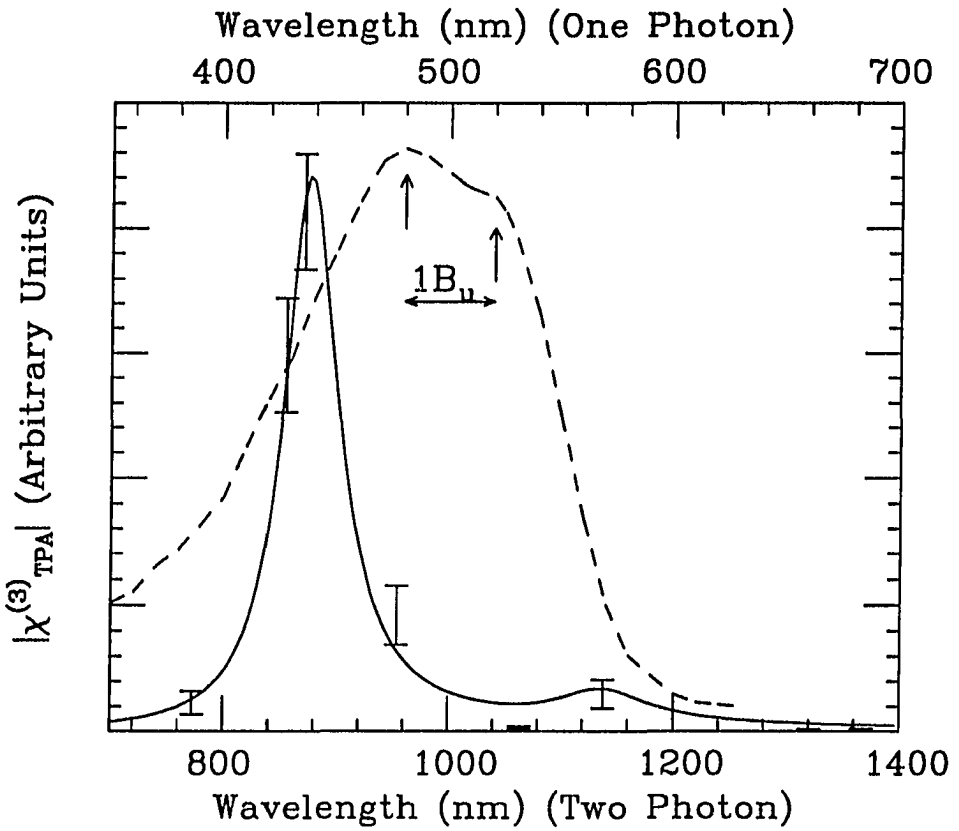

Figure 4.27: Experimental two-photon absorption spectrum $\chi^{(3)}_{TPA}(\omega)$ (solid curve) and the corresponding linear (one-photon) absorption spectrum (dashed curve).

except that due to the mA_g, which is located just above the $1B_u$, and only one strong two-photon resonance is expected in the $\chi^{(3)}_{TPA}$ spectrum.

The experimental two-photon absorption spectrum in Fig. 4.27 was measured in a polydiacetylene thin film 4-BCMU with side group $(CH_2)_4OCONHCH_2COO(CH_2)_3CH_3$) (Torruellas, 1991). In the figure, the linear absorption spectrum (dashed curve) is also given in order to identify the relative locations of the $1B_u$, the mA_g, and the sub-gap A_g states. The maximum of the linear absorption is between 480-520 nm (2.4-2.6 eV), indicating that the $1B_u$ is in this region. The two-photon absorption spectrum (solid curve) has a *sharp* peak at 865 nm (1.4 eV), implying a *single* two-photon state located at 433 nm (2.8 eV), which is about 0.2-0.4 eV above the $1B_u$. Based on the essential states theory, this two-photon state is the

mA_g since its contribution to the $\chi^{(3)}_{TPA}$ and $\chi^{(3)}_{THG}$ is not cancelled out completely due to the presence of longer range electron-electron Coulomb interactions ($V \neq 0$), and, therefore, a gap between the exciton $1B_u$ and the conduction band threshold. A very small peak at about 1140 nm (1.1 eV) is attributed to a two-photon state at 570 nm (2.2 eV). From the previous argument, this state is a sub-gap A_g state that is expected to be present in the interacting-electron models and to have a very weak resonance intensity. The nonzero two-photon resonance intensity of the sub-gap A_g states in the spectrum could be due to the effects that reduce the effective lengths of the molecular chains and hence nonperfect cancellations.

4.3 Electro-Absorption

The most important contribution of this work to the theory of optical nonlinearity in conjugated polymers is the recognition of the roles played by the conduction band threshold (nB_u), which leads to the more complete understanding of the mechanism of the nonlinearity. However, it is hard to observe the the conduction band threshold in the linear absorption spectrum $\alpha(\omega)$[3],

$$\alpha(\omega) = K \times \omega Im\{\sum_{g,n} |\langle n|\mu|g\rangle|^2 [\frac{1}{\omega + \omega_{ng} + i\Gamma_{ng}} - \frac{1}{\omega - \omega_{ng} + i\Gamma_{ng}}]\} , \qquad (4.52)$$

where K is a constant, due to the weaker nB_u-$1A_g$ coupling compared to the $1B_u$-$1A_g$ coupling and larger nB_u-$1A_g$ energy separation. An alternative way of identifying the nB_u is to study the electro-absorption spectrum that gives the changes in the linear absorption induced by an applied electric field F. Electro-absorption experiments measure $\Delta\alpha(\omega) \equiv \alpha_F(\omega) - \alpha_0(\omega)$

Applying an electric field F to a molecular chain breaks the mirror plane symmetry and mixes the states of different parities. The strength of mixing between two states is proportional to the dipole moment between them. The resultant effects in the absorption spectrum α are the energy shifts (Stark shifts, see Fig.

[3]See, Shen, 1984

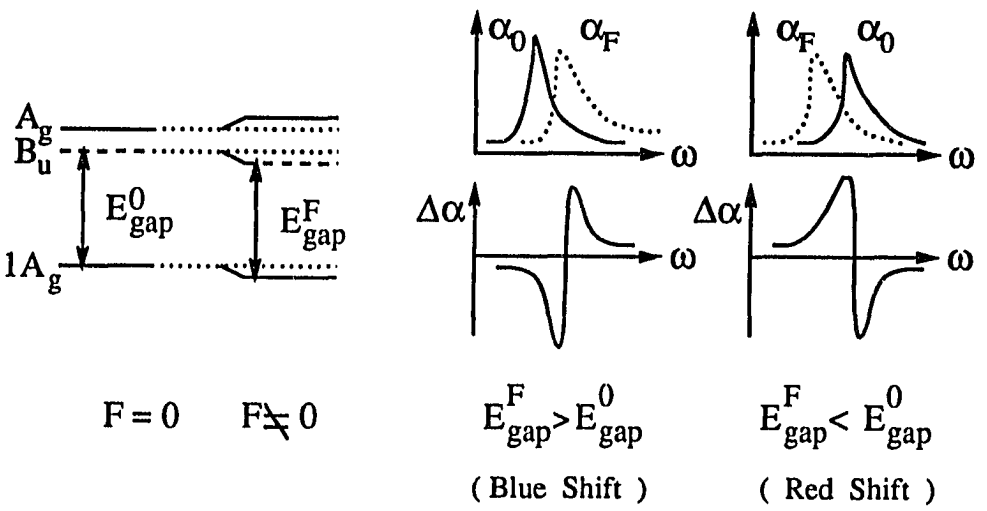

Figure 4.28: Schematic illustration of Stark shifts in the energy spectrum and the electro-absorption spectrum. $\Delta\alpha = \alpha_F - \alpha_0$.

4.28) and the field-induced $1A_g$-A_g transitions. Due to the strong intra-band couplings between the $1B_u$ and the mA_g and between the conduction band states, large changes are expected for the $1B_u$ exciton, the mA_g exciton, and for the band threshold nB_u and other band states. However, for the states deep inside the conduction band, the field-induced losses in $1A_g$-B_u absorptions cancel the gains in $1A_g$-A_g absorption due to small energy separations between the band states, and only the changes at the band edge are observable. For the sub-gap A_g states, cancellations in the field induced transition moments exist, and, as a result, sub-gap A_g states are also not observable in electro-absorption spectra. A detailed analysis of field-induced effects is given in Appendix B. Therefore, in an electro-absorption spectrum $\Delta\alpha(\omega)$, there are only three major features — the $1B_u$ red shift because the mA_g is above and very strongly coupled to the $1B_u$ (see Appendix B), the field-induced $1A_g$-mA_g absorption, and the field induced changes at the conduction band edge. Consequently, from an electro-absorption experiment one can, in principle, determine the locations of all the three excited essential states.

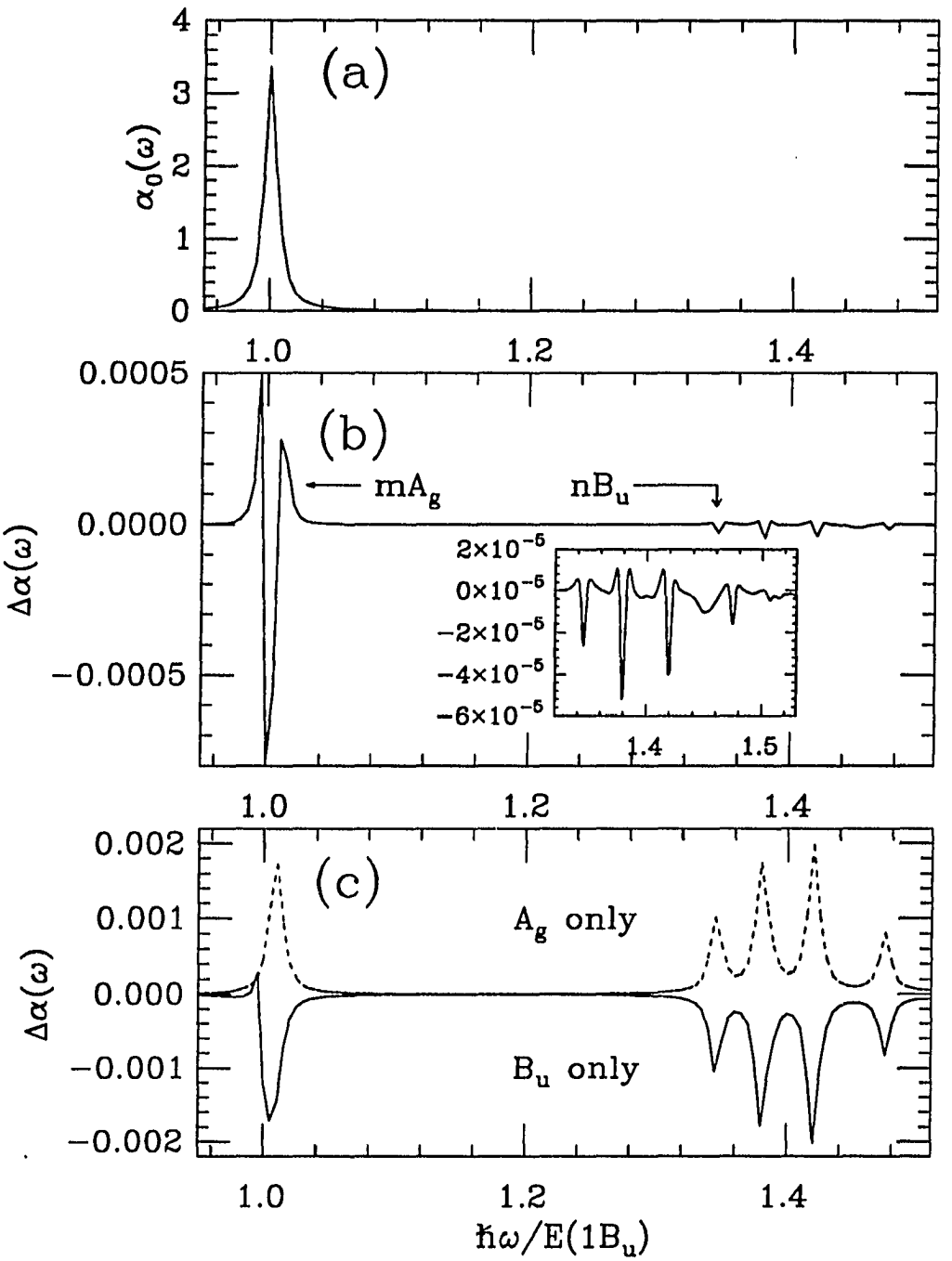

Figure 4.29: Electro-absorption for $N = 8$, $U = 50$, $V = 15$, $\delta = 0.1$, $\Gamma = 0.005E(1B_u)$. The energies of the mA_g and the nB_u are, respectively, $1.007E(1B_u)$ and $1.345E(1B_u)$. (a) Linear absorption $\alpha_0(\omega)$; (b) Difference spectrum $\Delta\alpha(\omega)$ with field $F = 0.005$ in dimensionless units. (c) The difference spectra for the A_g absorption (dashed curve) and the B_u absorption (solid curve).

In order to recognize the band threshold unambiguously, the theoretical calculation of the electro-absorption spectrum is first carried out in the large parameter limit, in which the conduction band is well separated from the excitons. The electro-absorption for $N = 8$, $U = 50$, $V = 15$, $\delta = 0.1$ is given in Fig. 4.29. The $1B_u$ and the mA_g are recognized in the spectrum. The cancellation inside the conduction band is demonstrated by showing the field effects on the A_g or the B_u states only (Fig. 4.29(c)). The onset of the weaker higher energy feature is at the nB_u ($20B_u$), which is attributed to the band threshold.

The electro-absorption and zero-field absorption spectra for moderate interaction case, which is considered to be comparable with experiments, are shown in Fig. 4.30 for $N = 8$, $U = 10$, $V = 3$, $\delta = 0.1$. The feature similar to that of the band threshold in strong correlation limit is observed at the energy of the nB_u ($9B_u$), which has been known from the previous chapter to be the band threshold for this set of parameters.

Although the nB_u is recognized as the conduction "band" threshold from small cluster calculations, its band character has been proved by experiments in real materials with long chain molecules. The experimental electro-absorption spectra are given in Fig. 4.31, which is measured in a polydiacetylene thin film (DCH-PDA) (Kawabe *et al.*, 1991). There is a good agreement between the experimental spectrum $\Delta\alpha$ and that of theory in Fig. 4.30(b). The $1B_u$, which is recognized as an exciton state according to the fact that the photo-conductivity is absent in the corresponding energy region[4], is red-shifted as predicted theoretically. From the resemblance between the nB_u feature in the theoretical spectrum in Fig. 4.30 and the feature in the experimental spectrum in Fig. 4.31, the conduction band threshold of DCH-PDA is considered as being at about 2.4 eV. This assignment is confirmed by the photon-conduction experiment (K. C. Yee and Chance, 1978) carried out in the same material, which finds the onset of photo-conduction being at 2.4 eV.

[4]See, Yee and Chance, 1978.

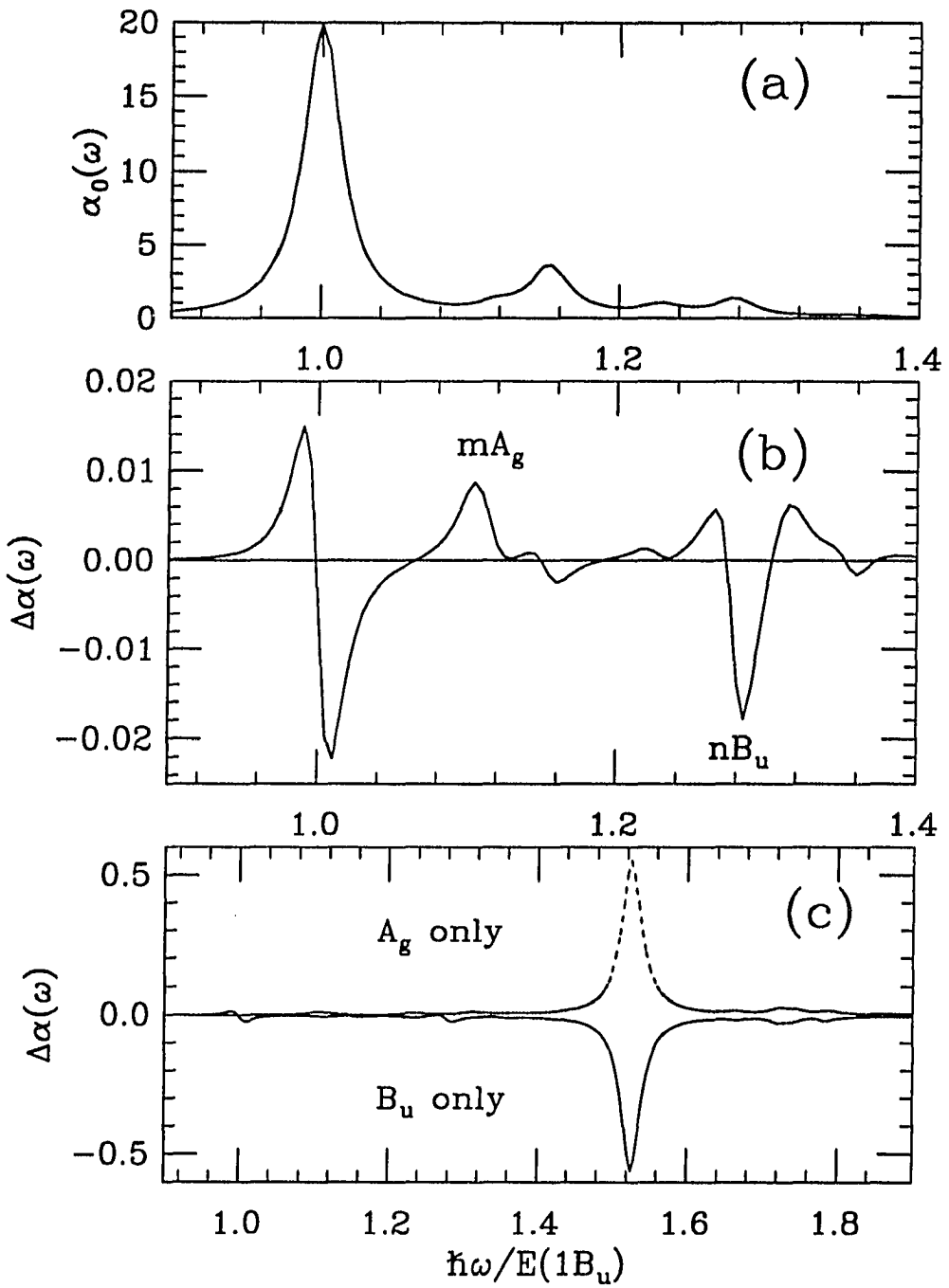

Figure 4.30: Electro-absorption for $N = 8$, $U = 10$, $V = 3$, $\delta = 0.1$, $\Gamma = 0.016E(1B_u)$. The energies of the mA_g and the nB_u are $1.107E(1B_u)$ and $1.278E(1B_u)$ respectively. (a) Linear absorption $\alpha_0(\omega)$; (b) Difference spectrum $\Delta\alpha(\omega)$ with field $F = 0.005$ in dimensionless units. (c) The difference spectra for the A_g absorption (dashed curve) and the B_u absorption (solid curve).

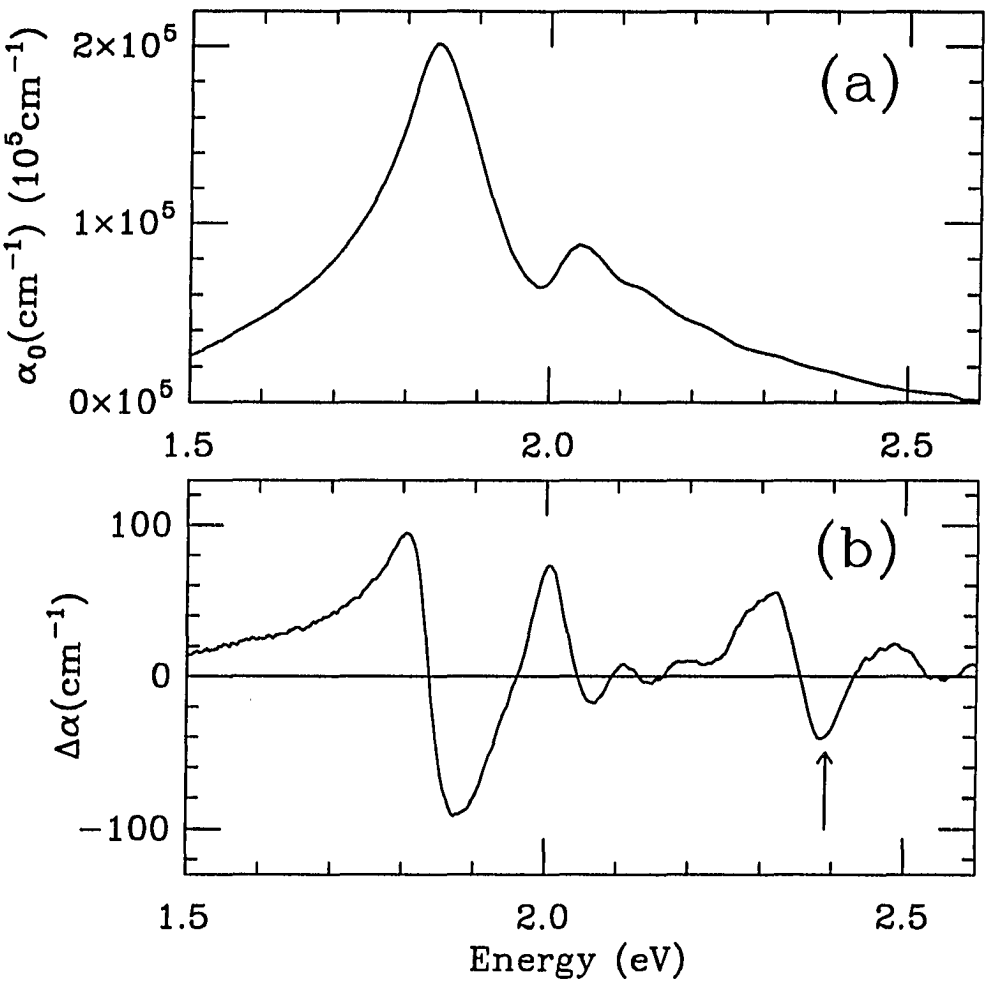

Figure 4.31: Experimental electro-absorption spectra in DCH-PDA film. (a) Linear absorption α_0. (b) Difference spectrum $\Delta\alpha$ with applied field being $120kV/cm$ (Kawabe *et al.*, 1991).

In summary, electro-absorption and photo-conduction experiments have proved that the nB_u, one of the essential states for understanding the third order optical nonlinearity of π-conjugated polymers, is the conduction band threshold. The comparisons with experiments have shown that the conduction band of an infinite chain is recognizable from small cluster calculations.

4.4 Others

Besides the experiments mentioned above, other experiments have shown that the essential states mechanism is valid in many π-conjugated polymers.

The $\chi^{(3)}_{THG}$ measurement in β-carotene (van Beek *et al.*, 1992) shows that the only important two-photon state (mA_g)is above and close to the $1B_u$, and the energy difference between the $1B_u$ and the mA_g is about $0.05E(1B_u)$. This observation is consistent with the theory.

The $\chi^{(3)}_{THG}$ spectra of poly-4BCMU, polythiophene-3BUTY, polythiophene-3DECY, and β-carotene all show the presence of the three-photon resonance due to the band threshold nB_u. The experimental $\chi^{(3)}$ and theoretical fitting are given in Fig. 4.32 to 4.35. The theoretical curves fitted to the experimental spectra are calculated in the following way. The energies of the $1B_u$, mA_g, and nB_u are obtained from the experimental data and are used in the four-state $\chi^{(3)}$ calculations. The dipole moments are chosen to get the curves that are well fitted to the experimental data. The fitting parameters are listed in Table 4.4 and are compared with those of theoretical values for $N = 8$, $U = 10$, $V = 3$, $\delta = 0.1$.

The quantitative deviation of the experimental results from the theoretical predictions can be due to the following reasons. The mA_g may not be very close to the $1B_u$ in certain materials with large bond alternation (for example, polydiacetylenes), or the defects that lead to shorter effective chain lengths, or amorphous structures that contain bent (nonlinear) molecular chains and cause

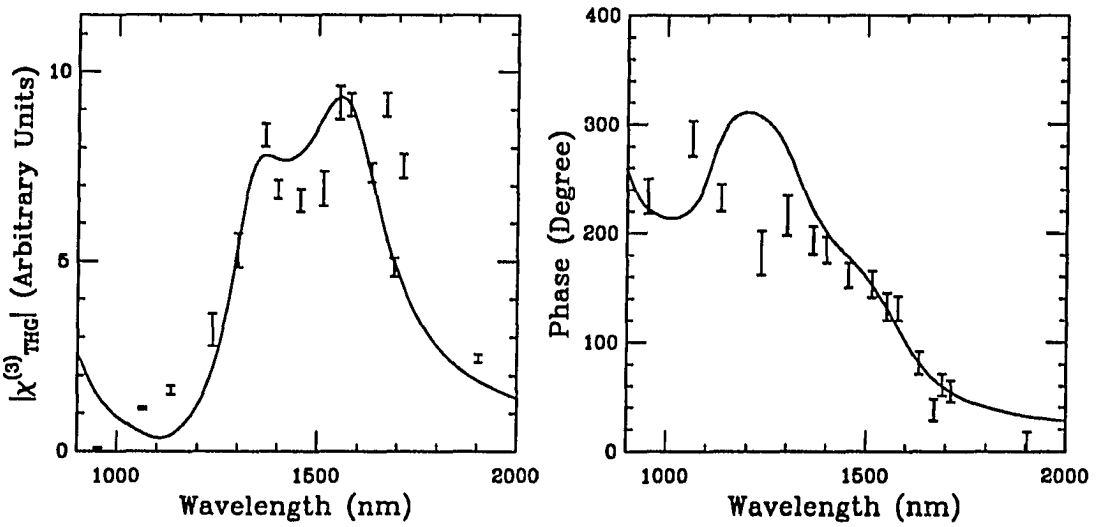

Figure 4.32: Experimental $\chi^{(3)}$ and its phase in poly-4BCMU and theoretical fits (solid curve).

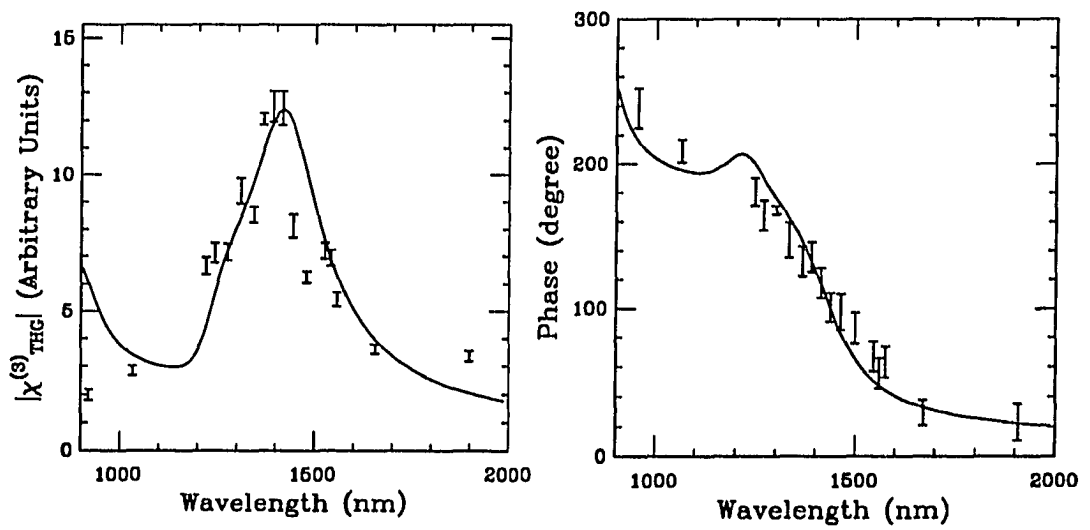

Figure 4.33: Experimental $\chi^{(3)}$ and its phase in β-carotene and theoretical fits (solid curve).

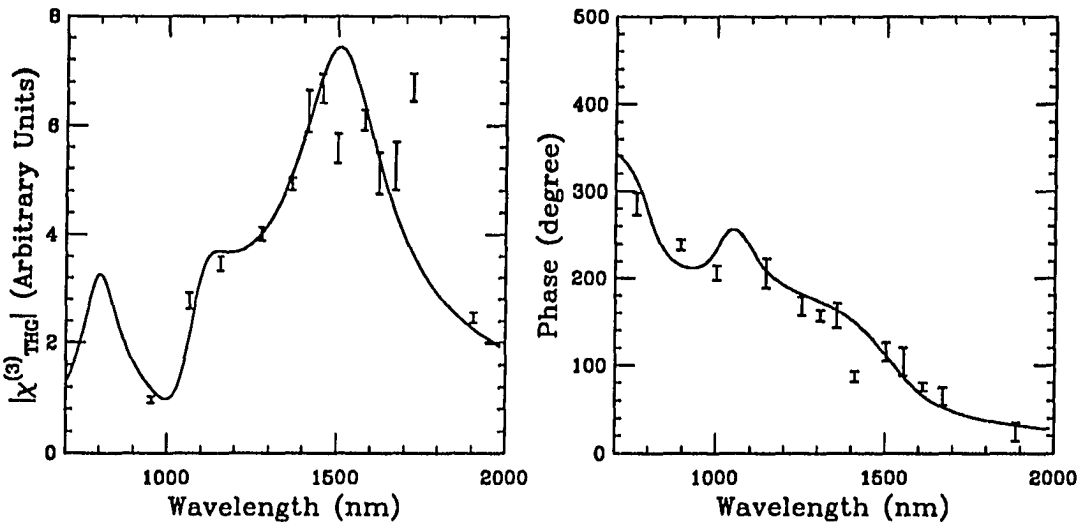

Figure 4.34: Experimental $\chi^{(3)}$ and its phase in polythiophene-3BUTY and theoretical fits (solid curve).

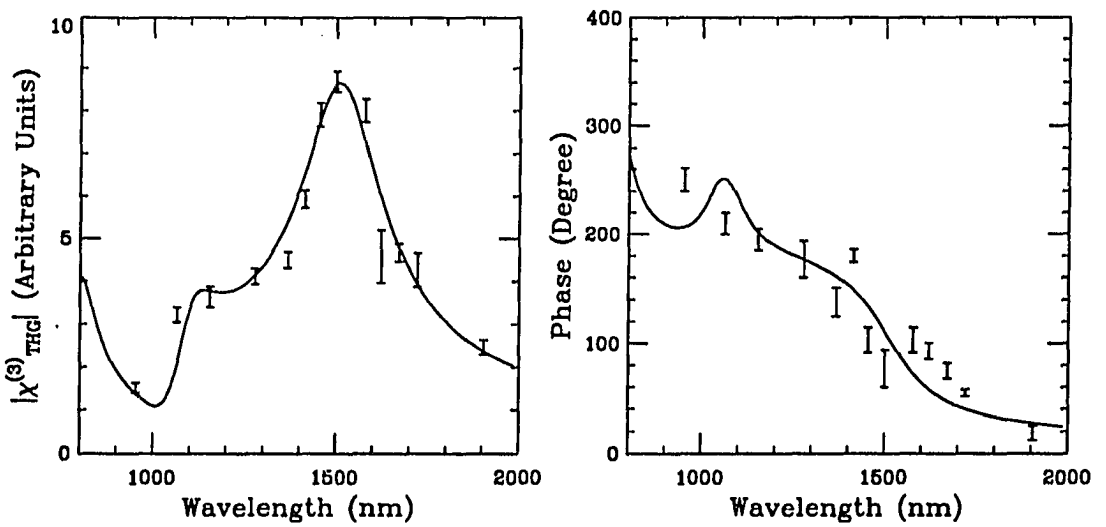

Figure 4.35: Experimental $\chi^{(3)}$ and its phase in polythiophene-3DECY and theoretical fits (solid curve).

Material	$\frac{E(mA_g)}{E(1B_u)}$	$\frac{E(nB_u)}{E(1B_u)}$	$\frac{\langle mA_g\|\mu\|1B_u\rangle}{\langle 1A_g\|\mu\|1B_u\rangle}$	$\frac{\langle mA_g\|\mu\|nB_u\rangle}{\langle 1A_g\|\mu\|1B_u\rangle}$	$\frac{\langle 1A_g\|\mu\|nB_u\rangle}{\langle 1A_g\|\mu\|1B_u\rangle}$
Poly-4BCMU	1.17	1.22	2.2	2.0	-0.35
β-carotene	1.08	1.15	2.2	2.0	-0.15
poly(3-butythiophene)	1.26	1.39	2.2	2.0	-0.14
poly(3-decythiophene)	1.26	1.39	2.2	2.0	-0.12
PDA-C_4UC_4	1.28	1.46	2.2	1.6	-0.25
polyacetylene	1.01	1.29	2.0	1.3	-0.2
Theory N U V 8 10 3	1.14	1.37	2.9	2.6	-0.18

Table 4.4: Comparisons between parameters obtained from the 4-level theoretical calculation with $N = 8$, $U = 10$, $V = 3$, $\delta = 0.1$ and those used in the fit to the experimental spectra. The energies of the essential states are obtained from the experimental data.

mixing of symmetries. However, the essential two-photon state is always below the conduction band threshold because of its excitonic nature.

4.5 On Polyacetylene

As mentioned in the first chapter, the research on the nonlinear optical properties in conjugated polymers was originally focused on interpreting the $\chi^{(3)}_{THG}$ spectrum of polyacetylene. Polyacetylene has long been considered as the prototype of π-conjugated polymers because of its simplest molecular structures of all. However, it is its structure that makes polyacetylene a special case in its polymer family.

The distinction of polyacetylene from most of the π-conjugated polymers such as polydiacetylenes and polythiophenes is due to its two-fold degenerate

ground state. As a result of such degeneracy, even in a defect (topological defect) free polyacetylene, optical excitation of electron-hole pairs can generate soliton/antisoliton pairs (Su and Schrieffer, 1980) or sub-gap soliton states. Therefore, the optical excitations that lead to generation of real electrons and holes give rise to absorption spectra with soliton contribution.[5].

Since soliton states can be photo-generated, the origin of optical nonlinearity in polyacetylene has been considered as solitonic rather than excitonic as in most of conjugated polymers (Sinclair *et al.*, 1989). I do not agree with the assumption of soliton nonlinearity for polyacetylene based on the following considerations, although quantitative studies are needed for a more conclusive answer.

According to the electro-absorption and photoconduction experiments (Phillips *et al.*, 1989), the onset of photo-generated soliton absorption in an initially soliton-free polyacetylene is at about 1.3 eV. Namely, for the photon energy less than 1.3 eV, there is no soliton generation, which is consistent with the fact that the photo-generation of solitons results from the real creation of electron-hole pairs that can be produced only when the input photon energy is close to that of the gap (1.78 eV for polyacetylene). The resonance features in the experimental $\chi^{(3)}_{THG}$ spectrum of polyacetylene (Fann *et al.*, 1989) are in the frequency regime in which photon energy is less than 1 eV (well below the gap energy), and, according to the above argument, no soliton can be generated in that frequency region.

In conclusion, it is highly unlikely that the optical nonlinearity of polyacetylene in the frequency range < 1 eV have soliton contributions.

Although the experimental $\chi^{(3)}$ spectrum of polyacetylene has been considered as a two-peak spectrum, it can be fitted by the four-level model. Because of the soliton conduction, the electron and hole conduction threshold of polyacetylene cannot be determined from the photo-conduction experiment. However, if

[5]See, for example, Phillips *et al.*, 1989.

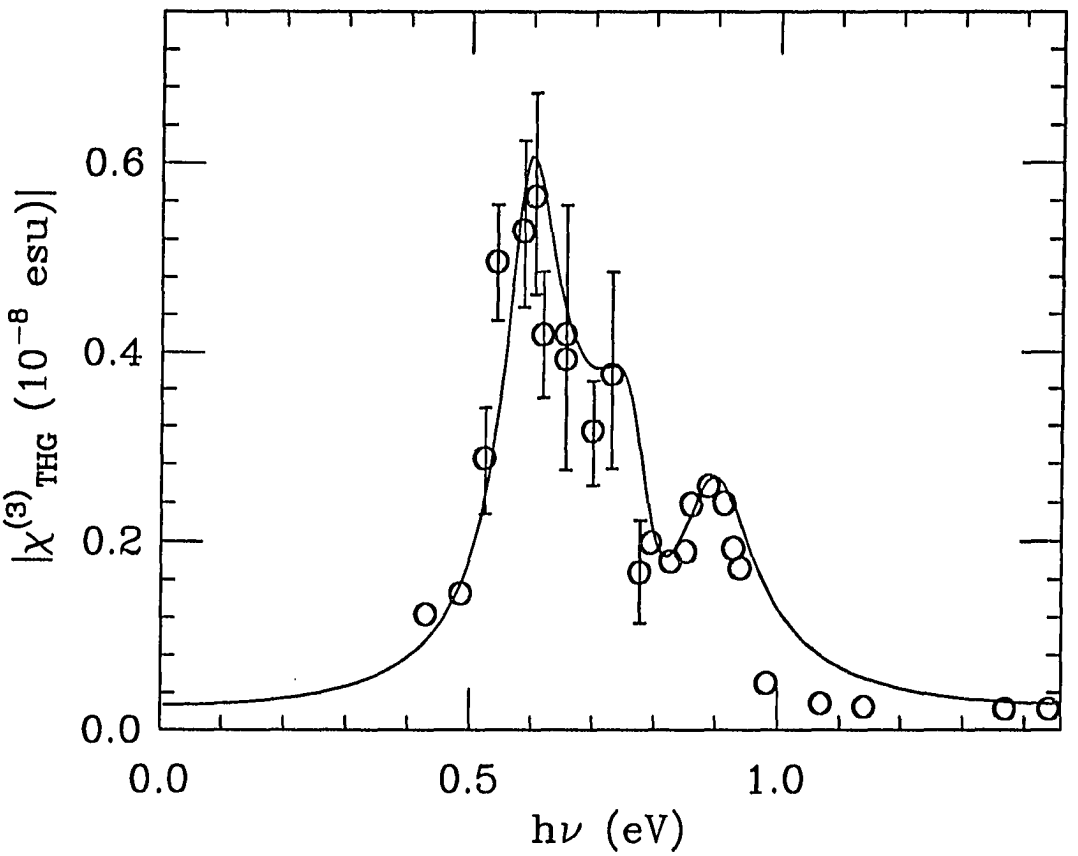

Figure 4.36: Experimental $\chi^{(3)}$ in a polyacetylene and the theoretical fit (solid curve) within the four essential states model.

one estimates the threshold according to the electro-absorption spectrum of *cis*-polyacetylene (Phillips *et al.*, 1989) and the role for finding the band threshold, which has been discussed in the previous section, the threshold can be considered at 2.3 eV. Knowing that the $1B_u$ is at 1.78 eV and assuming the mA_g is at 1.8 eV, the experimental spectrum can be fitted well. The theoretical fit to the experimental $\chi^{(3)}_{THG}$ spectrum is given in Fig. 4.36. In the figure, a three-peak structure is revealed, indicating that the origin of nonlinearity of polyacetylene is not qualitatively different from that of polydiacetylenes and many other π-conjugated polymers.

CHAPTER 5

SUMMARY AND CONCLUSIONS

In this research, a microscopic many-body theory for the third order optical nonlinearity in π-conjugated polymers is developed within the extended Hubbard model.

It is found that in spite of huge amount of optical states involved in nonlinear processes, the bulk of the optical nonlinearity is determined by four essential states. Within the extended Hubbard model, the four essential states are determined as (1) the ground state, (2) the first odd-parity exciton state $1B_u$, (3) the first even-parity exciton state (two-photon state) mA_g, and (4) the conduction band threshold nB_u. The essential two-photon state mA_g is always bounded between the $1B_u$ exciton and the conduction band threshold independent of parameters. The three excited essential states lead to three-peak $\chi^{(3)}_{THG}$ spectra. The three peaks correspond to the three-photon resonance at $\frac{1}{3}E(1B_u)$, the three-photon resonance at $\frac{1}{3}E(nB_u)$, and the two-photon resonance at $\frac{1}{2}E(mA_g)$.

From the analysis of the nonlinear pathways it is shown that the sub-gap states are irrelevant to nonlinear optical properties.

The study on the intensity of two-photon resonances shows that the excitonic feature is essential to understanding the nonlinearity in π-conjugated polymers. Since the exciton formation require nonzero nearest neighbor electron-electron Coulomb interactions, the one-electron theory and the simple Hubbard model are not appropriate for describing nonlinear optical properties of these materials.

It is revealed that a cancellation effect is present in the optical nonlinear processes in one-dimensional chains, which limits the magnitude of the third order nonlinearity of conjugated polymers. The effort to increase the nonlinearity should be directed towards eliminating such cancellations.

Based on both physical arguments and numerical computations, the natures of the essential states are determined. Particularly, the determination of the conduction band leads to more complete understanding of the mechanism of the third order electronic nonlinearity for the first time. There are good agreements between theoretical predictions and experiments, indicating that infinite chain behavior can be understood from small cluster results.

At the time when this work was first published (Guo *et al.*, 1992), Abe *et al.* (Abe *et al.*, 1992) also found a three-peak $\chi^{(3)}$ spectrum in their numerical result. One of the resonances is also attributed to the conduction band threshold. However, the approximations in their calculations are such that there exist no sub-gap A_g states, which is inconsistent with many experimental observations in π-conjugated polymers. It is accidental that their three-peak spectrum agrees with that of the essential states theory.

Generalization of the Essential States Mechanism

The essential states mechanism can be generalized to include other A_g and B_u states at the edge of a "band". For example, for the fifth order nonlinearity $\chi^{(5)}$, the A_g state (or states) at the conduction band edge and strongly coupled to the nB_u and the first bi-exciton B_u state become essential. Even for the third order nonlinearities, the two-photon resonances due to the conduction-band-edge A_g states and the three-photon resonance due to the first bi-exciton B_u state can be observable in short chains because the dominance of the four most essential states is weakened by finite size effects.

In conclusion, the band edge states are always the most relevant states

to nonlinear optical properties since they give rise to the dominant inter-band dipole couplings, where the "bands" can be classified as collections of excitons, conduction states, bi-excitons, tri-excitons, and even localized or delocalized states such as those in polyaraphenylene etc. . Any kind of optical nonlinearity in an infinite system should be understood by examing the roles played by the states at the relevant "band" edges.

APPENDIX A

VALENCE BOND THEORY: INTRODUCTION

A.1 Historical Review

Valence-bond (VB) theory was originally developed for understanding the chemical structure of molecules. The modern version of the theory was formed in the early time of quantum mechanics and characterized by the work of Heitler and London on hydrogen molecule H_2 (Heitler and London, 1927). A close correspondence between the chemical bonds and VB "spin-pairing" structures was found due to the works of Rumer (Rumer, 1932), Pauling (Pauling, 1932), and Eyring and co-workers (Eyring *et al.*, 1932). However, in the application to solid state physics and quantum chemistry, VB theory was not as popular as the band theory or the molecular orbital theory mostly due to the difficulties in computations. After nearly 60 years, the VB theory have been developed into a stage that the qualitative understanding of many-body effects can be obtained within simple and intuitive physical pictures with quantitative accuracy and less computational efforts, although the development is still continuing[1].

The increased interests in the VB theory stemmed from the recognition of electron-electron correlations that are crucial to many chemical and physical problems. The theory has been applied in various "peripheral" areas of condensed matter physics such as the Born's theory of ionic solids (Born, 1954), Frenckel

[1] For a detailed review, see "*Valence Bond Theory and Chemical Structures*", edited by Klein and Trinajstic, 1990.

exciton theory (Frenckel, 1962), Heisenberg model for ferromagnetism and antiferromagnetism (see, e.g., Van Vleck, 1932), and high-temperature superconductivity (Anderson, 1987) etc., where conventional band theory cease to work. Since it was designed to understand the electron Coulomb pairings in molecules, the VB representation naturally takes into account electron-electron interactions. Although VB calculations have been limited to small size molecules and careful finite size analysis is required, it has become a powerful tool in solving problems in narrow-band systems in which electron correlations are pronounced.

A.2 Valence Bond Representation

In the VB theory, a coordinate-space representation is chosen for solving quantum mechanical problems. The basis functions are the VB diagrams that show explicitly the electronic configurations in real space and provide intuitive physical pictures of real-space electron transfers in excitations.

The VB basis $\{|k\rangle\}$ is complete, nonorthogonal and spin invariant, namely, the VB diagrams are the eigenfuctions of the total spin operators $\mathbf{S}^2$ and $\mathbf{S}_z$. The second quantized form of the basic elements of VB diagrams are constructed in the following way. Since the ground state for one-dimensional chains is a singlet ($\mathbf{S}$=0), and the total spin is conserved in optical excitations, we shall be interested only in the cases of $\mathbf{S}$=0. If one denotes the up-spin and down-spin by α and β respectively, a site doubly occupied with two electrons of opposite spins by a cross ($\times$), an empty site by a dot ($\cdot$), and a pair of singlet-coupled singly occupied sites by a line or "bond" joining them, then, using the creation operators c^+s the two basic VB diagrams can be expressed as

$$\underset{site\ \ i\ \ j}{|\text{—}\rangle} \equiv \frac{1}{\sqrt{2}}(c^+_{i,\alpha}c^+_{j,\beta} - c^+_{i,\beta}c^+_{j,\alpha})|0\rangle, \tag{A.53}$$

$$\underset{site\ \ i\ \ j}{|\times\ \cdot\rangle} \equiv c^+_{i,\alpha}c^+_{i,\beta}|0\rangle. \tag{A.54}$$

where only two sites (i, j) are shown. All the other possible diagrams can be generated from the covalent diagram (A.53) and the ionic diagram (A.54) for arbitrary large systems. For example, for a chain of 4 sites,

$$\underset{site\ \ 1\ 2\ 3\ 4}{|\ \frown\ \rangle} \equiv \tfrac{1}{\sqrt{2}}c^+_{2,\alpha}c^+_{2,\beta}(c^+_{1,\alpha}c^+_{4,\beta} - c^+_{1,\beta}c^+_{4,\alpha})|0\rangle, \tag{A.55}$$

The legal VB diagrams are restricted by the rule in which only nested (i.e. non-crossing) bonds are allowed. Any diagram with crossing bond can be expressed as linear combinations of the legal diagrams. Therefore, for a N-site half-filled system, the total number of VB diagrams N_T is given by

$$N_T = \sum_{m=0}^{N/2} \binom{N}{m} \binom{N-m}{N-2m} \frac{(N-2m)!}{(N/2-m)!(N/2-m+1)!}\,. \tag{A.56}$$

It is clear that the dimension of the Hamiltonian matrix increases very rapidly as N increases even if the electron-hole and mirror plane symmetries are included in the construction of the basis functions. As a result, the VB calculations are limited to relatively small systems.

APPENDIX B

ELECTRO-ABSORPTION

Optical Absorption Coefficient

The linear optical absorption coefficient is defined as[1]

$$\alpha(\omega) = \omega Im\{\chi^{(1)}\}$$

$$= K \times \omega Im\{\sum_{g,n} |\langle n|\mu|g\rangle|^2 (\frac{1}{\omega + \omega_{ng} + i\Gamma_{ng}} - \frac{1}{\omega - \omega_{ng} + i\Gamma_{ng}})\} \qquad \text{(B.57)}$$

Perturbation Theory of Electro-Absorption

Assuming a weak applied field F parallel to the chain direction, the Hamiltonian is, therefore, the sum of that of zero field and that of nonzero field $H_F = -\mu F$, i.e.

$$H = H_0 + H_F \ .$$

To the first order, the new wave functions in the presence of the field are

$$|n\rangle = |n^{(0)}\rangle - F \sum_{m \neq n} \frac{\langle m^{(0)}|\mu|n^{(0)}\rangle}{E_n^{(0)} - E_m^{(0)}} |m^{(0)}\rangle \qquad \text{(B.58)}$$

where $|n^{(0)}\rangle$ and $E_n^{(0)}$ etc. are the unperturbed wave functions and energies. Within the perturbation theory, the following results are obtained.

[1]See Shen, 1984.

(1) Energy Shifts of the $1B_u$ and the nB_u:

Since the $1B_u$ is strongly coupled to only two A_g states, the new wave function $|1B_u\rangle$ in the presence of the field can be written as

$$|1B_u\rangle = |1B_u^{(0)}\rangle - F\frac{\langle 1A_g^{(0)}|\mu|1B_u^{(0)}\rangle}{E_{1B_u}^{(0)} - E_{1A_g}^{(0)}}|1A_g^{(0)}\rangle - F\frac{\langle mA_g^{(0)}|\mu|1B_u^{(0)}\rangle}{E_{1B_u}^{(0)} - E_{mA_g}^{(0)}}|mA_g^{(0)}\rangle \ , \quad \text{(B.59)}$$

where only essential states are considered, and the change in the energy of the $1B_u$, to the second order of F, is

$$\begin{aligned}\Delta E(1B_u) &\equiv \langle 1B_u|H_F|1B_u\rangle \\ &\simeq 2F^2\frac{|\langle 1A_g^{(0)}|\mu|1B_u^{(0)}\rangle|^2}{E_{1B_u}^{(0)} - E_{1A_g}^{(0)}} + 2F^2\frac{|\langle mA_g^{(0)}|\mu|1B_u^{(0)}\rangle|^2}{E_{1B_u}^{(0)} - E_{mA_g}^{(0)}} \qquad \text{(B.60)}\end{aligned}$$

Since $|\langle mA_g^{(0)}|\mu|1B_u^{(0)}\rangle|$ is comparable to or larger than $|\langle 1A_g^{(0)}|\mu|1B_u^{(0)}\rangle|$ and $E_{1B_u} - E_{mA_g} < 0$, while $0 < E_{mA_g} - E_{1B_u} < E_{1B_u} - E_{1A_g}$, the second term in Eq. B.60 is negative and larger in magnitude. Therefore, the energy of the $1B_u$ is lowered by the field due to the presence of the mA_g that is just above and strongly coupled to the $1B_u$. Correspondingly, a red shift of the $1B_u$ exciton is expected in the electro-absorption spectrum $\Delta\alpha(\omega) \equiv \alpha_F - \alpha_0$. The energy shift of the ground state $1A_g$ can be neglected because of its large energy separations (by a gap) from the B_u states.

Similarly, the energy of the conduction band threshold nB_u is also expected to be lowered because the nB_u is strongly coupled to one or more band A_g states that are close to and above it.

(2) Field Induced A_g—$1A_g$ Couplings:

In the presence of the field, the new wave functions are the mixing of the A_g and the B_u states (see Eq. B.58). As a result, the dipole couplings between the perturbed A_g states become possible. Considering that each A_g state is strongly coupled to two B_u states and the ground state is hardly changed, the field induced

dipole coupling between a perturbed A_g state, say $|kA_g\rangle$, and the ground state $|1A_g^{(0)}\rangle$ is given by

$$\langle 1A_g^{(0)}|\mu|kA_g\rangle =$$

$$-F\frac{\langle k_1B_u^{(0)}|\mu|kA_g^{(0)}\rangle}{E_{kA_g}^{(0)}-E_{k_1B_u}^{(0)}}\langle 1A_g^{(0)}|\mu|k_1B_u^{(0)}\rangle - F\frac{\langle k_2B_u^{(0)}|\mu|kA_g^{(0)}\rangle}{E_{kA_g}^{(0)}-E_{k_2B_u}^{(0)}}\langle 1A_g^{(0)}|\mu|k_2B_u^{(0)}\rangle \quad \text{(B.61)}$$

where k_1B_u and the k_2B_u are the two B_u states coupled to the kA_g.

<u>mA_g—$1A_g$ Coupling</u>

For the mA_g, the k_1B_u and the k_2B_u are the $1B_u$ and the nB_u respectively, and the two denominators in Eq. B.61 have different signs since $E_{1B_u} < E_{mA_g} < E_{nB_u}$. On the other hand, it is known, from Chapter 4, that the two numerators $\langle 1B_u^{(0)}|\mu|mA_g^{(0)}\rangle\langle 1A_g^{(0)}|\mu|1B_u^{(0)}\rangle$ and $\langle nB_u^{(0)}|\mu|mA_g^{(0)}\rangle\langle 1A_g^{(0)}|\mu|nB_u^{(0)}\rangle$ also have opposite signs. Therefore, the two terms in Eq. B.61 add constructively and a sizable absorption intensity is expected in the $\Delta\alpha$ spectrum.

<u>$2A_g$—$1A_g$ Coupling</u>

In the noninteracting-electron models, the $2A_g$ is the mA_g and the two essential B_u states are the $1B_u$ and the $2B_u$ with $E_{1B_u} < E_{2A_g} < E_{2B_u}$, and field induced $2A_g$—$1A_g$ is expected since the two terms in in Eq. B.61 add. While in the interacting electron models, the $2A_g$ becomes a subgap state and $E_{2A_g} < E_{1B_u} < E_{2B_u}$. Hence the energy denominators in Eq. B.61 have the same signs and the two terms in the equation cancel since $\langle 1B_u^{(0)}|\mu|2A_g^{(0)}\langle 1A_g^{(0)}|\mu|1B_u^{(0)}\rangle \simeq -\langle 2B_u^{(0)}|\mu|2A_g^{(0)}\langle 1A_g^{(0)}|\mu|2B_u^{(0)}\rangle$ and $E_{1B_u} = E_{2B_u}$ in the infinite chain limit. Consequently, $2A_g$—$1A_g$ coupling is strongly suppressed by the cancellation. Similarly, for other sub-gap A_g states, the cancellations are present in the field induced A_g-$1A_g$ dipole coupling moments.

REFERENCES

[1] Abe, S., Schreiber, M., Su, W. P., and Yu, J., 1992, *Phys. Rev. B 45*, 9432.

[2] Abe, S., Schreiber, M., Su, and W. P., 1992, *Chem. Phys. Lett. 192*, 425.

[3] Agrawal, G. P., Cojan, C. and Flytzanis, C., 1978, *Phys. Rev. B 17*, 776.

[4] Anderson, P. W., 1959, *Phys. Rev. 115*, 2.

[5] Anderson, P. W., 1987, *Since, 235*, 1196.

[6] Aspnes, D. E. and Rowe, J. F., 1972, *Phys. Rev. B 5*, 4022.

[7] Aspnes, D. E. 1967, *Phys. Rev. 153*, 972.

[8] Baeriswyl, D., Campbell, D. K. and Mazumdar, S. 1992, in *Conjugated Conducting Polymers*, edited by Kiess, H., (Springer-Verlag, Berlin), 7.

[9] Baker, G. L., Etemad, S. and Kajzar, F., 1987, *SPIE Proc. 824*, 102.

[10] Bassler, H., 1985, in *Polydiacetylene* edited by Bloor, D. and Chance, R. R., (Martinus Nijhoff, Dordrecht), 135.

[11] Batchelder, D. N., 1985, in *Polydiacetylenes*, edited by Bloor, D. and Chance, R. R., NATO ASI Series, (Martinus Nijhoff, Dordrcht), 187, and references therein.

[12] Bloor, D. and Chance, R. R., 1985, eds. *"Polydiacetylenes", NATO ASI Series E: Applied Sciences - No. 102.*

[13] Bondeson, S. R. and Soos, Z. G., 1979, *J. Chem. Phys. 71*, 3807.

[14] Bonner, J. C. and Blöte, H. W. J., 1982, *Phys. Rev. B 25*, 6959.

[15] Bonner, J. C. and Fisher, M. E., 1964, *Phys. Rev. 135*, 640.

[16] Campbell, D. K., DeGrand, T. A., and Mazumdar, S., 1984, *Phys. Rev. Lett. 52*, 1717.

[17] Chance, R. R., Shand, M. L., Hogg, C. and Silbey, R., 1980, *Phys. Rev. B 22*, 3540.

[18] Chemla, D. S. and Zyss, J., eds., 1987, *Nonlinear Optical Properties of Organic Molecules and Crystals*, (Academic, New York)

[19] Chiang, L. Y., Garito, A. F., and Sandman, D. J., eds, 1991, *Mater. Res. Soc. Symp. 247.*

[20] Chollet, P. A., Kajzar, F. and Messier, J., 1985, in *Polydiacetylenes*, edited by Bloor, D. and Chance, R. R., NATO ASI Series E. No. 102 (Martinus Nijhoff, Dordrecht), 317.

[21] Cohen-Tannoudji, C., 1977, *Quantum Mechanics* by Hermann and by John Wiley & Sons, Inc. .

[22] Cojan, C., Agrawal, G. P. and Flytzanis, C., 1977 *Phys. Rev. B 15*, 909.

[23] Delong, K. W., Rochford, K. B. and Stegeman, G. I., 1989, *Appl. Phys. Lett. 55*, 1823.

[24] Demelo, C. P. and Silbey, R., 1987, *Chem. Phys. Lett. 140*, 537.

[25] Dewar, M. I., 1952, *J. Chem. Soc.*, September, 3532.

[26] Dixit, S. N. and Mazumdar, S., 1984, *Phys. Rev. B. 29*, 1824.

[27] Dixit, S. N., Guo, D. and Mazumdar, S. 1991, *Phys. Rev. B 43*, 6781.

[28] Ducasse, I. R., Miller, T. E., and Soos, Z. G., 1982, *J. Chem. Phys. 76*, 4094.

[29] Fann, W. -S., Benson, S., Madey, J. M. J., Etemad, S., Baker, G. L. and Kajzar, F., 1989, *Phys. Rev. Lett. 62*, 1492.

[30] Ficher, C. R., Chen, C. -E., Heeger, A. J., MacDiarmid, A. C., and Hastings, J. B., 1982, *Phys. Rev. Lett. 48*, 100.

[31] Guo, Dandan and Mazumdar, S., 1992a, *J. Chem. Phys. 97*, 2170.

[32] Guo, Dandan, Mazumdar, S. and Dixit, S. N., 1992b, *Synth. Metals 49*, 1.

[33] Guo, Dandan, Mazumdar, S., Stegeman, G. I., Cha, M., Neher, D., Aramaki, S., Torruellas, W. and R. Zanoni, 1992c, in *Electrical, Optical, and Magnetic Properties of Organic Solid State Materials* edited by Chiang, L. Y., Garito, A. F., and Sandman, D. J., 151.

[34] Guo, Dandan, Mazumdar, S. and Dixit, S. N., 1992d, *J. Nonlinear Optics*, submitted.

[35] Guo, Dandan, Mazumdar, S., Dixit, S. N., Kawabe, Y., Jarka, F. and Peyghambrian, 1992e, Phys. Rev. B, submitted.

[36] Guo, F. and Mazumdar, S., 1992, unpublished.

[37] Guo, F., Guo, D., and Mazumdar, S., 1993, *Bulletin of American Physical Society 38*, 57.

[38] Guo, F., Guo, D., and Mazumdar, S., 1993, to be published.

[39] Haarer, D. and Philpott, M. R., 1983 in *Spectroscopy and Excitation Dynamics of Condensed Molecular Systems*, edited by Agranovich, V. M. and Hochstrasser (North Holland), 27.

[40] Hanna, D. C., Yuratich, M. A. and Cotter, D., 1979, *Nonlinear Optics of Free Atoms and Molecules*, (Springer-Verlag, Berlin Heidelberg New York).

[41] Hanna, M. W., McLachlan, A. D., Dearman, H. H., and McConnell, H. M., 1962, *J. Chem. Phys. 37*, 361.

[42] Hanna, M. W., McLachlan, A. D., Dearman, H. H., and McConnell, H. M., 1962, *J. Chem. Phys. 37*, 3008.

[43] Hasegawa, T., Ishikawa, K., Kanetake, T., Koda, T., Takeda, K., Kobayashi, H., and Kubodera, K., 1990, *Chem. Phys. Lett. 171*, 239.

[44] Hasegawa, T., Ishikawa, K., Koda, T., Takeda, K., Kobayashi, H., and Kubodera, K., 1991, *Synth. Metals, 41-43*, 3151.

[45] Hasegawa, T., Iwasa, Y., Sunamura, H., Koda, T., Tokura, Y., Tachibana, H., Matsumoto, M., and Abe, S., 1992, *Phys. Rev. Lett. 69*, 668.

[46] Hayden, G. W. and Mele, E. J., 1986, *Phys. Rev. B 34*, 5484.

[47] Hayden, G. W. and Soos, Z. G., 1988, *Phys. Rev. B 38*, 6075.

[48] Heflin, J. R., Wong, K. Y., Zamani-Khamiri, O. and Garito, A. F., 1988, *Phys. Rev. B 38*, 1573.

[49] Heitler, W. and London, F., 1927, *Z. Physik, 44*, 455.

[50] Hermann, J. P., Richard, D. and Ducuing, J., 1973, *Appl. Phys. Lett. 23*, 178.

[51] Hermann, J. P. and Ducuing, J., 1974, *J. Appl. Phys. 45*, 5100.

[52] Hiroaki, T., Kawabata, Y., Koshihara, S., and Tokura, Y., 1990, *Solid State Comm. 75*, 5.

[53] Hirsch, J. E., 1983, *Phys. Rev. Lett. 51*, 296.

[54] Hirsch, J. E. and Grabowski, M., 1984, *Phys. Rev. Lett. 52*, 1713.

[55] Hubbard, J., 1963, *Proc. R. Soc. London, A 276*, 238; 1964, *Proc. R. Soc. London, 277*, 237.

[56] Hudson, B. S., Kohler, B. E. and Schulten, K., 1982, in *Excited States*, edited by Lim, E. C., (Academic, New York), Vol. 6.

[57] Iwasa, Y., Hasegawa, T., Koda, Tokura, Y., Tachibana, H. and Kawabata, Y., 1992, *Synth. Metals 50*, 415.

[58] Kajzar, F., Etemad, S., Baker, G. L. and Messier, J., 1987, *Synth. Met. 17*, 563.

[59] Kajzar, F., Etemad, S., Baker, G. L. and Messier, J., 1987, *Solid State Commun. 63*, 1113.

[60] Kajzar, F. and Messier, J., 1985, *Thin Solid. Films 132*, 11.

[61] Kajzar, F. and Messier, J., 1987, in *Nonlinear Optical Properties of Organic Molecules and Crystals*, edited by Chemla, D. S. and Zyss, J. (Academic, New York).

[62] Kanetake, T., Ishikawa, K., Hasegawa, T., Koda, T., Takeda, K., Hasegawa, M., Kubodera, K., and Kobayashi, H., 1989, *Appl. Phys. Lett. 54*, 2287.

[63] Kawabe, Y., Jarka, F., Peyghambarian, N., Guo, D., Mazumdar, S., Dixit, S. N. and Kajzar, F., 1991, *Phys. Rev. B 44*,6530.

[64] Kawabe, Y., Jarka, F., Peyghambarian, N., Guo, D., Mazumdar, S., Dixit, S. N. and Kajzar, F., 1992, *Synth. Metals 50*, 517.

[65] Kepler, R. G. and Soos, Z. G., 1991, *Phys. Rev. B 43*, 12530.

[66] Kepler, R. G., Zeigler, J. M., Harrah, L. A., and Kurtz, S. R., 1987, *Phys. Rev. B 35*, 2818.

[67] Klümper, A., Schadschneider, A., and Zittartz, J., 1990, *Z. Phys. B 78*, 99.

[68] Koda, T, Haseegawa, T., Ishikawa, K., Kubodera, K., Kobayashi, H., and Takeda, K., 1991, *J. Lumin 48-49*, 321.

[69] Kohler, B. E. and Schilke, D. E., 1987, *J. Chem. Phys. 86*, 5214.

[70] Kohler, B. E., Sprangler, C. and Westerfield, C., 1988, *J. Chem. Phys. 89*, 5422, and references therein.

[71] Kubo, K., 1971, *J. Phys. Soc. Jpn. 31*, 30.

[72] Kurihara, T., Oba, N., Mori, Y., Tomaru, S., and Kaino, T., 1991, *J. Appl. Phys. 70*, 17.

[73] Le, H. Q. and Cecca, S. Di, 1991, *Opt. Lett. 16*, 901.

[74] Le Moigne, J., Thierry, A., Chollet, P. A., Kajzar, F. and Messier, J., 1988, *J. chem. Phys. 88*, 6647.

[75] Le Moigne, J., Thierry, A. and Kajzar, F., 1989, in *Thin Films in Optics*, edited by Tschudi, T., SPIE Proc. Vol. 1125, p. 9.

[76] Le Moigne, J., Thierry, A. Chollet, P. A., Kajzar, F. and Messier, J. 1988, *J. Chem. Phys. 88*, 6647.

[77] Lieb, E. H. and Wu, F. Y., 1968, *Phys. Rev. Lett. 20*, 1445.

[78] Lochner, K., Bassler, H., Tieke, B. and Wegner, G., 1978, *Phys. Stat. Solidi (b)88*, 653, and references therein.

[79] Mataga, N. and Nishimoto, K., 1957, *Z. Physik. Chem. Neue Folge, 13*, 140.

[80] Mazumdar, S. and Campbell, D. K., 1985, *Phys. Rev. Lett. 55*, 2067.

[81] Mazumdar, S. and Campbell, D. K., 1986, *Synth. Met. 13*, 163.

[82] Mazumdar, S. and Dixit, S. N., 1983, *Phys. Rev. Lett. 51*, 292.

[83] Mazumdar, S. and Dixit, S. N., 1989, *Synth. Met. 28*, D463.

[84] Mazumdar, S., Guo, D. and Dixit, S. N., 1991, *SPIE Proc. 1436* 137.

[85] Mazumdar, S., Guo, D. and Dixit, S. N., 1992, *J. Chem. Phys. 96*, 6962

[86] McConnell, H. M. and Chesnut, D. B., 1957, *J. Chem. Phys. 27*, 984.

[87] McIntyre, E. F. and Hameka, H. F., 1978, *J. Chem. Phys. 68*, 3481.

[88] McWilliams, P. C. M., Hayden, G. W., and Soos, Z. G., 1990, *Chem. Phys. Lett. 171*, 14.

[89] McWilliams, P. C. M. and Soos, Z. G., 1991, *J. Chem. Phys. 95*, 2127.

[90] Messier, J., Kajzar, F., Prasad, P. and Ulrich, D., eds. 1989, , *Nonlinear Optical Effects in Organic Polymers*, NATO Series AIS series, Vol. 162, (Kluwer Academic Publishers, Dordecht).

[91] Misurkin, I. A., and Ovchhinnikov, A. A., 1970, *Fiz. Tverd. Tela 12*, 2524.

[92] Misurkin, I. A., and Ovchhinnikov, A. A., 1971, *Sov. Phys. Solid State 12*, 2031.

[93] Mori, Y. and Okano, Y., 1990, *Mat. Res. Symp. Proc. 173*, 665.

[94] Musurkin, I. A. and Ovchinnikov, A.A., 1971, *Soviet Physics 12*, 2031.

[95] Nunzi, J. M. and Charra, F., 1991, *Appl. Phys. Lett. 59*, 13.

[96] Ohno, K., 1964, *Chim. Acta 2*, 219.

[97] Orr, B. J. and Ward, J. F., 1971, *Mol. Phys. 20*, 513.

[98] Ovchinnikov, A. A., 1970, *Sov. Phys.-JETP, 30*, 1160.

[99] Pariser, R., 1956, *J. Chem. Phys. 24*, 250.

[100] Pariser, R. and Parr, R. G., 1953, *J. Chem. Phys. 21*, 767.

[101] Pauling, L., 1948, *The nature of Chemical Bonds*, (Cornell University Press, Ithaca, second edition).

[102] Peierls, R. E., 1955, *Quantum Theory of Solids*, (Oxford Univ. Press, London).

[103] Phillips, S. D., Worland, R., Yu, G., Hagler, T., Freedman, R. Cao, Y., Chiang, J., Walker, W. C. and Heeger, A. J., 1989, *Phys. Rev. B 40*, 9751.

[104] Pople, J. A. 1953, *Trans Faraday Soc. 42*, 1375.

[105] Ramasesha, S. and Soos, Z. G., 1984 (a), *Synth. Metals 9*, 283.

[106] Ramasesha, S. and Soos, Z. G., 1984 (b), *J. Chem. Phys. 80*, 3278.

[107] Roos, B. and Skancke, P. N., 1967, *Acta Chem. Scand. 21*, 233.

[108] Rumer, G., 1932, *Göttingen Nachrich. Tech.*, 377.

[109] Salem, L., 1966, *The Molecular Orbital Theory of Conjugated Systems*, (W. A. Benjamin, Inc.).

[110] Sauteret, C., Hermann, J. -P., Frey, R., Pradere, F., Ducuing, J., Baughman, R. H. and Chance, R. R., 1976, *Phys. Rev. Lett. 36*, 956.

[111] Schulten, K., Ohmine, I. and Karplus, M., 1976, *J. Chem. Phys. 64*, 4422.

[112] Sebastian, L. and Weiser, G., 1981, *Phys. Rev. Lett. 46*, 1159.

[113] Sebastian, L. and Weiser, G., 1981, *Chem. Phys. 62*, 447.

[114] Shen, Y. R., 1984, *The Principles of Nonlinear Optics*, (John Wiley & Sons).

[115] Shuai, Z. and Brédas, J. L., 1991, *Phys. Rev. B 44*, 5962.

[116] Sinclair, M., 1988, *Phys. Rev. B 38*, 10724.

[117] Sinclair, M., Moses, D., McBranch, D., Heeger, A. J., Yu, J., and Su, W. P., 1989, *Synth. Metals 28*, D655.

[118] Soos, Z. G. and Ramasesha, S., 1983, *Chem. Phys. Lett. 101*, 34.

[119] Soos, Z. G. and Ramasesha, S., 1984, *Phys. Rev. B 29*, 5410.

[120] Soos, Z. G. and Hayden, G. W., 1988, in *Electroresponsive Molecular and Polymeric Systems*, ed. by Skotheim, T. A. (Dekker, New York), 197.

[121] Soos, Z. G. and Ramasesha, S., 1989, *J. Chem. Phys. 90*, 1067.

[122] Stegeman, G. I., Zanoni, R. and Seaton, C. T., 1987 in *Mat Res. Soc. Symp. Proc. 53.*

[123] Stegeman, G. I., Seaton, C. T., and Zanoni, R., 1987, *Thin Solid Films 152*, 231.

[124] Stegeman, G. I., Torruellas, W., Rochford, K. B., Zanoni, R., Krug, W., Miao, E. and Beranek, M. W., 1991, *Proc. Mat. Res. Soc.*.

[125] Su, W. P., Schrieffer, J. R., and Heeger, A. J., 1979, *Phys. Rev. Lett. 42*, 1698.

[126] Su, W. P., Schrieffer, J. R., and Heeger, A. J., 1980, *Phys. Rev. B 22*, 2099.

[127] Su, W. P. and Schrieffer, J. R., 1980, *Proc. Natl. Acad. Sci. 77*, 5626.

[128] Suzuki, H., 1967, *Electronic absorption Spectra and Geometry of Organic Molecules*, (Academic Press, New Yourk).

[129] Suzuki, N., Ozaki, M., Etemad, S., Heeger, A. J., and MacDiarmid, A. G., 1980, *Phys. Rev. Lett. 45*, 1209.

[130] Thakur, M. and Krol, D. M., 1990, *Appl. Phys. Lett. 56*, 1213.

[131] Tavan, P. and Schulten, K., 1987, *Phys. Rev. B 36*, 4337.

[132] Tokura, Y., Oowaki, Y., Koda, T. and Baughman, R. H., 1984, *Chem. Phys. 88*, 437.

[133] Tokura, Y., Koda, T., Itsubo, A., Miyabayashi, M., Okuhara, K. Ueda, A., 1986, *J. Chem. Phys. 85*, 99.

[134] Torruellas, W. E., Neher, D., Zanoni, R., Stegeman, G. I., Kajzar, F. and Leclerc, M., 1990, *Chem. Phys. Lett. 175*, 11.

[135] Torruellas, W. E., 1991, *Ph.D. thesis.*

[136] Torruellas, W. E., Rochford, K. B., Zanoni, R., Aramaki, S. and Stegeman, G. I., 1991, *Opt. Commun. 82*, 94.

[137] Townsend, P. D., Baker, G. L., Klausner, C. F. and Etemad, S., 1988, *Appl. Phys. Lett. 53*, 1782.

[138] Townsend, P. D., Fann, W. S., S. Etemad, Baker, Soos, Z. G. and McWilliams, P. C. M., 1991, *Chem. Phys. Lett. 180*, 485.

[139] Vardeny, Z. V. and Baker, G. L., eds, 1992, *Synth. Metals 49.*

[140] van Beek, J. B., Kajzar, F. and Albrecht, A. C., 1991, *J. Chem. Phys. 95*, 6400.

[141] van Beek and Albrecht, A. C., 1991, *Chem Phys. Lett. 187*, 269.

[142] van Tomme, E., Van Daele, P. P., and Baets, R. G., 1991, *IEEE J. Quant. Electr. 27*, 778.

[143] Weinberger, B. R., Roxlo, C. B., Etemad, S., Baker, G. L., and Orenstein, J., 1984, *Phys. Rev. Lett. 53*, 86.

[144] Williams, V., Ho, Z. Z., Peygambarian, N., Gibbons, W. M., Grasso, R. P., O'Brien, M. K., Shannon, P. J. and Sun, S. T., 1990, *Apply. Phys. Lett. 57*, 2399.

[145] Willson, E. G., 1975, *J. Phys. C 8*, 727.

[146] Woynarovich, F., 1982, *J. Phys. C15*, 85.

[147] Wu, W. K., 1988, *Phys. Rev. Lett. 61*, 1119.

[148] Wu, W. and Kivelson, S., 1989, *Synth. Metals 28D*, 575.

[149] Wynne, J. J., 1969, *Phys. Rev. 178*, 1295.

[150] Yee, K. C. and Chance, R. R., 1978 , *J. Polym. Sci. Polym. Phys. Ed. 16*, 431.

[151] Yannoni, C. S. and Clarke, T. C., 1983, *Phys. Rev. Lett. 51*, 1191.

[152] Yu, J., Friedman, B., Baldwin, P. R. and Su, W. P., 1989, *Phys. Rev. B 39*, 12814.